AD-A207 454 DEEP SPACE LADAR SBIR PHASE 1(U) AUTONOMOUS TECHNOLOGIES CORP ORLANDO FL R W FREY ET AL. 27 MAR 89 1/2
DASG60-88-C-0076

UNCLASSIFIED F/G 17/5.1 NL

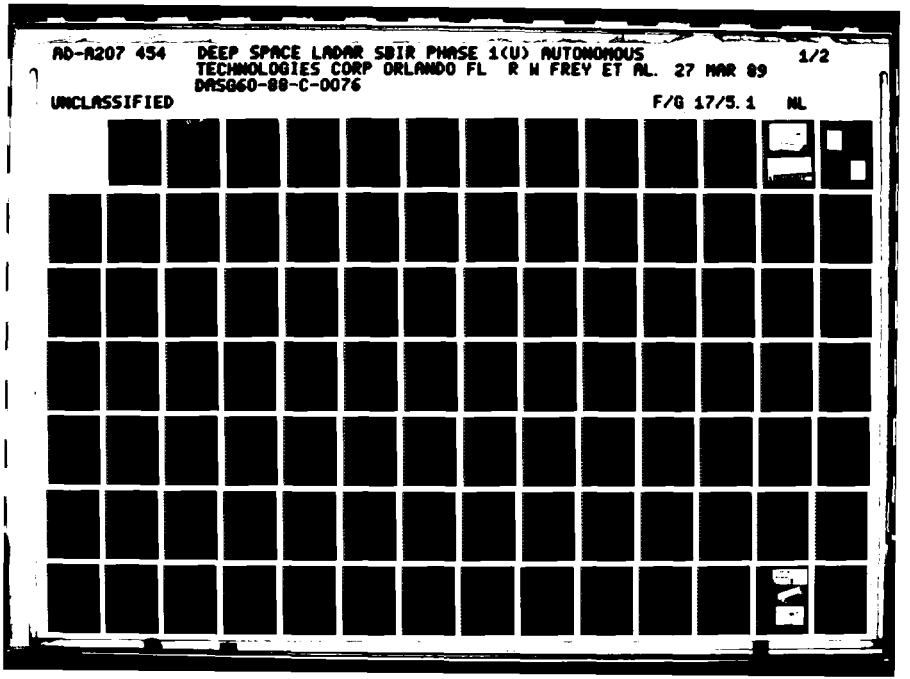

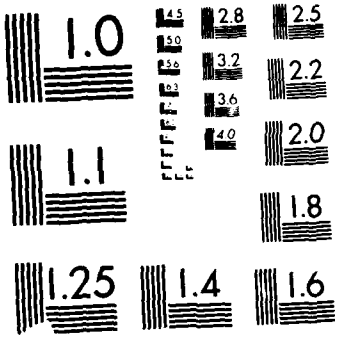

UTION TEST CHART

AUTONOMOUS TECHNOLOGIES CORPORATION

DEEP SPACE LADAR

CONTRACT #DASG60-88-C-0076

SBIR PHASE I. FINAL REPORT

27 MARCH 1989

SUBMITTED BY:

AUTONOMOUS TECHNOLOGIES CORPORATION

ORLANDO, FL

SPONSORED BY:

SDIO/INNOVATIVE SCIENCE AND TECHNOLOGY OFFICE

MANAGED BY:

U.S. ARMY STRATEGIC DEFENSE COMMAND

UNCLASSIFIED
SECURITY CLASSIFICATION OF THIS PAGE

REPORT DOCUMENTATION PAGE

Form Approved
OMB No. 0704-0188

1a. REPORT SECURITY CLASSIFICATION UNCLASSIFIED	1b. RESTRICTIVE MARKINGS NONE
2a. SECURITY CLASSIFICATION AUTHORITY N/A	3. DISTRIBUTION/AVAILABILITY OF REPORT UNLIMITED
2b. DECLASSIFICATION/DOWNGRADING SCHEDULE N/A	
4. PERFORMING ORGANIZATION REPORT NUMBER(S) N/A	5. MONITORING ORGANIZATION REPORT NUMBER(S) DI-S-3591A/M
6a. NAME OF PERFORMING ORGANIZATION Autonomous Technologies Corp. 6b. OFFICE SYMBOL (If applicable) N/A	7a. NAME OF MONITORING ORGANIZATION U.S. ARMY STRATEGIC DEFENSE COMMAND
6c. ADDRESS (City, State, and ZIP Code) 520 N. SEMORAN BLVD., SUITE 180 ORLANDO, FLORIDA 32807	7b. ADDRESS (City, State, and ZIP Code) CSSD-H-V P.O. BOX 1500 HUNTSVILLE, ALABAMA 35807-3801
8a. NAME OF FUNDING/SPONSORING ORGANIZATION SDIO/INNOVATIVE SCIENCE & TECHNOLOGY OFFICE 8b. OFFICE SYMBOL (If applicable) IST	9. PROCUREMENT INSTRUMENT IDENTIFICATION NUMBER DASG60-88-C-0076
8c. ADDRESS (City, State, and ZIP Code) 1717 H STREET WASHINGTON, D.C. 20301-7100	10. SOURCE OF FUNDING NUMBERS PROGRAM ELEMENT NO.: P63222C PROJECT NO.: N/A TASK NO.: N/A WORK UNIT ACCESSION NO.: N/A

11. TITLE (Include Security Classification)
DEEP SPACE LADAR SBIR PHASE I FINAL REPORT

12. PERSONAL AUTHOR(S)
RANDY W. FREY, GREG RAWLINS, NEIL ZEPKIN, JOHN BOHLIN

13a. TYPE OF REPORT	13b. TIME COVERED	14. DATE OF REPORT (Year, Month, Day)	15. PAGE COUNT
FINAL REPORT	FROM 88, 10 TO 89, 3	1989, MARCH, 27	117

16. SUPPLEMENTARY NOTATION
N/A

17. COSATI CODES			18. SUBJECT TERMS (Continue on reverse if necessary and identify by block number)
FIELD	GROUP	SUB-GROUP	LADAR, PSEUDO-RANGING, PSEUDO-NOISE MODULATION, SIE, AMOS, LASE
N/A	N/A	N/A	
N/A	N/A	N/A	

19. ABSTRACT (Continue on reverse if necessary and identify by block number)

A pseudo-ranging laser radar (PRLADAR) concept is proposed to provide extended range capability to tracking LADAR systems meeting the long-range requirements of SDI mission scenarios such as the SIE midcourse program. The project will investigate the payoff of several transmitter modulation techniques and a feasibility demonstration using a breadboard implementation of a new receiver concept called the Phase Multiplexed Correlator (PMC) will be accomplished. The PRLADAR concept has specific application to spaceborne LADAR tracking missions where increased CNR/SNR performance gained by the proposed technique may reduce the laser power and/or optical aperture requirement for a given mission. The reduction in power/aperture has similar cost reduction advantages in commercial ranging applications. A successful Phase I program will lay the groundwork for a quick reaction upgrade to the AMOS/LASE system in support of near term SIE measurement objectives.

20. DISTRIBUTION/AVAILABILITY OF ABSTRACT ☐ UNCLASSIFIED/UNLIMITED ☒ SAME AS RPT. ☐ DTIC USERS	21. ABSTRACT SECURITY CLASSIFICATION UNCLASSIFIED
22a. NAME OF RESPONSIBLE INDIVIDUAL MR. RICHARD LENNING	22b. TELEPHONE (Include Area Code) 22c. OFFICE SYMBOL CSSD-H-V

DD Form 1473, JUN 86 *Previous editions are obsolete.*

SECURITY CLASSIFICATION OF THIS PAGE
UNCLASSIFIED

PN LADAR PHASE I SBIR
FINAL REPORT
Table of Contents

		PAGE
1.0	Executive Summary	7
2.0	PN Theoretical Overview:Results of Phase I Design/Analyses Tasks	11
2.1	Introduction/Overview	11
2.2	Signal Design	14
2.2.1	Phase Multiplexed Correlator	
2.2.2	PN Code Generator Properties	
2.2.3	Delayed Sequences	
2.2.4	Gold Code Generators	
2.2.5	PMC Correlator Performance Bounds	
2.2.6	Partial Auto-correlation and Cross Correlation Variance	
2.2.7	Codes for Phase I Experiment	
2.3	Acquisition	57
2.3.1	Coarse Acquisition	
2.3.1.1	Number of Cells to be Searched	
2.3.1.2	Sequential Testing with the PMC	
2.3.2	Fine Acquisition	
2.4	System Considerations	75
2.4.1	Range & Range Rate: Range Resolution	
2.4.2	Doppler Ambiguity	
2.4.3	Doppler Invariant Design	
3.0	Phase I PN LADAR Optical Implementation	92
3.1	Opto-Mechanical Hardware	92
3.1.1	Laser	
3.1.2	Compact Interferometer	
3.1.3	CI Mechanical Design Considerations	
3.1.4	PN LADAR Transmitter Optical Carrier Modulation	

		PAGE
4.0	Phase I Receiver Hardware	98
4.1	Receiver Noise Considerations	98
4.2	Receiver Intermediate Frequency (IF) Electronics	98
4.2.1	Optical Detector	
4.2.2	Bias network	
4.2.3	Pre-amp and Filter	
4.2.4	Additional RF Components	
4.2.5	RF Conversion to Baseband	
4.3	Pseudo Random Bit Sequence Test Set: Hardware Description	102
4.3.1	Transmit Sequence	
4.3.1.1	Phase Multiplex Correlator Signal	
4.3.2	Inputs	
4.3.3	Outputs	
4.3.4	Programming Interface	
4.3.5	Shift	
4.3.6	Delay	
4.3.7	Reset	
4.4	Theory of Operation	106
5.0	Phase I Experimental Configuration and Results	107
5.1	Definition of Experiment Configuration	107
5.2	Results	107
5.3	Conclusion	113

LIST OF FIGURES FOR PN FINAL REPORT

Figure #	Page #	Figure Title
1-1	9	Hardware Photos
1-2	10	Composite Data
2.1-1	13	DSSS Receiver
2.2-1	15	Phase Multi-plexed Correlator, Basic Structure
2.2-2	17	DSSS Modulator
2.2-3	19	PN Sequence Generator Basic Structure
2.2-4	19	Gold Code Generator Basic Structure
2.2-5	21	Generator for a Sequence with ?? Delay
2.2-6	24	Linear Maximal Length Sequence Generator, n = 10
2.2-7	27	Shift and Add Tapped Delay Generator for 16 Chip Delay
2.2-8	29	Gold Code Generator for n = 10
2.2-9	32	Receiver Correlator with Matched Filter
2.2-10	32	Synchronous Multiplication of a Message Sequence with a Spreading Sequence
2.2-11	38	Impulse response for an Ideal Finite Time Integrator
2.2-12	42	Identification of the Correlated Phase
2.2-13a	45	Prebias Concept to Improve Acquisition Performance
2.2-13b	53	PMC Sequence Generator for, L=8, $g(X) = X^9+X^8+X^6+X^3+X^2+1$
2.2-14	54	Polynomial Delay Generator for $g(X) = X^{10}+X^3+1$

2.2-15	55	Sequence Generated by $X^{10}+X^9+X^8+X^6+X^3+X^2+1$
2.2-16	56	Sequence Generated by $X^{10}+X^3+1$
2.3-14	58	Serial Search State Diagram
2.3-15	60	Phase Multi-plexed Correlator Signal
2.3-16	64	Likelihood Ratio Test Boundaries
2.3-17	68	Sequential Detector Block Diagram
2.3-18	72	Probability of Miss vs SNR with SNR_D, β_1, β_μ as Parameters
2.3-19	73	Lower Threshold Sensitivity vs the Mean Number of Samples to Dismiss Given SNR_D
2.4-1	77	(Costas Loop) Doppler Trackers
2.4-2	78	Quadrature Doppler Tracking Approach
2.4-3	80	Phasor Diagram of Quadrature Doppler
2.4-4	81	Ambiguity Function 3 dB Contours for Simple Pulse, Linear FM Pulse and 13 bit Barker Code
2.4-5	83	Non-coherent Detector
2.4-6	84	Loss in Convolver Peak Output Due to Doppler for the Input and Reference Waveforms Being 10μs Pulses
2.4-7	84	Normalized Correlation Function for Output of Convolver with the Input and Reference Waveforms Being 10μs Pulses with 10kHz of Doppler
2.4-8	85	Normalized Correlation Function for Output of Convolver with the Input and Reference Waveforms Being 10μs Pulses with 500 kHz of Doppler

2.4-9	85	Normalized Correlation Function for Output of Convolver with the Input and Reference Waveforms Being 10μs Pulses with 800kHz of Doppler
2.4-10	87	Loss in Convolver Mean Square Output Due to Doppler and Random Phase Variations
2.4-11	87	Normalized Mean Square Value of Convolver Output with Random Phase Input
2.4-12	88	Normalized Mean Square Value of Convolver Output with Random Phase Input
2.4-13	88	Normalized Mean Square Value of Convolver Output with Random Phase Input
2.4-14	89	Normalized Mean Square Value of Convolver Output with Random Phase Input
2.4-15	90	Doppler Invariant Design
3-1	93	Photo of Laser
3-2	93	Photo of CI and Mounts
3-3	93	Photo of Complete Transceiver
3-4	94	PN LADAR Optical Schematic
4-1	99	PN LADAR RF-IF Processing Block DIagram
4-2	101	SAT Bias Network
4-3	103	PN Transmitter
4-4	104	PMC Correlator Receiver
5-1	108	Shot Noise Limited Heterodyne Detection
5-2	109	Return From Center of Target
5-3	109	Return From Approaching Side of Target

5-4	109	Return From Receding Side of Target
5-5	111	PN Transmit Sequence Waveform and PMC Local Correlator Reference Waveform
5-6	111	Spectrum of RF Bleedthrough with PN Modulation on the Optical Carrier
5-7	112	Spectrum of Pseudo Noise Return from the Center of the Diffuse Rotating Conical Target
5-8	112	Spectrum of the Pseudo Noise Return from Diffuse Rotating Conical Target with Receding Rotational Doppler
5-9	112	Spectrum of the Return from a Stationary GLint Target
5-10	114	Baseband Received PN Waveform from a Stationary Diffuse Target
5-11	114	Baseband Received PN Waveform from a Stationary Diffuse Target showing Phase Instability [In the Absence of a Carrier Tracking Loop]
5-12	115	Normalized Correlation Coefficients

1.0 EXECUTIVE SUMMARY

Autonomous Technologies Corporation (ATC) a three year old company specializing in laser radar technology is pleased to report the results of our Phase I SBIR program entitled "Deep Space LADAR".

Recalling the project objectives taken from the Phase I proposal verbatim:

> Phase I Objectives
>
> The overall objective of Phase I will be to quantify the payoff of a PR LADAR approach to deep space ranging. The specific issues addressed will be:
>
> 1) The determination of PN code parameters optimized for SDI tracking missions
>
> 2) The analytic signal processing gain for the PR LADAR approach compared to incoherent averaging of a matched IF filter will be determined
>
> 3) Laboratory demonstration of a Simplified PN transmitter modulation technique
>
> 4) Investigation of the new phase multiplexed correlator (PMC) receiver concept
>
> 5) Measured data and analytic support extending the PR LADAR concept to a viable Phase II upgrade to the AMOS/LASE CW system

ATC is pleased to report successful completion of the above objectives with the demonstration of what we believe is the first reported operating heterodyne CO_2 laser radar (LADAR) employing a pseudo-random code modulation format. (See Figures 1-1 and 1-2)

The principle technology developments were in the successful demonstration of coherent transmission and reception of the double sideband suppressed carrier (DSSC) optical modulation which is electronically equivalent to the desired 0 to 180° phase shift keying (PSK); and the successful demonstration of the correlation properties of the new phase multiplexed correlator (PMC) receiver that substantially reduces acquisition time compared to serial search methods.

Although less progress was made on the determination of the detailed analytic signal processing gain of the PN approach over other LADAR approaches, we have made considerably more progress then expected in defining PN code parameters for high payoff SDI mission scenarios where many quantitative advantages of the PN approach are identified.

Foremost among the newly envisioned SDI mission payoffs is the utility of the correlation properties of the code (1 chip translation results in complete signal decorrelation) to produce a new range-Doppler imaging concept. Additionally there is reason to believe the PN approach may have superior performance in the presence of a retro-reflective counter measure based on the one chip (one range bin) decorrelation effect. Finally, high data rate precision range and range rate measurements are envisioned through sub chip code tracking techniques which may be used for discrimination. In addition to addressing the newly defined system concepts above, the recommended Phase II program will examine the original payoff of SNR improvement and reduction in system power-aperture.

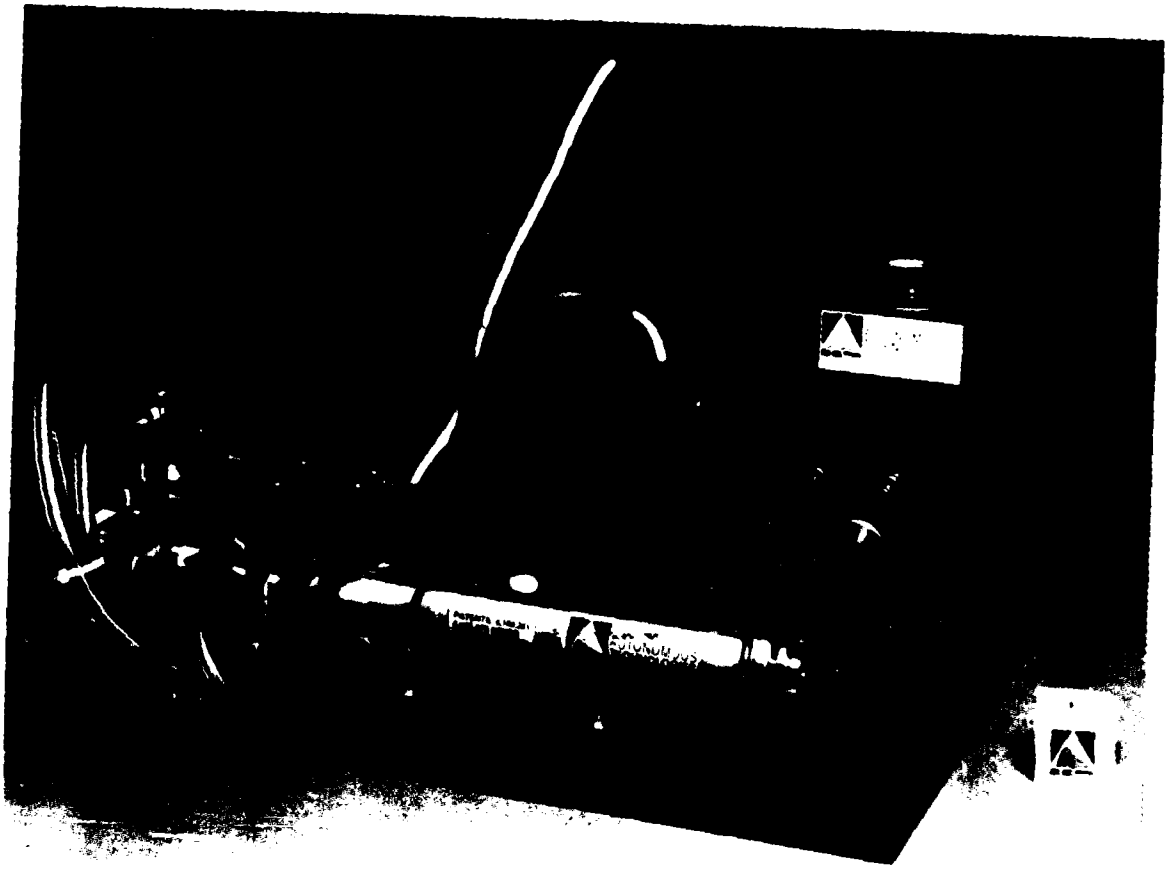

ATC LADAR WITH PHASE I AO MODULATOR

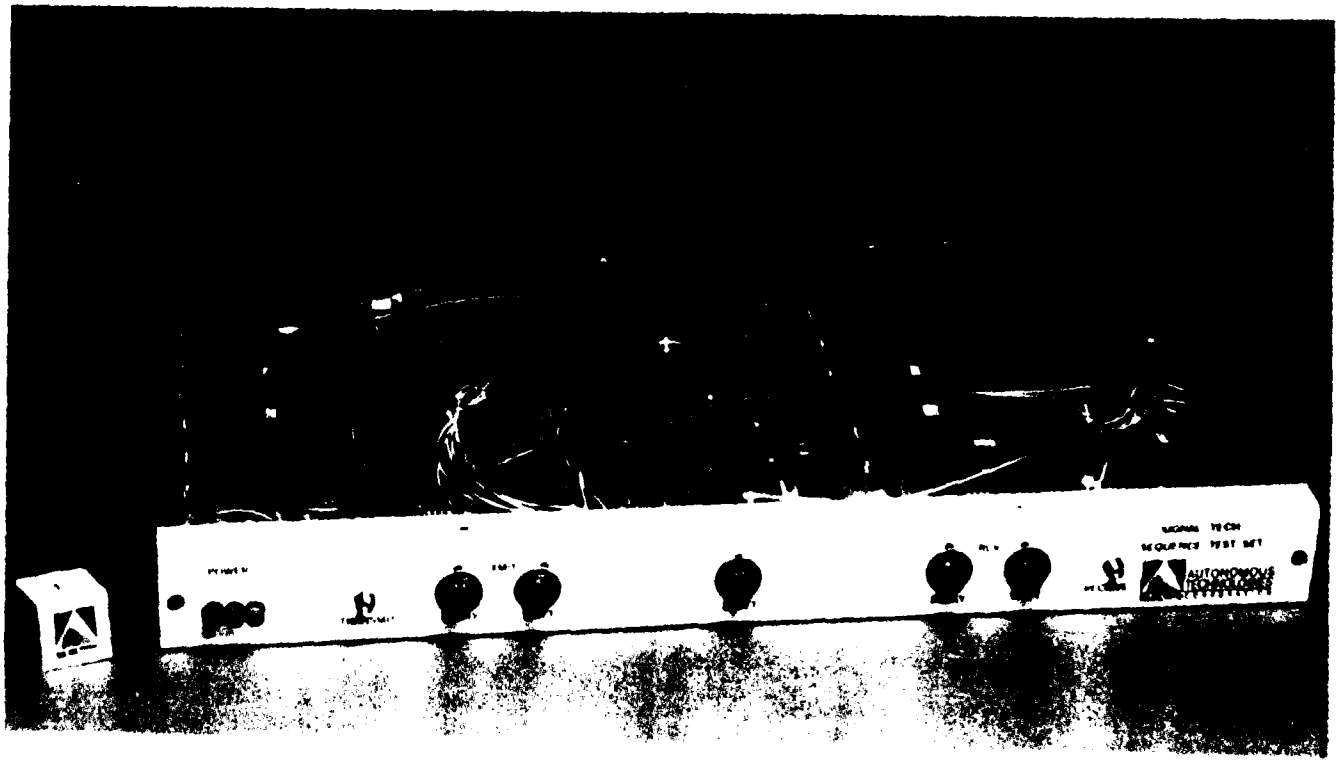

PHASE I PN TRANSMIT/PMC RECEIVE CORRELATION ELECTRONICS

Phase I PN LADAR Hardware Implementation

FIGURE 1-1

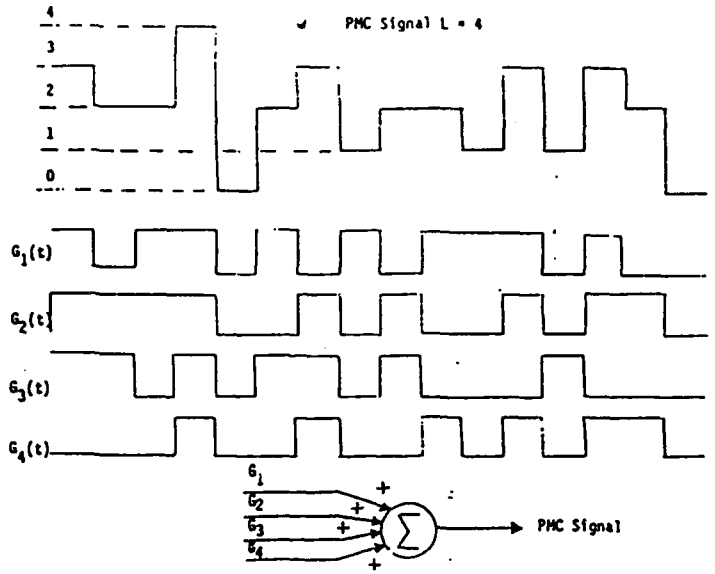

PHASE MULTIPLEXED CORRELATOR (PMC) CONCEPT

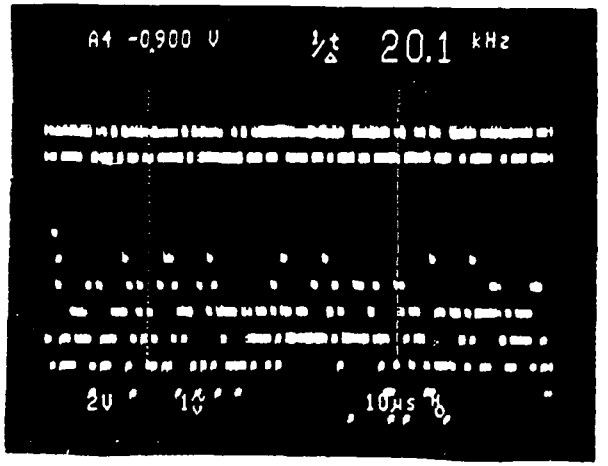

TRANSMIT WAVEFORM

RECEIVE PMC SIGNAL

CORRELATION REFERENCE

PHASE I PROGRAM: 8 LEVEL IMPLEMENTATION

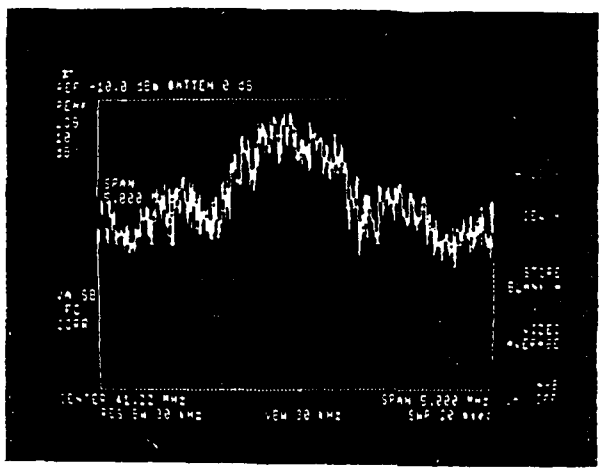

HETERODYNE CARRIER RETURN SPREAD BY PN MODULATION

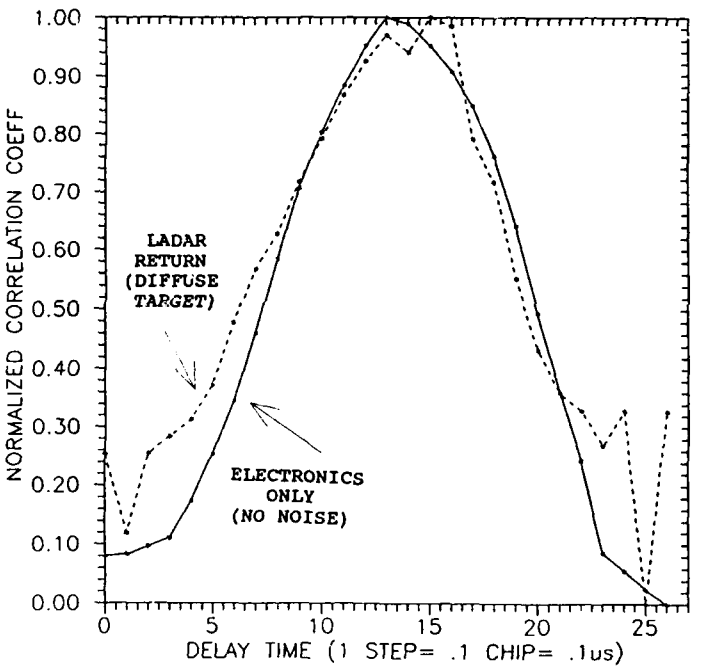

END-TO-END CORRELATION

FIGURE 1-2

2.0 PN THEORETICAL OVERVIEW: RESULTS OF PHASE I DESIGN/ANALYSIS TASKS

Historically, pseudo-noise or pseudo random sequences have been used to obtain ranging information in radar, altimeter, and navigational receiver applications. Maximum range, minimum range, acquisition speed, resolution, and range rate requirements all impact the design of such systems. Perhaps the most severe requirement is acquisition speed because of its dependence on the other system considerations, particularly max/min range and range resolution. An improvement in acquisition speed over conventional PN sequence techniques is a natural consequence of the proprietary techniques proposed. The following sections address the critical theoretical aspects of the signal design, code design and acquisition improvement.

2.1 Introduction/Overview

Synchronization of spread spectrum systems has become an important topic in recent years due to increased covert military application and expanded commercial interest. The Global Positioning System (GPS) and Tracking Relay Data Satellite System (TRDSS) spread spectrum links are the two most notable system examples. There are two very broad categories of synchronizing strategies which encompass the majority of approaches. Matched filters can be used to recover the spread symbols or various types of sliding correlators are often employed. There are several other schemes which have limited application, such as the Rapid Acquisition by Sequential Estimation (RASE) or maximum-likelihood algorithm techniques (Simon 1985). However, the focus of the ensuing discussion deals with a modification to the sliding correlator implementation and heretofore has not been found in the literature. The most similar publicized technique is the conventional sliding correlator with parallel processors. The parallel processing approach quickly becomes cumbersome in terms of hardware. Therefore, a novel solution has been conceived to be integrated with a serial search coarse acquisition synchronizer. This technique can be implemented in digital or analog hardware, depending on the system specifications, and is entirely compatible with the code tracking stage of synchronization.

Typically, a binary pseudo-noise (PN) sequence is used to modulate a much slower random binary message sequence which is translated by carrier to the channel. In the case of a ranging radar m(t) is a constant. This is called Direct Sequence Spread Spectrum (DSSS). A receiver down converts the spread signal to an Intermediate Frequency (IF) where the composite signal is despread by multiplication with an exact replica of the modulating PN sequence. The difficulty lies in the time uncertainty between transmitter and receiver clocks. The link platforms may be extremely dynamic in nature, undergoing high acceleration and experiencing severe Doppler shift. In the most general case, the transmit and receive clocks have entirely independent statistics. Of course, in the radar case target velocity, range, and trajectory determine this instability. This requires that the receive clock must adapt as required for synchronization between the platforms. The sliding correlator or serial search correlator reduces the time or phase uncertainty between the modulating PN sequence and local receiver PN sequence. This is usually accomplished by moving the

receiver PN sequence relative to the received signal by a fraction of the PN sequence characteristic symbol or chip. Eventually, the received and transmitted sequences will overlap partially, resulting in a high cross correlation value out of the local multiply. This large correlation peak is detected, verified, then further used for fine synchronization. Each cell or portion to the PN sequence must be searched until such a correlation peak is obtained (Holmes 1982). The proposed multiphase correlator will reduce the number of cells that must be searched before correlation is achieved. Since the number of cells searched is lower, the mean time to acquire synchronization, T_{aq}, must also be reduced, compared to conventional correlators.

Figure 2.1-1 illustrates a typical system configuration. the acquisition loop is responsible for obtaining synchronization within a fraction of a PN code chip. This is sometimes referred to as coarse acquisition. The code tracking loop is responsible for fine synchronization between the received signal and the local correlation signal. The proprietary scheme presented in this report is intended to be employed during the coarse acquisition phase. The fundamental binary time unit of the PN sequence is known as a chip. Traditionally, all phases of the locally generated PN code are explored chip by chip until synchronization is achieved. The sequential detection algorithm is the optimal search process for acquisition (Simon 1985). Originally developed by Abraham Wald, this algorithm is slightly modified to suit the purpose of the Phase Multiplexed Correlation (PMC) signal presented here. The key to the success of the proposed technique lies in the low cross-correlation properties of the despreading codes. The bounds on the local correlation signal design will be developed in detail.

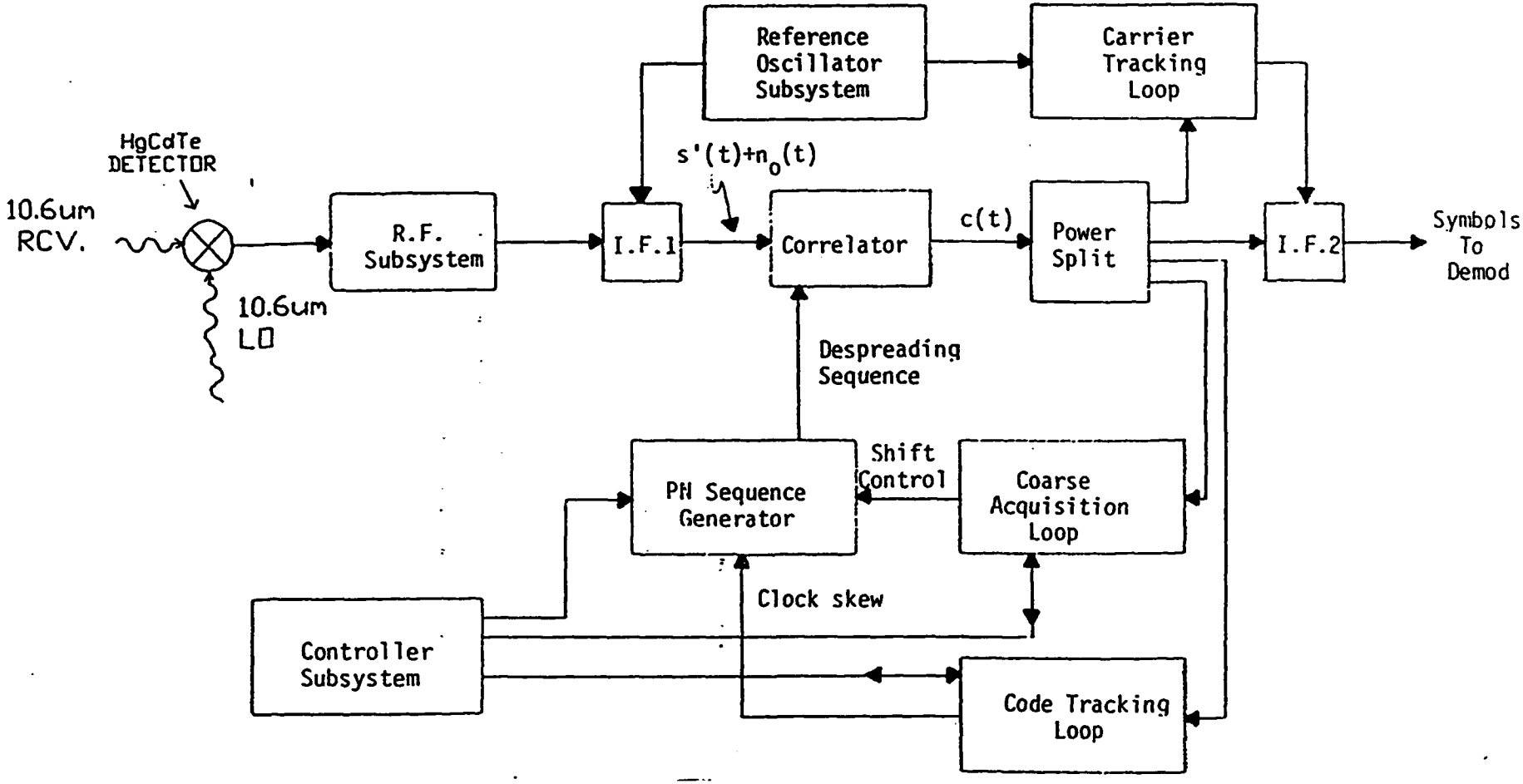

Figure 2.1-1 DSSS Receiver

2.2 SIGNAL DESIGN

2.2.1 Phase Multiplexed Correlator (PMC)

The locally generated correlation signal is composed of L equally spaced phases of the spreading sequence. If the length of the sequence is N, then the number of phase shifts between adjacent sequences is simply,

$$(N + 1)/L = \lambda, \quad L < N + 1$$

$$N = 2^n - 1, \quad N > 0 \text{ (N is an integer)}$$

Although, one of the L code epochs will contain at least one less chip than the rest because $N = 2^n - 1$. The linear sum of the L equally spaced code phases, P(t), is multiplied by the received spread signal, s'(t). Subsequently, the correlator signal formed by P(t) can be shifted in phase, chip by chip, until correlation is achieved. The advantage over classical sliding correlators is that the maximum number of chips that must be searched to achieve correlation is only (Rawlins 1987),

$$(N + 1)/L = \lambda, \; L < N + 1$$

This assumes that the probability of detecting correlation is equal to one. If the spreading sequence is properly selected, then all ancillary phases of the local correlator signal will have low cross-correlation coefficients with respect to s'(t). Only one phase of P(t) will produce a high correlation value. Once that correlation is recognized, all subordinate phases of the locally generated correlation signal are terminated leaving only the correlated portion of P(t). Gold codes are well suited to construct P(t). For example, Figure 2.2-1 on the next page, illustrates how P(t) is formed in a system using L equally spaced shifts of a Gold code, G(t). Let n denote the generator order, and $G_1(t)$, $G_2(t)$, ..., $G_L(t)$ denote the successive phases of G(t). Because of acquisition algorithm properties, it is useful to further constrain L by,

$$L = 2^k, \; k < N$$

where k is an integer. This restriction is not required but can simplify hardware and software design.

Consider a system design with L = 8. If a Gold code with n = 10 is employed for the spreading code, the uniform phase distance between $G_1(t)$, $G_2(t)$, ..., $G_L(t)$ is

$$\lambda = (N + 1)/L = 2^n/L = 2^{10}/8 = 128$$

Of course, one of the $G_L(t)$ codes will have a spacing of 127.

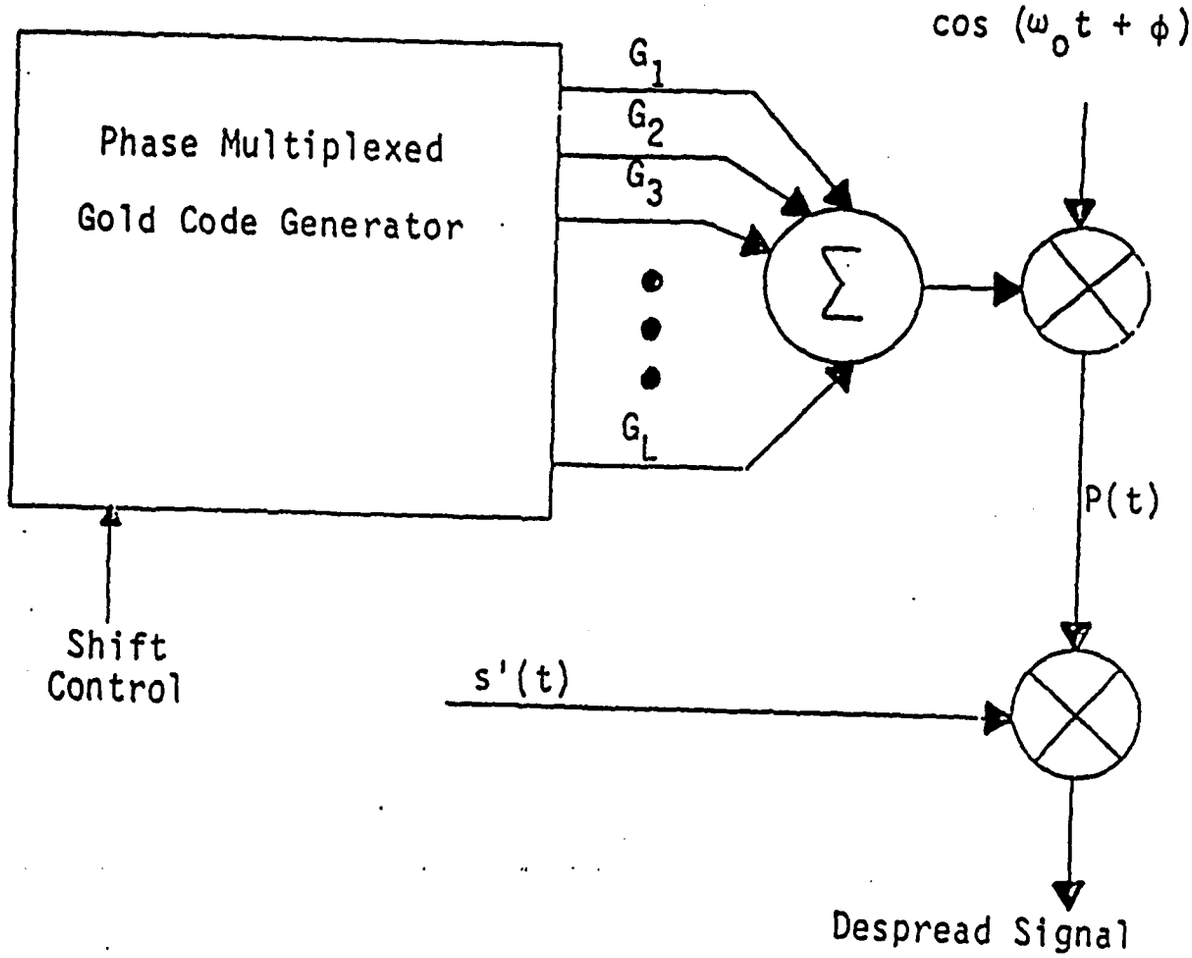

Figure 2.2-1 Phase Multiplexed Correlator, Basic Structure.

There are several straightforward brute force techniques for creating the desired phase shifts. However, these methods are hardware intensive and cumbersome to build. There is a procedure for implementing the PMC signal using a single Gold code generator. Several properties of maximal length PN sequences and Gold code sequences must be examined in order to establish the design method.

2.2.2 PN Code Generator Properties

Two linear maximal length sequences of identical order n can be summed by mod 2 addition to create a Gold code sequence. Selection of an appropriate pair of codes is not arbitrary. Specifically, there are three randomness properties which should be possessed by the Gold code. The balance property states that a sequence of length N possesses the same number of "one" states as "zero" states, plus or minus one. This property is extremely important for systems requiring low probability of intercept (LPI). An unbalance in the sequence creates d.c. offset in the modulating signal, thus causing carrier insertion. Obviously, if a carrier is detected, then an operational scenario could be compromised (Torrierri 1981).

Figure 2.2-2 depicts a typical modulator.

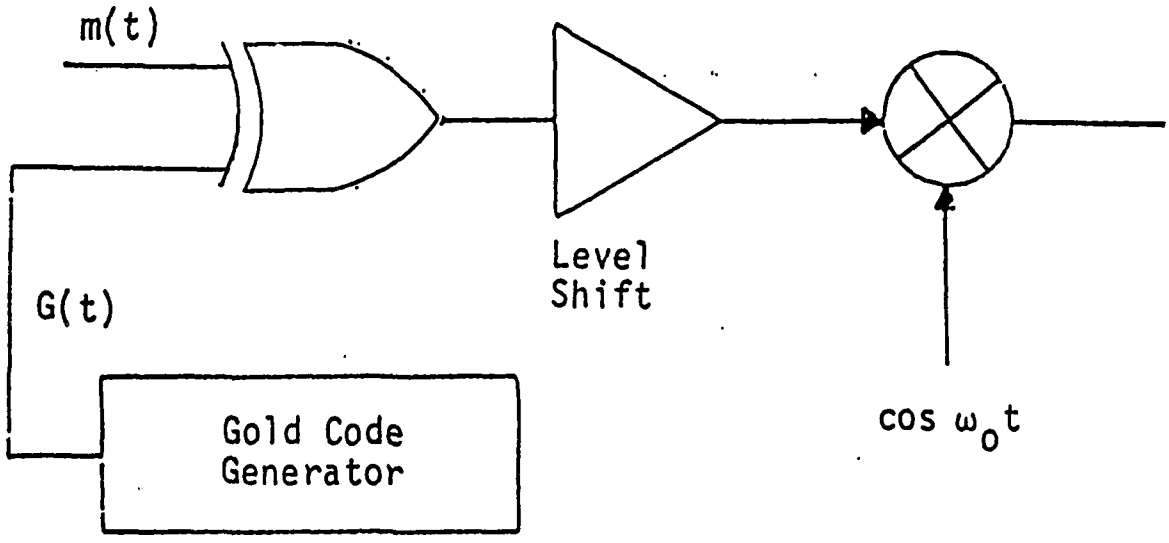

Figure 2.2-2 DSSS Modulator.

Another important randomness property requires that the distribution of chips within the sequence be statistically independent. This further reduces the probability of intercept because the spectral density of such wave forms is more evenly distributed. The final and most important property involves the auto-correlation features of the code. Ideally, the auto-correlation of a sequence should be binary valued. That is, when a sequence is compared to a phase shifted version of itself, the correlation is given by:

Correlation=Total Agreements-Total Disagreements

If the phase shift is "zero," then the correlation value is (N-1), and if the phase shift is between one and N-1, then the correlation value should be zero. However, this is not practical for many useful code types. Maximal length pseudo-noise sequences satisfy the randomness properties better than any other class of sequences (Young 1985). Gold codes are not maximal length pseudo-noise codes, but satisfy the first two randomness properties in a strict sense. Even though Gold codes do not exhibit binary valued auto-correlation functions, the auto-correlation function can be designed to have specific bounds. In fact, the auto-correlation for a non-zero phase shift can be designed to be arbitrarily small (Young 1985). The PMC design exploits this auto-correlation property.

In addition to the randomness properties, three linear addition properties are vital to this development. When two maximal length sequences of different orders, n_1 and n_2, are mod two added, then a sequence of length $(2^{n_1}-1)(2^{n_2}-1)$ will result. Also, when two sequences of the same length N are added (mod two), the result is a non-maximal length sequence of length N. Finally, if a linear maximal length pseudo-noise sequence is mod two added to a phase shifted version of itself, then an identical sequence will be generated with a predictable phase. The shift and add property, along with the auto-correlation properties of Gold codes, are essential to the correlator design (Holmes 1982).

2.2.3 Delayed Sequences

In order to create a desired delay of a sequence using the shift and add property, some mathematical representations of sequences must be developed. There are illustrations of the topologies of maximal length PN sequence and Gold code generators in Figures 2.2-3 and 2.2-4 respectively.

The given representations denote shifts, by the delay variable X^l where l is the number of shifts or the number of delayed chips. Each shift can be performed by a shift register and each mod two addition by an exclusive OR gate. The sequence g(X) in Figure 2.2-3 can be represented by a polynomial in X derived

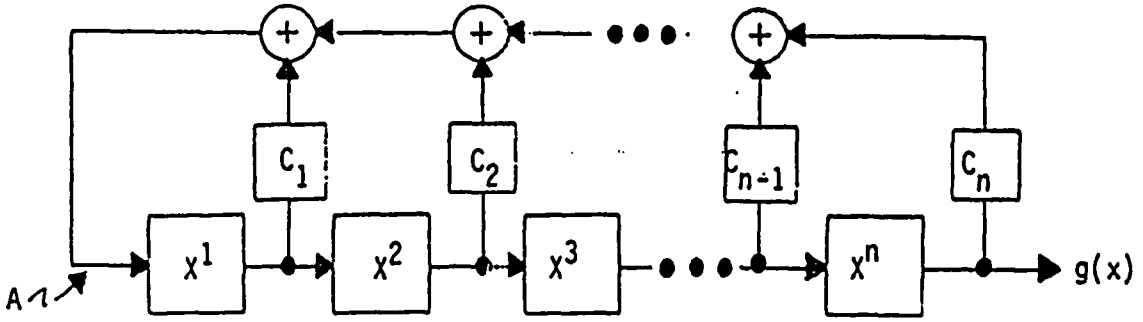

Figure 2.2-3 PN Sequence Generator basic structure.

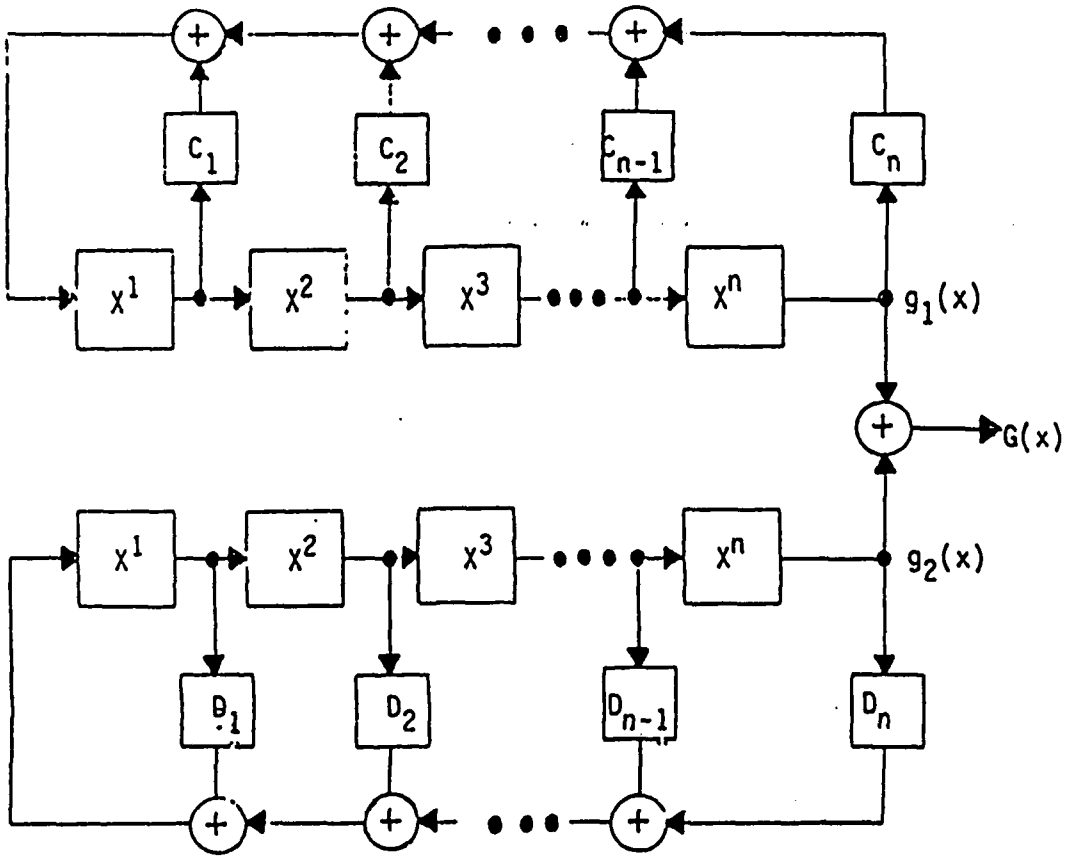

Figure 2.2-4 Gold Code Generator basic structure.

using Polynomial theory. For instance, point A in Figure 2.2-3 can be thought of as X^o. Thus, by inspection,

$$X^o=c_1X^1+c_2X^2+c_3X^3+\ldots+c_nX^n \qquad (2.1)$$

In mod two arithmetic, the following properties apply:

$$-a = +a,\ |a| < \infty$$
$$a + a = 0$$
$$a + 0 = a$$
$$\text{if } a + b = c, \text{ then } a = b + c\ |b|\ ,\ |c| < \infty$$

Thus, equation (2.1) becomes:

$$1+c_1X+c_2X^2+c_3X^3+\ldots+c_nX^n=0, 0\le n<\infty \qquad (2.2)$$

Therefore, the output is given by:

$$g(X)=c_nX^n=1+c_1X+c_2X^2+c_3X^3+\ldots+c_{n-1}X^{n-1} \qquad (2.3)$$

The tap weights C_1, C_2, ..., C_n are either one or zero, denoting a connection or no connection. C_n is always a one for maximal length sequences. Furthermore, maximal length sequences always have an even combination of feedback taps. The feedback taps cannot be chosen arbitrarily. Only specific combinations produce maximal length sequences. Theory for the design of these polynomials is beyond the scope of this report. Appendix A contains a table of maximal length sequences prepared from the work of Peterson (Lane 1983) based on the order n. Also, Holmes (1982) provides a tutorial on the polynomial generating functions of such generators.

In order to delay a given sequence by a desired number of chips, it is necessary to multiply the describing polynomial, g(x), by X^α, where α is the number of phases the sequence must be shifted. For instance, the sequence given by g(x) in eq. (3) may be delayed by the delay variable X by writing:

$$g(X)'=X^{n+\alpha}=X^\alpha+c_1X^{\alpha+1}+c_2X^{\alpha+2}+\ldots+c_{n-1}X^{\alpha+n-1} \qquad (2.4)$$

A corresponding shift register topology is given in Figure 2.2-5.

If α becomes large, the number of memory elements required to implement the topology of Figure 2.2-5 becomes prohibitive. Polynomial theory and mod two arithmetic facilitate the application of the shift and add property to create the necessary delay with a minimal amount of hardware. Any delay X^α may be factored into sub-polynomials that are of degree n or less. This technique allows successive simplification of each polynomial until a final polynomial of order n or less is obtained (Rawlins 1987). To create the delay, an easy hardware scheme may be realized by

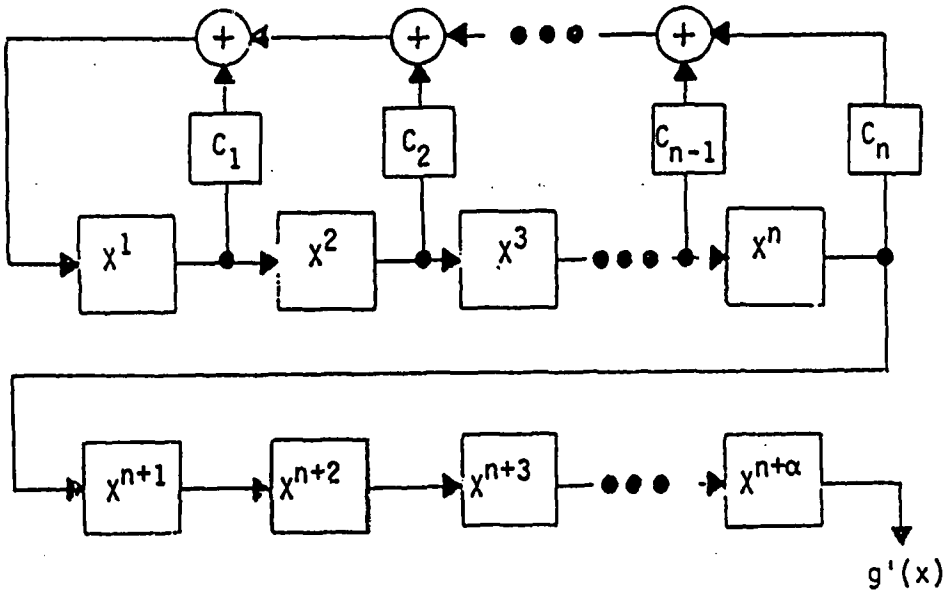

Figure 2.2-5 Generator for a sequence with α delay.

inspecting the reduced polynomial. Recalling equations (2.3) and (2.4) yields.

$$X^{n+\alpha}=X^{\alpha}g(X)=g(X)', \quad 0 \leq \alpha < \infty \tag{2.3}$$

$$X^{n+\alpha}=X^{\alpha}+c_1X^{\alpha+1}+c_2X^{\alpha+2}+\ldots+c_{n-1}X^{\alpha+n-1} \tag{2.6}$$

A method of constructing the polynomial $X^{n+\alpha}$ step by step is now considered. An equivalent representation of $X^{n+\alpha}$ by successively multiplying X^n by X can be obtained after simplification. An example of this process is as follows.

$$X^{n+1}=X+c_1X^2+c_2X^3+\ldots+c_{n-1}X^n$$

$$=X+c_1X^2+c_2X^3+\ldots$$

$$+c_{n-1}[1+c_1X+c_2X^2+\ldots+c_{n-1}X^{n-1}]$$

$$X^{n+2}=X^2+c_1x^3+c_2X^4+\ldots$$

$$+c_{n-1}\{X+c_1X^2+c_2X^3+\ldots+c_{n-1}X^n]$$

$$=X^2+c_1X^3+c_2X^4\ldots$$

$$+c_{n-1}[X+c_1X^2+\ldots c_{n-1}(1+c_1X+c_2X^2+\ldots$$

$$+c_{n-1}X^{n-1})]$$

$$X^{n+3}=X^3+c_1X^4+c_2X^5+\ldots$$

$$+c_{n-1}[X^2+c_1X^3+\ldots$$

$$+c_{n-1}(X+c_1X^2+c_2X^3+\ldots+c_{n-1}X^n)]$$

$$=X^3+c_1X^4+c_2X^5+\ldots$$

$$+c_{n-1}\{X^2+c_1X^3+\ldots c_{n-1}[X+c_1X^2+c_2X^3+$$

$$\ldots+c_{n-1}(1+c_1X+c_2X^2+\ldots+c_{n-1}X^{n-1})]\}$$

$$\vdots \qquad\qquad \vdots$$

$$X^{n+\alpha}= \qquad\qquad g(X)'$$

Each time X^n appears in a polynomial on the right-hand equation side, the relationship in equation (2.3) may be substituted. This will always result in a polynomial of order less than n by reduction. Of course, there are many other possible factors of $X^{\alpha+n}$ and it is not always necessary to reduce the polynomial by X^1. The first several delays can be reduced to form a table of polynomials that are used to synthesize $X^{n+\alpha}$ at a more efficient rate. An iterative example demonstrates the procedure for a generator with the topology in Figure 2.2-6. Hence, g(X) is given by inspection to be:

$$g(X)=X^{10}=X^9+X^8+X^6+X^3+X^2+1 \text{ (mod two)}$$

Likewise, successive delays are computed in Table 2-1. Even though the delay polynomials in Table 2-1 are formed by successive multiplication of X^1, the higher order polynomials can be synthesized by multiplying two lower order polynomials. For example (refer to Table 2-1):

$$X^{27} = X^{10}X^{17}=(X^9+X^8+X^6+X^3+X^2+1)(X^8+X^4)$$

$$=(X^{17}+X^{16}+X^{14}+X^{11}+X^{10}+X^8)$$

$$+(X^{13}+X^{12}+X^{10}+X^7+X^6+X^4)$$

$$= X^{17}+X^{16}+X^{14}+X^{13}+X^{12}+X^{11}+X^8+X^7+X^6+X^4$$

$$= (X^8+X^4)+(X^7+X^3)+(X^5+X)+(X^4+1)$$

$$+(X^9+X^8+X^7+X^5+X^3+X^2+X)$$

$$+(X^8+X^7+X^6+X^4+X^2+X+1)$$

$$+X^8+X^7+X^6+X^4$$

therefore: $X^{27} = X^{10}X^{17} = X^9+X$

Moreover, polynomials of arbitrary order may be created in this fashion. The significance of this method becomes evident in the hardware implementation of the delay. Suppose that the desired delay of the output sequence from the linear maximal length PN generator in Figure 2.2-6 is 16 chips. It is evident from Table 2-1 that:

$$X^{n+\alpha}=X^{10}X^{16}=X^{26}=X^8+1$$

where n = 10 and the delay is 16 chips. Figure 2.2-7 illustrates the application of the shift and add property to effect the 16 chip delay. The reduced polynomial g'(X) consists of mod two sums of delay variables of degree less than n. It follows that the taps required to implement the shift and add property are defined by the exponents of the delay variables of g'(X). Virtually any phase shift may be created using this method.

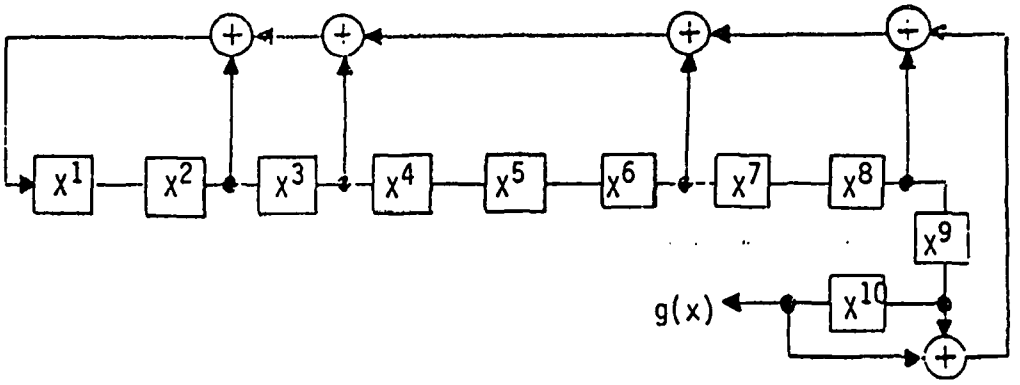

$$g(x) = X^9 + X^8 + X^6 + X^3 + X^2 + 1$$

Figure 2.2-6 Linear Maximal Length Sequence Generator, n+10.

TABLE 2-1

DELAY SYNTHESIS

$$X^{11} = X^{10} + X^9 + X^7 + X^4 + X^3 + X$$

$$= (X^9 + X^8 + X^6 + X^3 + X^2 + 1) + X^9 + X^7 + X^4 + X^3 + X \quad \text{(mod two)}$$

$$= X^8 + X^7 + X^6 + X^4 + X^2 + X + 1$$

$$X^{12} = X^9 + X^8 + X^7 + X^5 + X^3 + X^2 + X$$

$$X^{13} = X^{10} + X^9 + X^8 + X^6 + X^4 + X^3 + X^2 \quad \text{(mod two)}$$

$$= (X^9 + X^8 + X^6 + X^3 + X^2 + 1) + X^9 + X^8 + X^6 + X^4$$

$$= X^4 + 1$$

$$X^{14} = X^5 + X$$

$$X^{15} = X^6 + X^2$$

$$X^{16} = X^7 + X^3$$

$$X^{17} = X^8 + X^4$$

$$X^{18} = X^9 + X^5$$

$$X^{19} = X^{10} + X^6$$

$$= (X^9 + X^8 + X^6 + X^3 + X^2 + 1) + X^6 \quad \text{(mod two)}$$

$$= X^9 + X^8 + X^3 + X^2 + 1$$

TABLE 2-1 ..continued

$$X^{20} = X^{10} + X^9 + X^4 + X^3 + X$$

$$= (X^9 + X^8 + X^6 + X^3 + X^2 + 1) + X^9 + X^4 + X^3 + X \quad \text{(mod two)}$$

$$= X^8 + X^6 + X^4 + X^2 + X + 1$$

$$X^{21} = X^9 + X^7 + X^5 + X^3 + X^2 + X$$

$$X^{22} = X^9 + X^4 + 1$$

$$X^{23} = X^9 + X^8 + X^6 + X^5 + X^3 + X^2 + X + 1$$

$$X^{24} = X^8 + X^7 + X^4 + X + 1 \quad \text{(after being reduced)}$$

$$X^{25} = X^9 + X^8 + X^5$$

$$X^{26} = X^8 + 1$$

$$X^{27} = X^9 + X$$

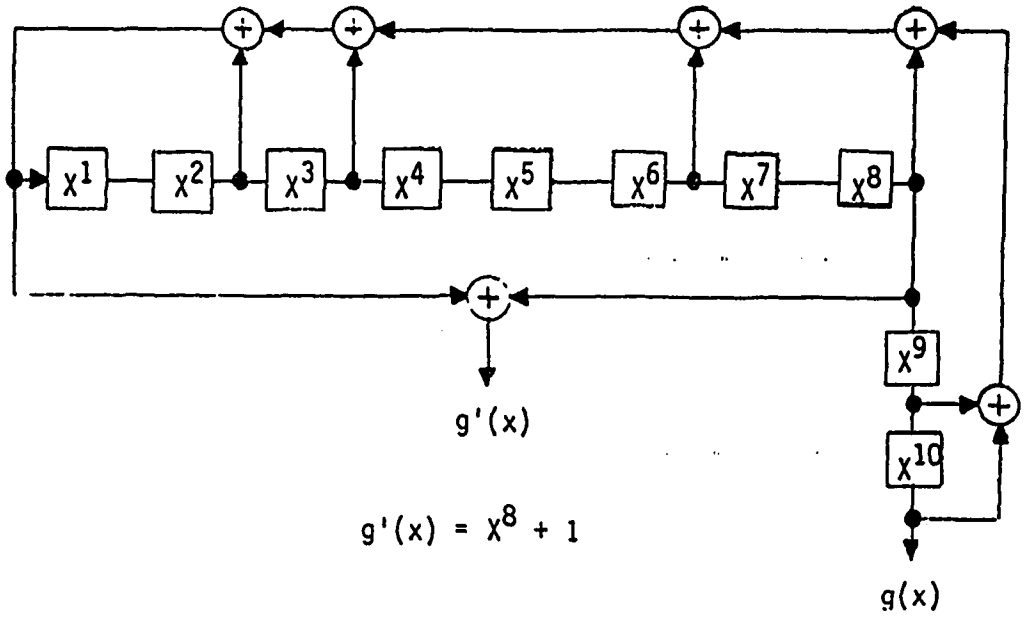

$g'(x) = X^8 + 1$

Figure 2.2-7 Shift and Add Tapped Delay Generator for a 16-chip delay.

2.2.4 Gold Code Generators

Since there exists a method for creating the desired phase shifts of the PN sequences via the shift and add property, the design of the PMC Gold Code Generator of Figure 2.2-1 is straightforward. A Gold Code Generator of order n=10 is given in Figure 2.2-8. Usually, the initial conditions of the registers of one of the sequence generators are altered to produce an entirely unique Gold code. However, delaying the output of one generator with respect to the other generator has the same effect. That is, equations (2.9) and (2.10) define two unique Gold codes, as seen below:

$$g_1(X)+g_2(X)=G(X) \pmod{\text{two}} \qquad (2.9)$$

$$g_1(X)X+g_2(X)=G'(X) \pmod{\text{two}} \qquad (2.10)$$

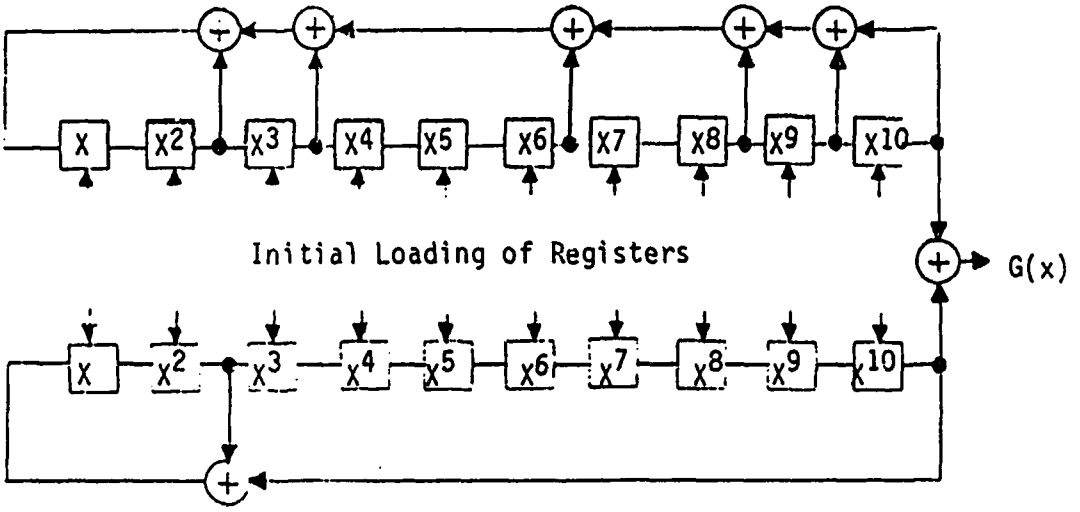

Figure 2.2.8 Gold Code Generator for n=10

Thus, by changing the initial conditions of the registers or the relative phases of $g_1(X)$ and $g_2(X)$, a set of 2^n+1 Gold codes may be generated. Not all members of the family of codes possess the desired randomness characteristics. However, enough codes are useful so that code division multiple access spread spectrum systems are realizable. Such systems rely on the low cross-correlation coefficients of the code families so that multiple codes may occupy the same channel frequency space without interference and information loss (Proakis 1983). Analogously, the low auto-correlation characteristics of phase shifted replicas of the same Gold code can produce nearly the same effect. That is why the structure in Figure 2.2-1 is plausible. Even though the different phases, $G_1(t)$, $G_2(t)$, ..., $G_L(t)$, are actually created from the same Gold code, they may occupy the same channel frequency space because of their low relative auto-correlations. This characteristic is precisely the motivation for labeling the signal structure as phase multiplexed. Work by Gold has established the bounds on the auto-correlation exactly. Table 2-2 shows the value of the auto-correlation of arbitrary phases of the Gold code. For N large, the auto-correlation for any phase, other than zero phase shift, is relatively small.

For instance, if n=10, then the possible auto-correlation values are:

$N=2^{10}-1=1023$ (no phase shift)

$-1 = -1$ (phase shift greater than one chip)

$-(2^6+1)=-65$ (phase shift greater than one chip)

$(2^6-1)=63$ (phase shift greater than one chip)

Hence, for n=10, approximately 6% of the chips will agree at worst case for any integer phase shift other than zero and different than some multiple of N. Such low auto-correlations are a must for a system employing a large number of equally spaced code phases, L (Rawlins 1987).

2.2.5 PMC Correlator Performance Bounds

One is tempted to develop a system with L=N+1. At first glance, this would seem to be a desirable method for minimizing , the maximum number of chips to be searched. L cannot be increased arbitrarily. The bound on L is similar to the bound placed on the number of codes that can occupy a Code Division Multiple Access (CDMA) spread spectrum system. Even though only one of the L phases will ultimately correlate, the other uncorrelated phases provide a background interference that cannot be ignored for large L. As in CDMA systems, the bound on L is related to the processing gain of the spread spectrum system and the channel noise (Proakis 1983). The received signal, s'(t), is given by:

$$s'(t)=Km(t)G(t)\cos(w_0t)+n(t) \qquad (2.11)$$

where m(t) is the transmitted message and G(t) is the spreading sequence. For the PN LADAR case m(t) can arbitrarily assigned a constant value of one. Channel noise is represented by n(t). After the signal passes through the correlator stage shown in Figure 2.2-1, it becomes:

$$P(t)s'(t)=[G_1(t)+G_2(t)+\ldots+G_L(t)][m(t)G(t)\cos(w_o t+\phi)]$$

$$\cos w_o t+[G_1(t)+G_2(t)+\ldots+G_L(t)]n(t)(\cos w_o t+\phi) \qquad (2\ 12)$$

Since P(t) is a linear combination of phase shifted replicas of G(t), it follows that:

$$G_1(t) = G(t+\epsilon)$$

$$G_2(t) = G(t+\epsilon+\tau)$$

$$G_3(t) = G(t+\epsilon+2\tau)$$

$$G_L(t) = G[t+\epsilon+(L-1)\tau]$$

$$\vdots \qquad \vdots$$

$$P(t) = [G(t+\epsilon)+G(t+\epsilon+2\tau)+\ldots+G(t+\epsilon+L)]\cos w_o t \qquad (2.13)$$

The time uncertainty between the transmitter and receiver is absorbed by ϵ. τ represents the planned phase shift between the L locally generated despreading signals. The object of the receiver correlator is to reduce the phase between one of the sequences, $G_1(t)$ through $G_L(t)$, and G(t). After multiplication with a local reference sequence, the signal usually passes through some type of a finite time integrator or averager to complete the correlator. This amounts to matched over multiple chip periods when the local and received coded are in sync. Figure 2.2-9 illustrates the process. If the averaging process takes place over the message bit period, then a decision can be made about whether or not a digital "1" or "0" was sent by observing C(t) (Cooper and McGillem 1986). If the application is radar or ranging oriented, the integration time must correspond to an associated code tracking loop bandwidth to accommodate a robust code sync in the presence of range rate.

In order to understand the despreading process, the power spectral density function of s'(t) should be analyzed. Assume that m(t) is a random binary process. At any point in time, m(t) may possess the value of plus or minus one. G(t) is a psuedo-random sequence of plus and minus ones. Hence, a multiplication of m(t) and G(t) results in a waveform that alternates the phase of G(t) according to m(t). For convenience, it is assumed that the transitions of m(t) are synchronous with the transitions of the spreading waveform, G(t). Also, the rate of the spreading sequence, Rc, is assumed much greater than the message rate, Rb. Figure 2.2-10 depicts how m(t)G(t) is formed step by step. It is emphasized once again that m(t) = 1 for the PN LADAR application.

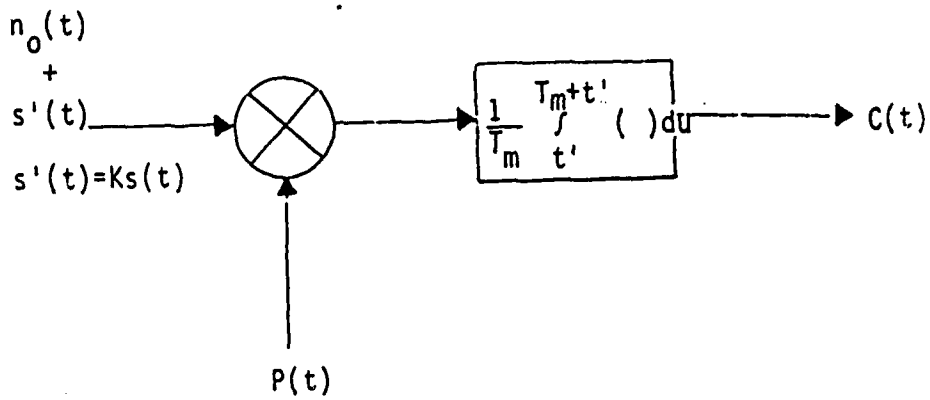

Figure (2.2-9) Receiver Correlator with matched filter.

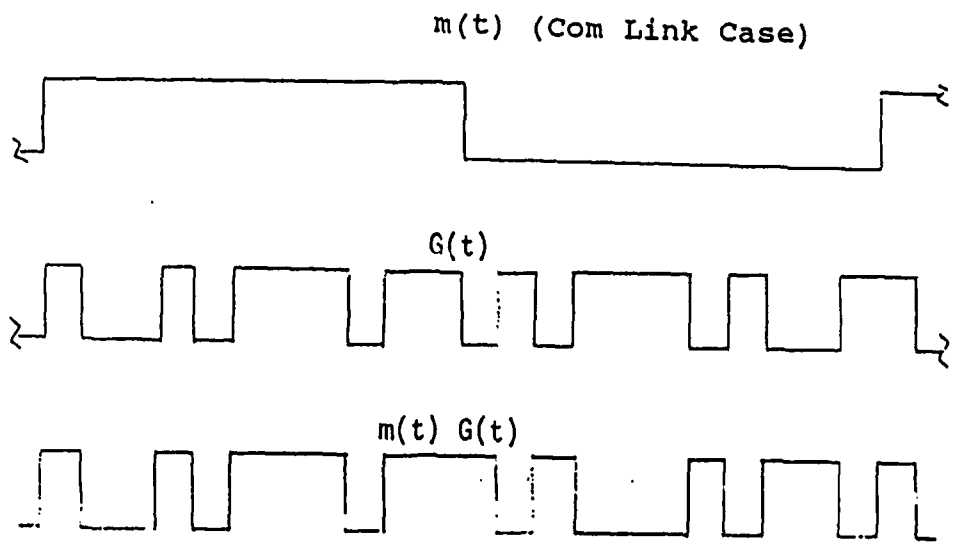

Figure 2.2-10 Synchronous Multiplication of a Message Sequence with a Spreading Sequence.

G(t)m(t) is then translated by a carrier to a frequency of f_o to form S(t). At baseband, the respective power spectral density (psd) functions of m(t) and G(t) are given by (Pickholtz and Schilling 1982):

$$S_M(f) = Tm\ \mathrm{sinc}^2(\pi fTm) \qquad (2.14)$$

$$S_G(f) = [(N+1)/N^2]\ \mathrm{sinc}^2(\pi fTc) \sum_{k=-\infty}^{\infty} \delta[f-(k/NTc)] - (1/N)\ [\delta(f)] \qquad (2.15)$$

$S_G(f)$ or $S_M(f)$ can be developed from the autocorrelation of the basic pulse shapes defining the two respective time waveforms. Therefore, by applying the modulation and linearity properties of the Fourier transform, we obtain the psd of s(t) (Holmes 1982).

$$S_S(f) =$$

$$Tm\ (N+1/2N^2)\ [\mathrm{sinc}^2(\pi[f-f_o])Tc] \sum_{k=-\infty}^{\infty} \mathrm{sinc}^2\ \pi Tm[f-f_o-k/NTc]$$

$$= \mathrm{sinc}^2(\pi[f+f_o])Tc \sum_{k=-\infty}^{\infty} \mathrm{sinc}^2 \pi Tm[f+f_o+k/NTc]$$

$$-(1/2N)[\delta(f+f_o)+\delta(f-f_o)] \qquad (2.16)$$

At the receiver s'(t)=Ks(t) where K is an attenuation constant signifying channel losses. If $G_1(t)$ of the PMC despreading signal is forced to be exactly in phase with G'(t) of s'(t), then m(t) will be recovered. From equations (2.15) and (2.16), it is easy to see that when G(t) is multiplied by itself, then the infinite series of sidebands will be translated back to f_o. Furthermore, if the locally generated replica of G(t) is out of phase, then the correlation output will be greatly reduced. This is apparent if the properties of equation (2.16) are fully understood. All sidebands of the infinite series do not coexist simultaneously. Equation (2.16) defines the spectral bounds of the waveform s(t) over the duration of time. Thus, sidebands will pop up and down at various times. Obviously, the only way to translate a particular sideband back to f_o is to multiply it by an exact replica at the same time that it is present. Therefore, a slight phase shift of less than Tc in the despreading waveform will give degraded correlating performance because the sidebands of equation (2.16) occupy the same signal space as the sidebands of the despreading waveform only a portion of time. Moreover, if a phase shift greater than Tc is experienced, then the sidebands of s'(t) will not often multiply against the proper translation sidebands of the local despreading signal and the correlation will be very low. Of course, Table 2-2 also predicts this phenomenon.

In addition to synchronization of the spreading and despreading functions, the local oscillator should track the incoming carrier. This can be accomplished with a carrier tracking loop. Assuming that this has been accomplished, C(t) can now be calculated.

$$C(t) = 1/Tm \int_{t'}^{Tm+t'} s'(u)P(u)+n(u)P(u)du$$

$$C(t) = 1/Tm \int_{t'}^{Tm+t'} [Km(u)G(u)\ \cos(w_o u+\phi)+n(u)][G(u+\epsilon)+G(u+\epsilon+t)$$

$$+G(u+\epsilon+(L-1)\tau]\ \cos\ w_o u\ du \qquad (2.17)$$

$$\phi \rightarrow 0,\ \epsilon \rightarrow 0$$

TABLE 2-2

CORRELATION COEFFICIENTS FOR GOLD CODES

REGISTER LENGTH	UN-NORMALIZED AUTOCORRELATION	NORMALIZED CROSS-CORRELATION
n = odd	N -1 $-[2^{(n+1)/2}+1]$ $[2^{(n+1)/2}-1]$	$-(1/N)$ $-[2^{(n+1)/2}+1]/N$ $[2^{(n+1/2)}-1]/N$
n = even and not divisible by 4	N -1 $-[2^{(n+2)/2}+1]$ $[2^{(n+2)/2}-1]$	$-(1/N)$ $-[2^{(n+2)/2}+1]/N$ $[2^{(n+2)/2}-1]/N$

SOURCE: Young 1985

The double frequency, $2f_o$, terms are low pass filtered. Therefore:

$$C(t) = (1/2Tm) \int_{t'}^{Tm+t'} Km(u)G(u)G(u)du$$

$$+(1/2Tm) \int_{t'}^{Tm+t'} Km(u)G(u)[G(u+2\tau)+...G(u+(L-1)\tau)]du$$

$$+ (1/Tm) \int_{t'}^{Tm+t'} n(u)[\ G(u)+G(u+\tau)+...G(u+(L-1)\tau)]\cos\ w_o u\ du \qquad (2.18)$$

The integration begins at the start of a message bit and ends precisely at the bit's conclusion or extends over an interval that is inversely proportional to the code tracking loop bandwidth for the PN LADAR application. This nullifies interference from adjacent bits. Equation (2.18) indicates that three separate expressions combine to form C(t). The first term is the average value of the message over one integration interval, since the spreading sequence G(u) is assumed to be in phase with $G_1(u)$ of the local PMC despreading sequence. The average value of term 2 tends toward zero. This is because the spreading sequence and the out of phase portion of the despreading sequence are uncorrelated. Since the PN sequence is balanced and the sample function taken over one bit contains many chips, it is reasonable to assume that the mean value is near zero. Term three contains the additive white gaussian noise from the channel. Hence, it follows that the average of that term will also tend to zero. However, it is the variance of the three terms that provides the most information. Because the variance of C(t) is directly related to the noise power, we can determine the signal to noise ratio. The first term in C(t) contributes to the desired signal energy and the second two terms contribute to the noise energy. Since m(t) consists of a sequence of bits with value ± 1 or a constant value of 1, the energy value of the despread message can be determined from (Cooper and McGillem 1986):

$$C_\alpha(TM) = (K/2Tm) \int_{t'}^{Tm+t'} \pm 1\ du)^2 = K^2/4 \qquad (2.19)$$

Since m(t) assumes a constant value over the message bit or integration interval, the square of the expected value is a good estimate of the power in the bit. The several terms of P(t) that are out of phase with the G(t) portion of s(t) will produce a self noise variance at the receiver output. As previously mentioned, $G_1(t)$ was selected as the local despreading phase of P(t) for purposes of example. Perfect synchronization has been assumed thus far. Because $G_1(t), G_2(t), \ldots G_I(t)$ have an established phase relationship based on an integral number of chip delays, the variance of the self noise of P(t) can be accurately calculated for the correlated case. The correlator implementation of Figure 2.2-9 contains an ideal finite time integrator. The impulse response of that filter is shown in Figure 2.2-11 and is given by:

$$h(t) = (1/Tm) \qquad 0 \leq t \leq Tm$$

$$= 0 \qquad \text{elsewhere}$$

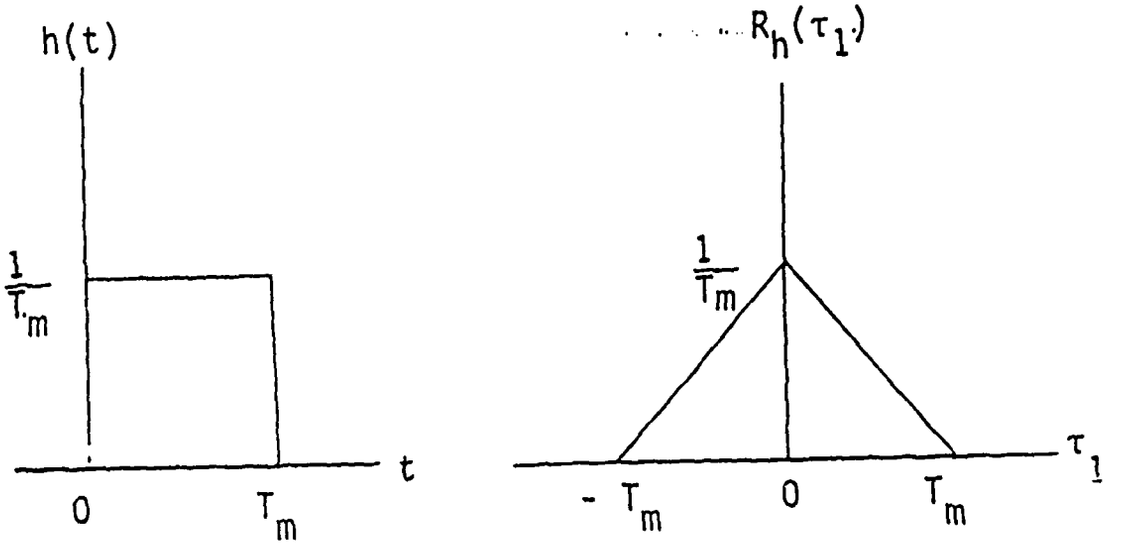

Figure 2.2-11 Impulse Response for an Ideal Finite Time Integrator.

This response is matched to the message bit pulse shape. The mean-square value of the output of a linear system can be obtained from the input autocorrelation function, R_{xx}, and autocorrelation of the system impulse response. Equation (2.20) describes this relationship (Papoulis 1965).

$$\sigma^2 = \int_{-\infty}^{\infty} R_{xx}(\tau_1) R_h(\tau_1) d\tau_1 \qquad (2.20)$$

After applying this result to the case involving a pseudo-random binary process of period Tc passing through the finite time integrator of period Tm, the output becomes:

$$R_{xx}(\tau_1) = A^2[1 - |\tau_1|/Tc], \quad |\tau_1| < Tc; \ 0 \text{ elsewhere}$$

$$R_h(\tau_1) = 1/Tm\ [1 - |\tau_1|/Tm], \quad |\tau_1| < Tm; \ 0 \text{ elsewhere} \qquad (2.21)$$

$$\sigma^2 = 2 \int_0^{Tc} (A^2/Tm)[1 - \tau_1/Tc][1 - \tau_1/Tm]\, d\tau_1, \quad Tc << Tm$$

$$\sigma^2 = A^2[Tc/Tm - Tc^2/3Tm^2] = A^2[1/PG - 1/3PG^2] \qquad (2.22)$$

A is an arbitrary constant that may be set to K/2 for this case. The ratios given in equation (2.22) illustrate that the self-noise or variance due to the chipping sequence can be made arbitrarily small by increasing the chipping rate, Rc, with respect to the message bit rate, Rm, or inverse integration time constant. Rc/Rm is known as the processing gain, PG, and is considered a figure of merit for DSSS systems. Careful examination of term #2 in equation (2.18) reveals that equation (2.22) applies. Since term #2 of equation (2.18) represents the uncorrelated portions of the despreading process, it may be treated as a sum of PN sequences. Of course, since it is assumed that one of the locally generated phases of the correlation signal is in sync with the incoming waveform, Km(t)G(t), it is certain that the chip period, Tc, is conserved. This will always result in the worst case self-noise variance. When synchronization is slightly skewed, then the apparent chipping period is smaller than Tc. Considering the multiplications of equation (2.18), this would reduce the variance indicated by equation (2.22). Therefore, at synchronization the total

self-noise variance due to the multiplied uncorrelated phases of $Km(t)G(t)G_L(t)$ is found to be (by equations 2.18 and 2.22):

$$\sigma_t^2 = (K^2/4)\ (Tc/Tm - Tc^2/3Tm^2)\ (L-1) \qquad (2.23)$$

Term #3 of equation (2.18) represents the additive white Gaussian (AWG) noise multiplied by the local correlation signal and averaged by the integrator. Again, equation (2.20) may be applied. The autocorrelation function is formed from the multiplication of the AWG noise at the receiver input. $N_o/2$ is the double-sided power spectral density of the AWG noise.

$$R_n(\tau_1) = N_o/2\ \delta(\tau_1) \qquad (2.24)$$

$$R_c(\tau_1) = [1 - |\tau_1|/Tc], \quad 0 \le |\tau_1| \le Tc$$

$$R_c(\tau_1) = 0, \quad |\tau_1| \ge Tc \qquad (2.25)$$

Equations (2.24) and (2.25) represent the autocorrelation functions of AWG noise and one phase of the local PN despreading sequence, respectively. After passing through the integrator, the output becomes:

$$\sigma_n^2 = (L/Tm) \int_{-Tc}^{Tc} (N_o/2\ \sigma(\tau_1)[1-|\tau_1|/Tc])[1-|\tau_1|/Tm]d\tau_1$$

$$\sigma_n^2 = (N_oL/2Tm) \int_{-Tc}^{Tc} \sigma(\tau_1)d\tau_1 = N_oL/2Tm \qquad (2.26)$$

Thus, equations (2.19), (2.23) and (2.26) calculate the signal energy and noise variance due to processing by the local correlator and integrator described by equation (2.18). Furthermore, to calculate the signal-to-noise ratio (SNR), equations (2.14), (2.23) and (2.26) are combined to obtain (Rawlins 1987):

$$SNR_o = \frac{K^2}{K^2\ [Tc/Tm - Tc^2/3Tm^2]\ (L-1) + 2N_oL/Tm} \qquad (2.27)$$

This expression describes the SNR for C(t) when ideal synchronization is assumed. Even if the code self-noise due to the ancillary phases of $G_L(t)$ becomes significant, the effect of this noise may be removed once synchronization is verified. The way that this can be accomplished is by simply turning the extra phases off. Having already accomplished their purpose, they are no longer necessary, once synchronization is achieved. The extra phases of $G_L(t)$ simply reduce the number of chips that must be searched in order to obtain synchronization. Of course, in cases where SNR_O is marginal, signal detection can deteriorate by using a complex correlation signal such as $G_L(t)$. In such cases, a receiver should adaptively reduce the number of available phases as required. After the extra phases of $G_L(t)$ are removed, the output SNR becomes (Cooper and McGillem 1986):

$$SNR_O'=(2S_rTm)/N_O \qquad (2.28)$$

where:

$$\text{received signal power} = K^2/4=S_r$$

For a given N_O, Tm and S_r, a suitable threshold may be optimally selected for demodulation of the message bits.

As suggested previously, to make the acquisition algorithm more convenient, and to enhance a digital implementation, convenient, and to enhance a digital implementation, the restriction of L by:

$$L=2^k, \quad k<N$$

might prove advantageous, although not required. For instance, it is assumed that the uncorrelated phases of $G_L(t)$ will be turned off once correlation is detected. However, we cannot know a priori which particular phase of the local correlator signal is providing synchronization. Therefore, it is necessary to obtain that information in order that the ancillary phases be removed discriminantly. The procedure is illustrated in Figure 2.2-12. It is easy to verify that k searches through the algorithm are required to identify the proper phase and to eliminate all uncorrelated phases.

During the search, it is possible that the proper phase is turned off, thus losing receiver synchronization. If the entire decision process is short-lived, with respect to resident clock instabilities, then this will not be a hindrance. That is, the proper phase will soon be reinstated and the receiver could still be considered in synch through the process. There are scenarios, though, where both the transmit and receive platforms will experience extreme dynamics and relative concomitant clock instabilities. An example might be a com link between a satellite and aircraft or illuminated tracking of a fast target. In such cases, a redundant local correlator should be employed to test the hypotheses of the search algorithm.

Equations (2.27) and (2.28) can be used to determine the pre-detection signal to noise ratio, SNR_D. SNR_D is an important performance spec for acquisition. The SNR_D is determined from equations (2.27) and (2.28), based on the minimum desired correlation sensitivity.

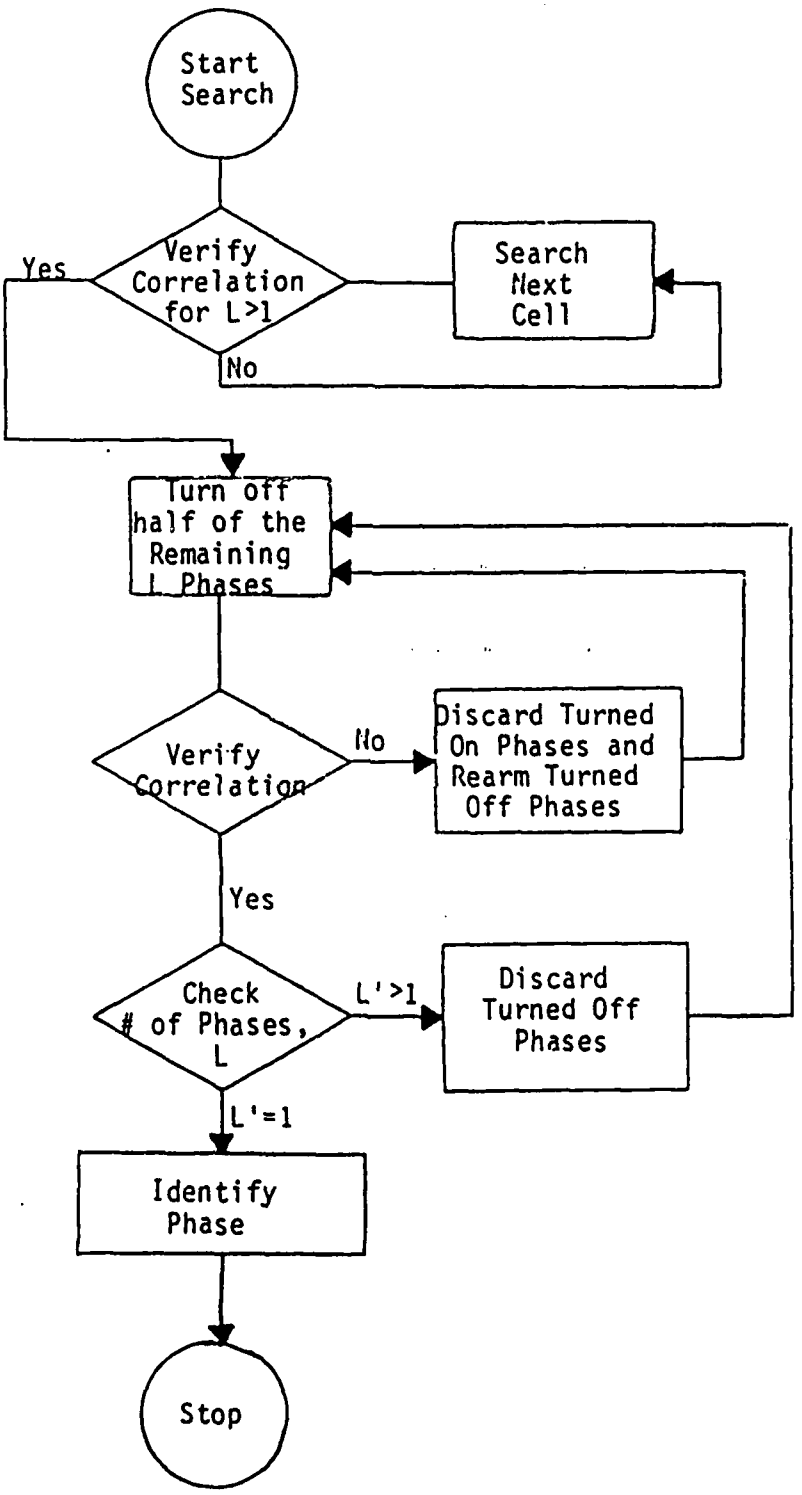

Figure 2.2-12 Identification of the correlated phase.

Since the transmitter and receiver clocks are independent, there may be very small overlap of the received and PMC sequences for some cells. In addition, some acquisition loops may step in one-eighth or one-tenth chip steps. Therefore, it is likely that SNR_D be as low a 0 dB or even lower. The lower SNR_D becomes, the longer it takes for acquisition. Thus, when SNR_D is specified, usually a specific acquisition time is implied (Simon 1985).

The PMC slides in half chip steps. Since the autocorrelation function of the PMC has significant values over a $\pm T_c$ range around the center, there are multiple cells that may produce noticeable correlation peaks. This means that a cell with moderate correlation will likely be adjacent to a cell with high correlation. Hence, rather than design for the low to moderate correlation case it is expedient to design for the high correlation case and degrade SNR_D by the PMC characteristics. On the average, the PMC implementation will suffer a penalty of one cell in terms of correlator sensitivity, as compared to the conventional sliding correlator. This is of little consequence because the PMC will significantly reduce the average total number of cells searched.

Once the link budget has been allocated for a specific BER performance, SNR_o' may be established in equation (2.28). Equation (2.28) can be solved in terms of N_o to obtain:

$$N_o = 2\ K^2\ Tm/\ 4\ SNR_o' \qquad (2.29)$$

Equation (2.29) is then substituted into equation (2.27) and solved for L, based on the partial correlation case of 0.75. When maximum correlation is desired, 0.75 is the worst case correlation for the half chip update scheme. This amounts to a .25 dB loss in signal power out of the correlator. For this partial correlation case, the noise variance from the multiplication of the PMC signal and the AWG channel noise is unchanged. The noise variance due to the ancillary code phases will be slightly reduced, yet equation (2.23) can be used as an upper bound. Therefore, substituting equation (2.29) into equation (2.27) and reducing the signal power by 0.75^2, the result is:

$$SNR_D = \frac{(K^2/4)\ (3/4)^2}{K^2/4\ [1/PG - 1/3PG^2]\ (L-1) + K^2L/SNR_o} \qquad (2.30)$$

$$SNR_D = \frac{(3/4)^2}{[1/PG - 1/3PG^2]\ (L-1) + 4L/SNR_o']}$$

Solving for L yields

$$L = \frac{(3/4)^2 + SNR_D/PG - SNR_D/3PG^2}{SNR_D\,[1/PG - 1/3PG^2 + 4/SNR_o']}$$

$$L = \frac{(3/4)^2\,(PG)SNR_o' + SNR_o'SNR_D}{4\,SNR_D(PG) + SNR_o'} \qquad (2.31)$$

For a given SNR_o' based on BER and link margin and for a desired SNR_D, L may be obtained. From equation (2.31), it is apparent that as SNR_o' is allowed to increase, L likewise may increase. In addition, lowering SNR_D allows L to increase. Unfortunately, for most practical values of SNR_o', increasing the processing gain does not increase L significantly. Nevertheless, certain scenarios may allow L to be large. Thus, equation (2.31) should be studied in each circumstance to determine the optimum trade offs.

Rawlins (1987) discussed a method for reducing the noise effect of using a complex signal with L phases of the correlating sequence for the PMC. The method requires a prebias of the sequential detection algorithm used in coarse acquisition of the received spread sequence. The prebias should consist of a term proportional to:

$$\text{prebias} \sim (K^2/4)[1/PG - 1/3PG^2]\,(L-1)$$

from the denominator term of 2.30. If this energy is detected and subtracted from the received signal during the sequential detection test, then the sensitivity in the detection process is greatly enhanced.

It is considered that a locally generated redundant PMC consisting of PN codes orthogonal to the primary PMC for the receiver could provide the reference channel for deriving an approximate prebias. Figure 2.2-13α illustrates the concept. It is expected that an improvement in acquisition on the order of

$$\text{Acquisition improvement} \approx 10\,\log_{10}(L-1)$$

can be attained using the prebias concept (Rawlins 1987).

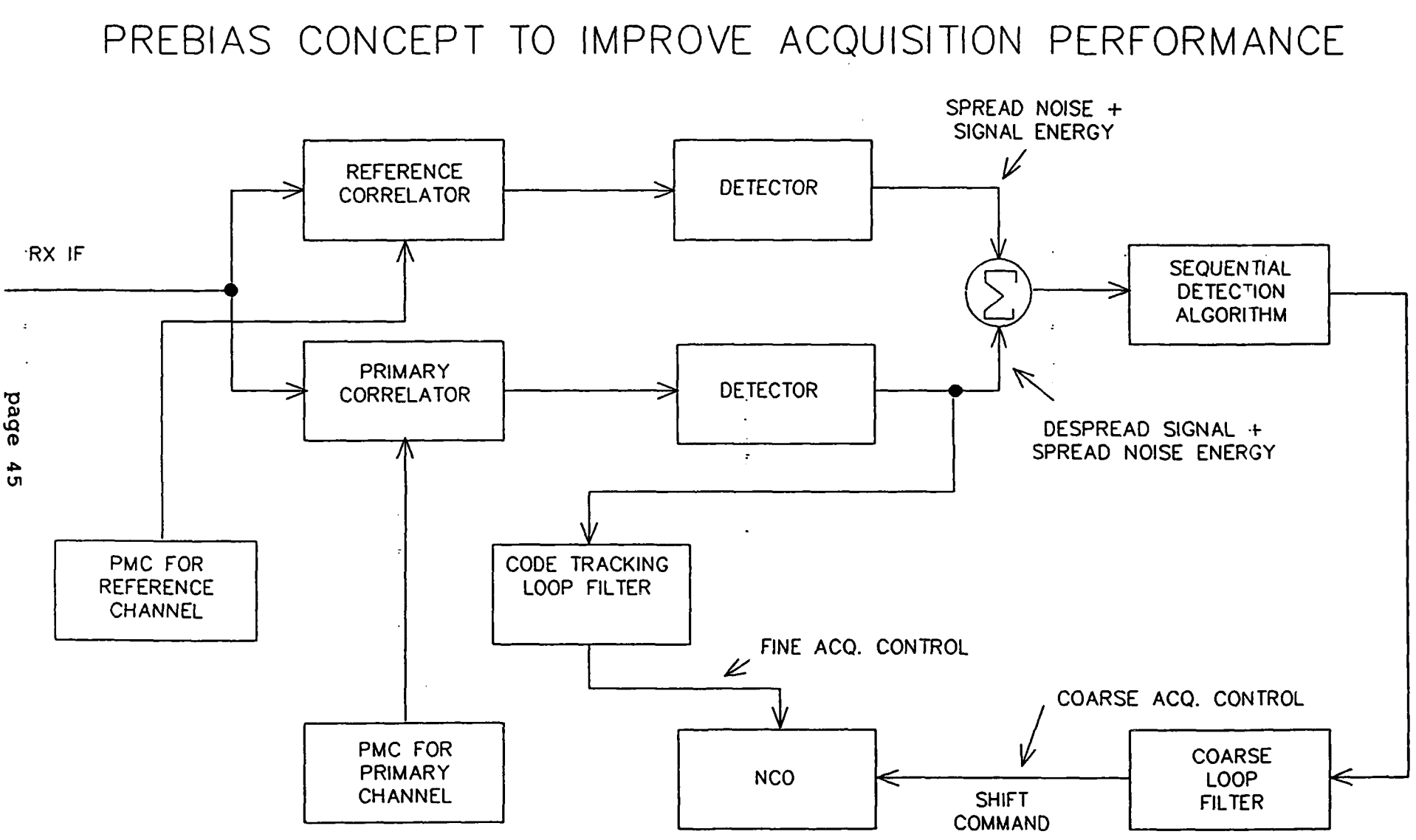

2.2-13q Prebias Concept to Improve Acquisition Performance

2.2.6 Partial Autocorrelation and Cross-correlation Variance

At this point, a note of caution should be sounded. Throughout the entire development, perfectly orthogonal codes have been assumed. In reality, partial correlation of the codes does exist. This finite cross-correlation is usually combatted by increasing the code length or detection filter memory. Nevertheless, this finite amount of code cross-correlation manifests itself as a noise variance and can degrade synchronization performance for large L.

Holmes has shown that for a linear maximal length PN sequence the variance of the partial correlation over W out of N total chips is given by (Holmes 1982):

$$\mathrm{var}[R^W(k)] = (1/W)\ (1 + 1/N)\ (1 - W/N),\ k \neq 0 \qquad (2.32)$$

For W = N, the variance tends toward zero as is expected. However, if the averaging cycle is significantly less than N chips, appreciable variance is introduced. Table 2-3 shows the results of work by Gold. The frequency of the various correlation values is shown in the last column.

Table 2-4 shows some maximum cross-correlation values for Gold code sequences of degree 5 to 21. Partial autocorrelations of Gold codes have the same normalized values as those given in Table 2-3, but at different frequency. Particular phase shifts of the same Gold code may have very different partial autocorrelations (Holmes 1982).

Because of the number of design considerations, it is probably better to simulate a potential code set and analyze the various trade offs. In that manner, a code can be custom tailored to the specific scenario. Young has developed three programs that are capable of an in-depth simulation (Young 1985). His polynomial sequence generator program can synthesize and derive all phases of linear maximal length PN sequences and Gold codes. In addition, the support program calculates autocorrelations, cross-correlations, as well as frequencies of occurrence. After the necessary partial autocorrelations are found by simulation, the variance may be calculated. If the variances are significant, then equation (2.23) is modified to (Rawlins 1987):

$$\sigma_t^{2\prime} = (K^2/4)[Tc/Tm - Tc^2/3Tm^2]\ (L-1) + \mathrm{var}[Rp] \qquad (2.33)$$

where:

$\mathrm{var}[R_p]$ =variance of the partial autocorrelations of the PMC signal with received signal.

TABLE 2-3

CORRELATION FREQUENCY OF GOLD CODES

n = REGISTER LENGTH	CODE LENGTH	NORMALIZED CROSS-CORRELATION COEFFICIENT	FREQUENCY OF OCCURRENCE
n odd	$N = 2^n - 1$	$-1/N$	$\simeq .5$
		$-(2^{(n+1)2} + 1)/N$	$\simeq .25$
		$-(2^{(n+1)/2} - 1)/N$	$\simeq .25$
n even and not divisible by 4	$N - 2^n - 1$	$-1/N$	$\simeq .75$
		$-(2^{(n+2)/2} + 1)/N$	$\simeq .125$
		$-(2^{(n+2)/2} - 1)/N$	$\simeq .125$

TABLE 2-4

MAXIMUM NORMALIZED CROSS-CORRELATION VALUES
FOR GOLD CODE SEQUENCE DEGREES FROM 5 TO 21

DEGREE n	SEQUENCE LENGTH	MAXIMUM NORMALIZED CROSS-CORRELATION
5	31	9/31 = .2903
6	63	17/63 = .2698
7	127	17/127 = .1339
9	511	33/511 = .0646
10	1023	65/1023 = .0635
11	2047	65/2047 = .0318
13	8191	129/8191 = .0157
14	16383	257/16383 = .0157
15	32767	257/32767 = .0078
17	131071	513/131071 = .0039
18	262143	1025/262143 = .0039
19	524287	1025/524287 = .0020
21	2097151	2049/2097151 = .0010

SOURCE: Young 1985

Therefore, SNR_D' becomes:

$$SNR_D' = \frac{K^2/4\ (3/4)^2}{K^2/4\ [Tc/Tm - Tc^2/3Tm^2]\ (L-1) + var[R_p] + K^2L/SNR_o'} \qquad (2.34)$$

The task of the designer should be to reduce the middle variance term in the denominator. This would then allow the results of equation (2.30) to be approached. In general, the additional variance will be a function of L, the number of PMC phases. If the statistics of equation (2.33) are considered over a large number of chip periods, then the effects of var $[R_p]$ will be reduced (Holmes 1982).

As a result of the previous discussions, several fundamental design concepts should be applied. These are listed as follows:

1. L should be the minimum required for a specified T_{aq}. (acquisition time)
2. As large a processing gain, PG, as possible should be used.
3. The narrowest possible pre-detection filters should be used, preferably matched filters to the message symbols.
4. Use as long as codes as possible for spreading and despreading.
5. The prebias concept via a reference channel correlator should be used.

Item one reduces unwanted variance terms produced by the PMC operation. Item two reduces the significance of additional PMC variance. Item three reduces the effects of AWGN from the receiver as well as PMC produced variances. Number four serves to maximize orthogonality or statistical independence of the sequences and therefore reduce long term false correlations. Number five could potentially reduce or eliminate all ancillary noise from the (L-1) unused/uncorrelated phases of the PMC generator.

2.2.7 Codes for Phase I Experiment

The basic building blocks for the sequences used in the Phase I transmitter and receiver are two maximal length PN sequences described by the generating polynomials, $X^{10}+X^3+1$ and $X^{10}+X^9+X^8+X^6+X^3+X^2+1$. These two sequences are mod two added to produce the Gold code used in the experiment. The basic experiment uses the Gold code at the transmitter to build the ranging waveform by modulating the optical carrier. Optimally, the modulation technique would be phase modulation (double sideband suppressed carrier). The receiver correlator waveform or PMC design employs a linear sum of time shifted versions of the Gold code. Figures 2.2-13band 2.2-14 show the Phase I hardware implementation block diagram of how the time shifted versions of the primitive polynomials are produced via the techniques of section 2.2.3. Tables 2-5 and 2-6 show the mod two arithmetic involved for implementing the delay functions. Figures 2.2-15 and 2.2-16 indicate the sequence of ones and zeros produced by the Proms used in the Phase I hardware implementation of the primitive maximal length generators.

TABLE 2-5

CODE DELAYS FOR L = 8, n = 10, AND
$g(X) = X^9+X^8+X^6+X^3+X^2+1$

$g(x) = g_1(X) = X^9 + X^8 + X^6 + X^3 + X^2 + 1,$	0 chip delay
$g_2(x) = g_1(X)\ X^{128} = X^9 + X^4 + X^2,$	128 chip delay
$g_3(x) = g_1(X)\ X^{256} = X^8 + X^7,$	256 chip delay
$g_4(x) = g_1(X)\ X^{384} = X^{10} + X^5 + X^3 + X^2,$	384 chip delay
$g_5(x) = g_1(X)\ X^{512} = X^6 + X^4,$	512 chip delay
$g_6(x) = g_1(X)\ X^{640} = X^9 + X^5 + X^3,$	640 chip delay
$g_7(x) = g_1(X)\ X^{768} = X^4 + X^3 + X^2 + X,$	768 chip delay
$g_8(x) = g_1(X)\ X^{896} = X^{10} + X^9 + X^8 + X^7 + X,$	896 chip delay

TABLE 2-6

Code delay for L=8, n=10

$g(X) = X^{10} + X^3 + 1$

PHASE I HARDWARE IMPLEMENTATION

$g_1 = X^{10} + X^3 + 1$	0 chip delay
$g_2 = X^9 + X^8 + X^5 + X^4 + X^3 + X + 1$	128 chip delay
$g_3 = X^{10} + X^8 + X^6 + X^5 + X^2 + 1$	256 chip delay
$g_4 = X^{10} + X^9 + X^7 + X^6 + X^4 + X^3$	384 chip delay
$g_5 = X^9 + X^7 + X^4$	512 chip delay
$g_6 = X^{10} + X^6 + X^3 + X^2$	640 chip delay
$g_7 = X^{10} + X^9 + X^6 + X^4 + X$	768 chip delay
$g_8 = X^{10} + X^9 + X^5 + X^2 + X$	896 chip delay

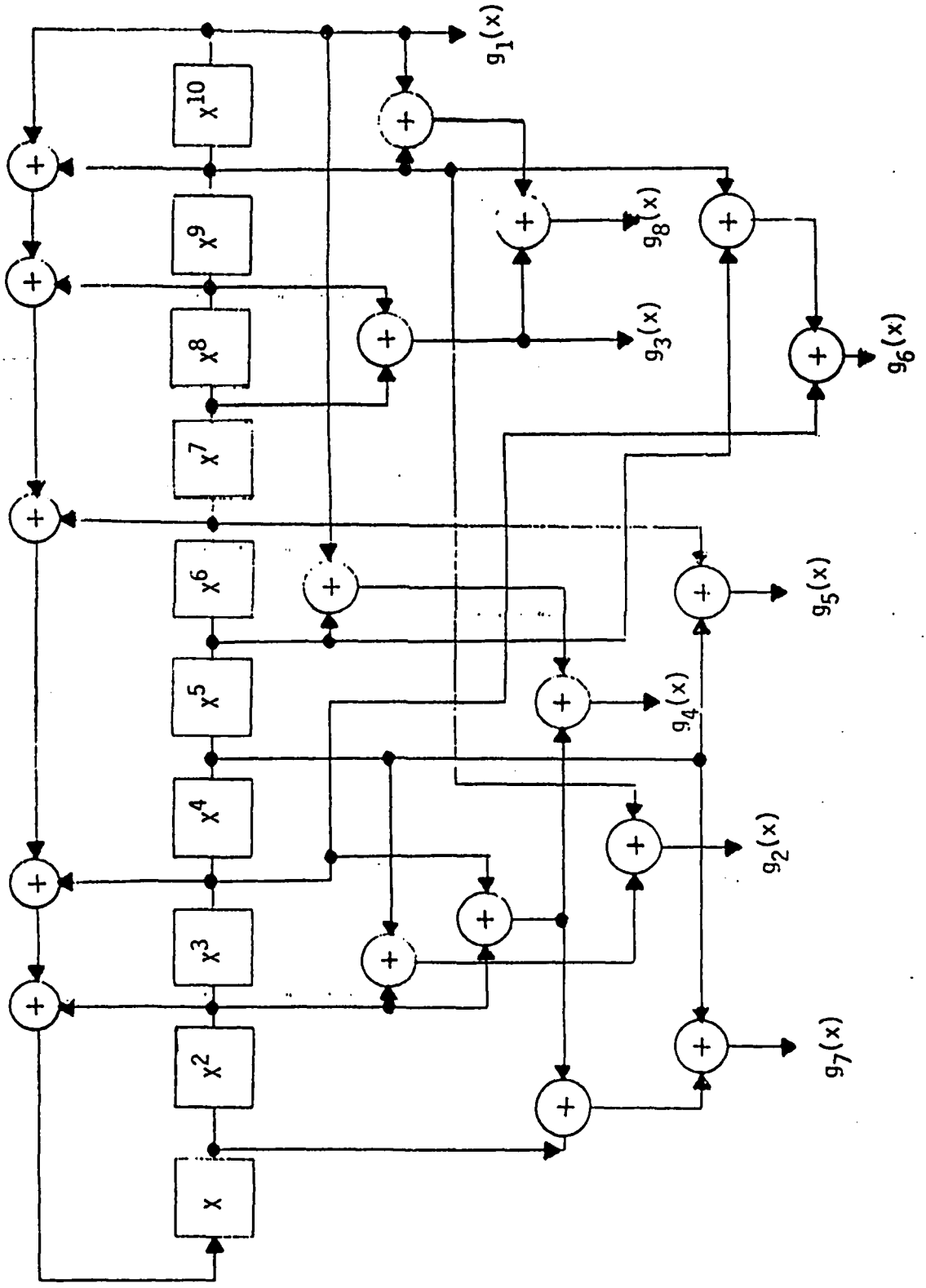

Figure 2.2-13b PMC sequence generator for L = 8
$g(X)=X^9+X^8+X^6+X^3+X^2+1$

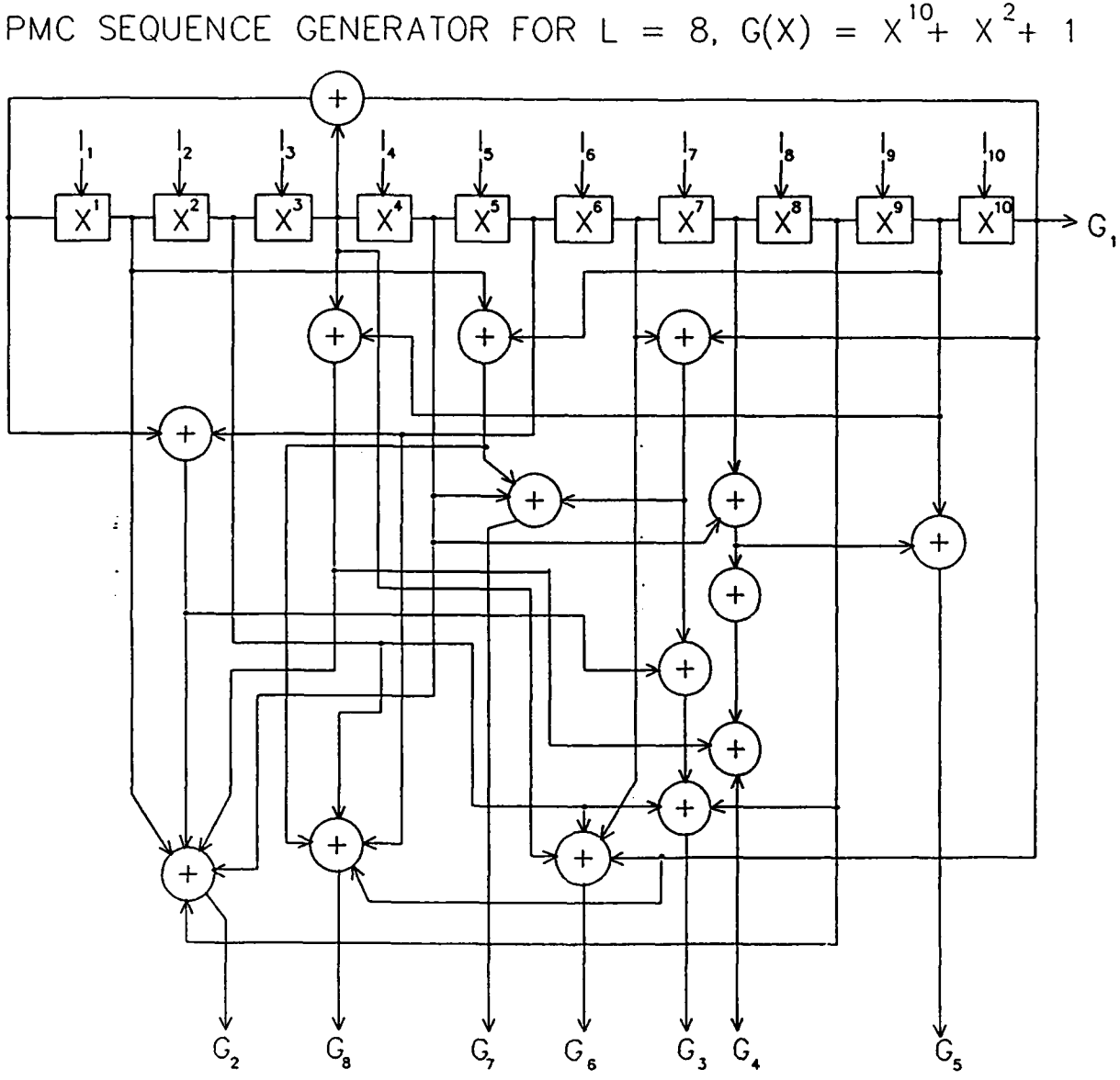

Polynomial Delay Generator for $g(X) = X^{10}+X^3+1$
Figure 2.2-14

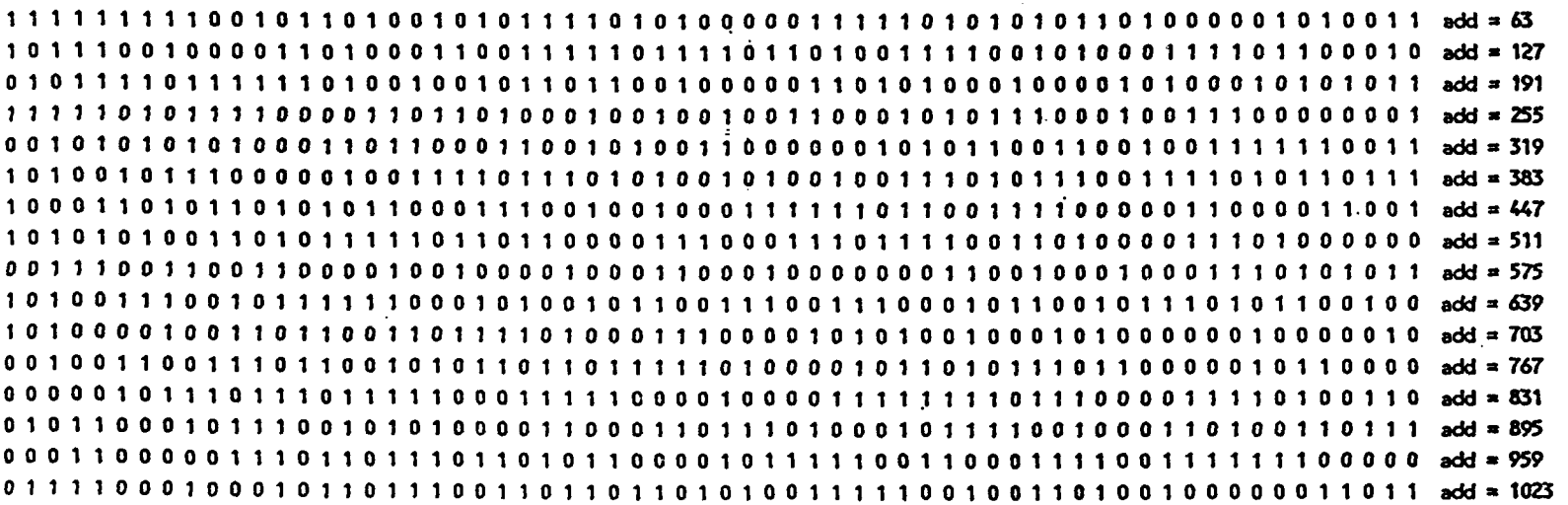

Figure 2.2-15 Sequence generated by
$X^{10}+X^9+X^8+X^6+X^3+X^2+1$

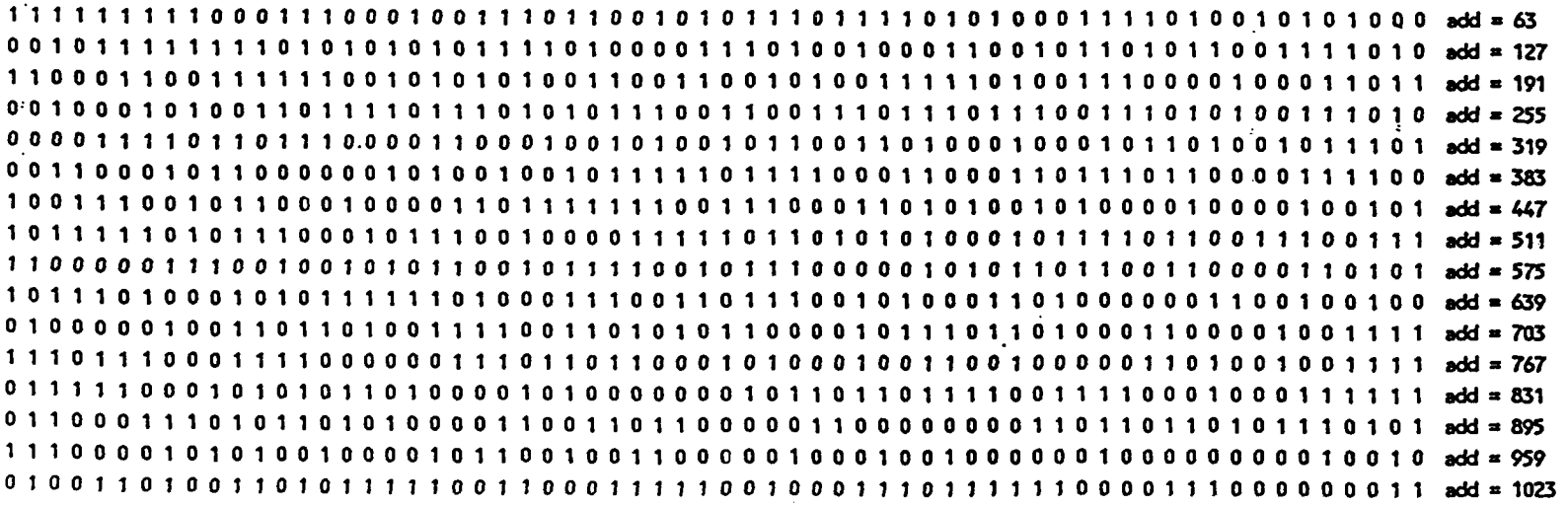

Figure 2.2-16 Sequence generated by $X^{10}+X^3+1$

2.3 ACQUISITION

2.3.1 Course Acquisition

For DSSS systems, numerous synchronization approaches are possible. Some strategies use redundant hardware to conduct parallel searches through the uncertainty region, yet most techniques fall into the class of serial search methods. The method proposed here appears to be serial from the hardware point of view, yet possesses some advantages of the parallel approach.

All systems must search through the region of uncertainty for the appropriate alignment of the transmitted and received PN sequences. This uncertainty region is divided up in cells that are usually some multiple of N, the sequence length (Simon 1985). The task of the acquisition loop in the receiver is to conduct the search and verify synchronization. Naturally, the most efficient search of this uncertainty region is desired and usually this efficiency is measured by the mean time to acquire synchronization, T_{aq}, for a particular predetection SNR_D. Historically, many sub-optimal solutions have been successfully implemented. Single and double dwell integration are the most often used sub-optimal approaches for serial searching. Abraham Wald pioneered an optimal solution in the 1940s while conducting radar research. The algorithm he developed is called the sequential detection algorithm and is useful for a wide class of problems where two hypotheses must be tested against one another (Holmes 1982). In the case of DSSS, the hypothesis of a correlated detected signal in the presence of noise must be tested against the hypothesis of an uncorrelated signal plus noise. The proposed phase multiplexed correlator (PMC) enhances the performance of the sequential detection algorithm by reducing the region of uncertainty. Although the PMC may be employed with other sub-optimal approaches, in this study, only a modified hardware implementation of the sequential detection algorithm has been considered for a coarse acquisition loop.

Figure 2.3-14 shows a state diagram for a serial search through all possible chips of a received PN sequence using a PMC with half chip steps. Thus, there are 2(N+1)/L cells to be searched. At the end of each cell, a decision is made based on the two hypotheses:

$$H_1 = \text{correlated}$$

$$H_o = \text{uncorrelated}$$

In the figure, each chip/multichip is represented by a circle and each semicircle represents the beginning of a new cell to be searched. The state variables, x and z, with their exponents are similar to those developed in the PN code delay synthesis

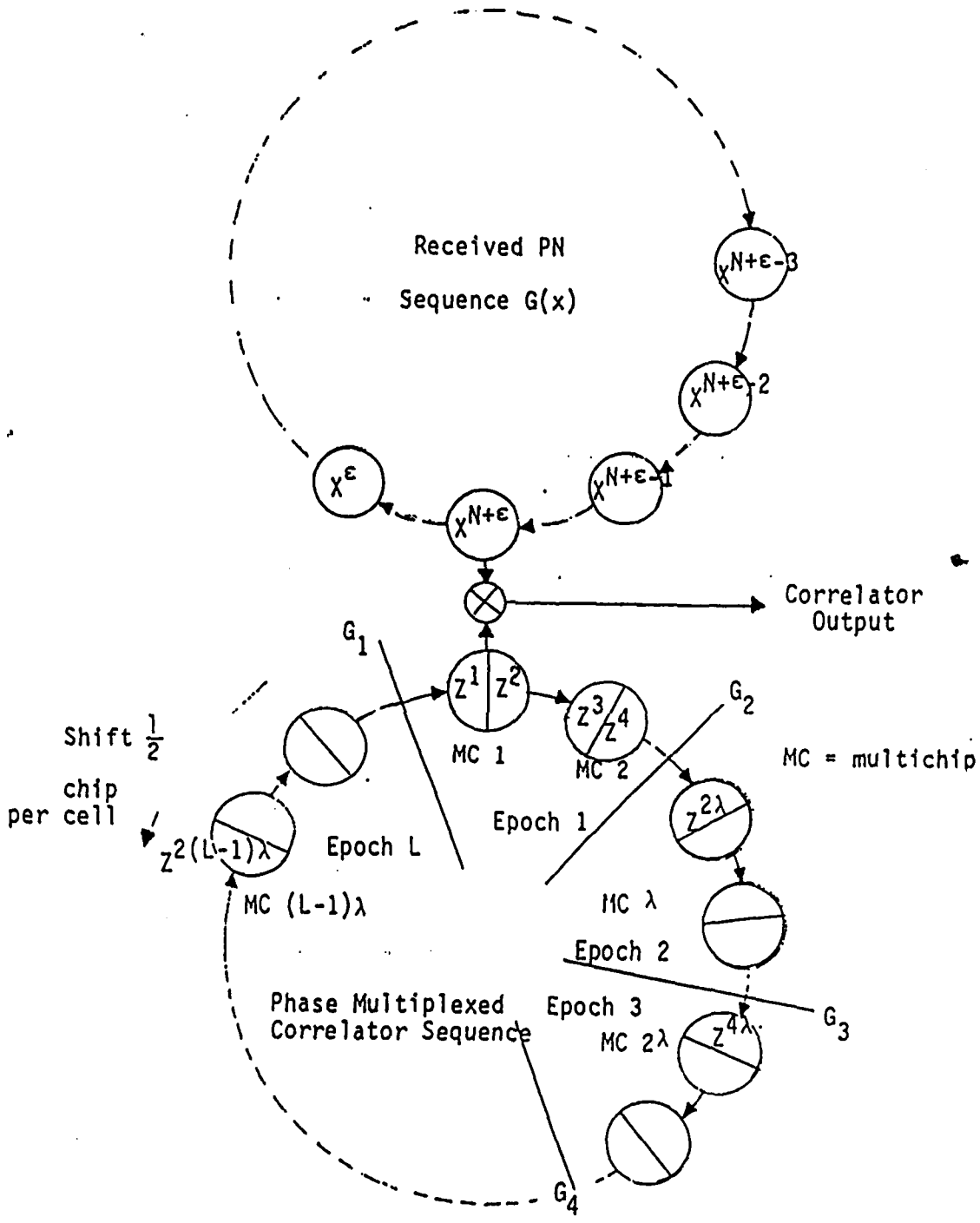

Figure 2.3-14 Serial Search State Diagram.

procedure presented earlier. The bottom wheel is divided into L boundaries corresponding to the L unique code members of the PMC signal. Each of these unique $G_L(t)$ phases coexist with their L identical replicas in equally spaced epochs. The term, multichip, has been chosen because the receiver PMC signal is not a binary sequence, but rather a linear sum of binary sequences. Hence, when examined in the time domain,, it can possess up to L+1 different, equally spaced, amplitude levels. Therefore, the PMC signal may vary in amplitude from zero to L, where zero corresponds to a state with (G_1, G_2, G_3 ..., G_L) = 0 and an amplitude of L implies (G_1, G_2, G_3,..., G_L) = 1 for that state. Figure 2.3-15 illustrates the synthesis of the PMC signal for L = 4 along with waveforms. Figure 2.3-14 shows that the receiver increments the PMC signal by a half chip to search a new cell. The time uncertainty between the clock of the received PN sequence and the PMC signal timing is given by . Since there is no a priori knowledge of the transmitter to receiver time uncertainty, the phase relationship between the PN sequence and local correlation signal is arbitrary. Hence, any received phase may be selected as a reference for the correlation procedure. Doppler shift is considered to be tracked elsewhere in the receiver by a carrier tracking loop. As such, the transmitter and receiver clocks are considered to be at the same rate, barring relativistic effects. The transmitter clock increments the chips for the received PN sequence, while the receiver clock controls the multichipping rate for the PMC signal. The chip/multichip states are represented as having a clockwise motion and the multichips are also allowed to shift by half chip increments in the counterclockwise direction pursuant to a shift command. The rate at which the counterclockwise shift occurs is directly related to the decision process of the coarse acquisition loop. Because of the random nature of the signals and the statistics of the noise in the channel, this shift happens in a random manner for optimal searching as dictated by the sequential detection algorithm (Bouvier 1980).

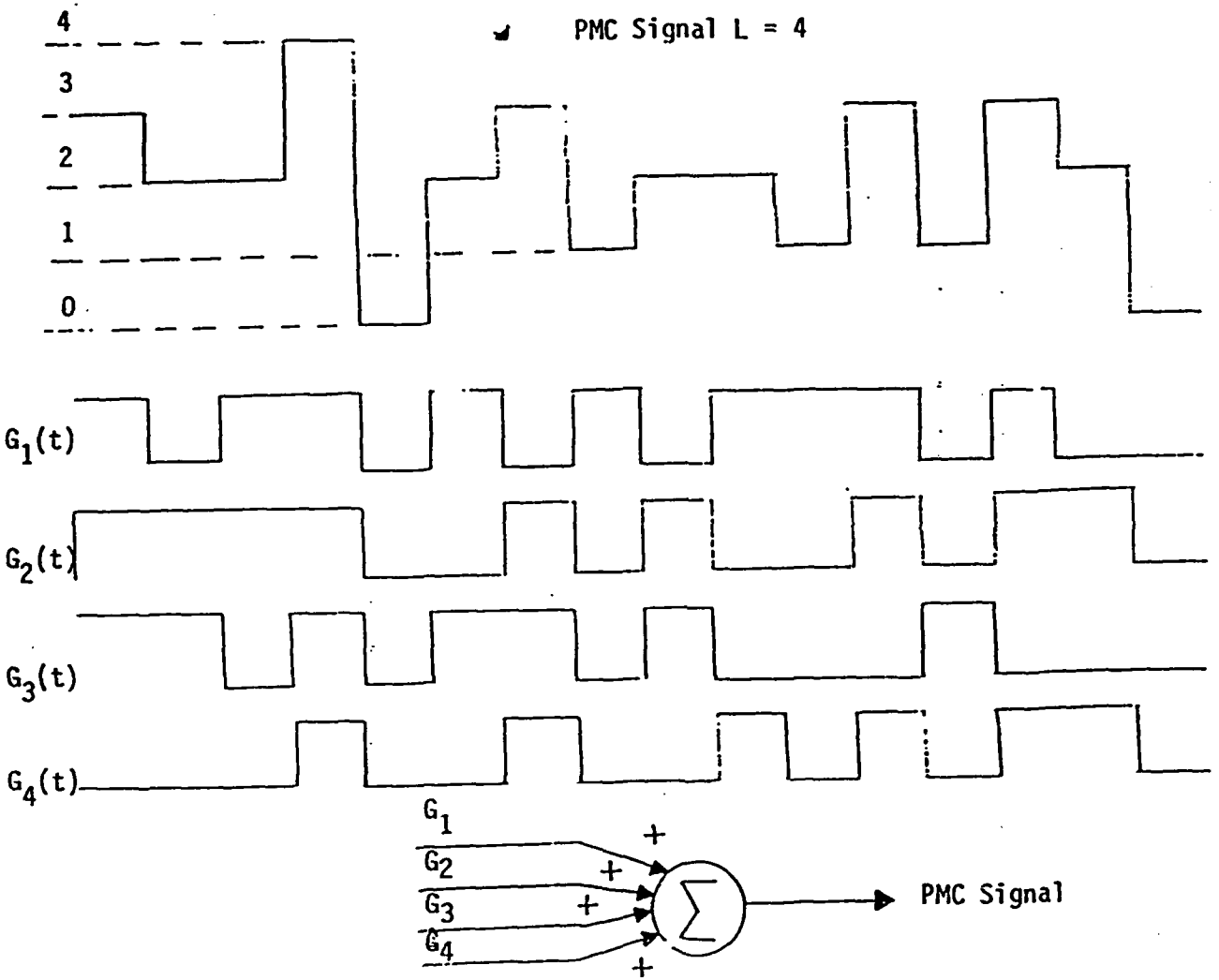

Figure 2.3-15 Phase multiplexed correlator signal

2.3.1.1 Number of Cells to be Searched

Up to this point, 2(N+1)/L has been used as a maximum number of cells to be searched before synchronization. This approximation holds for a probability of detection, P_d, very nearly equal to one. It is useful, though, to consider a more accurate expression which considers lower P_d. The following definitions will be helpful for the derivation.

2λ = 2(N+1)/L = average number of cells in the uncertainty region

P_d = probability of detecting correlation in a correct cell

P_{fa} = probability of a false alarm

Z = Average number of cells searched for detection

The probability that the correct cell is recognized after j searches of the uncertainty region is:

$$P_j = P_d(1 - P_d)^{j-1} \qquad (2.35)$$

which is the geometric probability law. This implies that P_d^{-1} searches on the average are required through the uncertainty region before detection occurs. The number of unsuccessful searches on the average is given by:

$$J = (P_d^{-1} - 1) \qquad (2.36)$$

Since the correct cell location is a random variable having a uniform distribution throughout the uncertainty region, the mean cell location will be at:

$$2\lambda/2 = \lambda = (N+1)/L \qquad (2.37)$$

Thus, the total number of cells searched on the average can be given by:

$$Z = (1/Pd - 1)(2(N+1)/L) + (N+1/L) \qquad (2.38)$$

$$Z = (N+1/L)(2/Pd - 1) = \lambda(2/Pd - 1) \qquad (2.39)$$

False alarms can impact the search process greatly (Bouvier 1980). After searching Z cells, P_d^{-1} are found to be correct. This implies that a possibility of false alarm exists on $(Z - P_d^{-1})$ trials. The number of false alarms, n_{fa}, out of n trials is subject to a binomial probability law given by:

$$P\left[\begin{array}{l} n_{fa} \text{ false alarms} \\ \text{in n trials} \end{array}\right] = \binom{n}{n_{fa}} P_{fa}^{n_{fa}} (1-P_{fa})^{n-n_{fa}} \qquad (2.40)$$

$$\text{for } \overline{n_{fa}} = 0,1,2,\ldots,n$$

The mean value is:

$$\overline{n_{fa}} = nP_{fa}$$

Therefore, the mean number of false alarms is given by:

$$\overline{n_{fa}} = (Z - 1/P_d)P_{fa} = (N+1/L)\ (2/P_d - 1)P_{fa} \qquad (2.41)$$

Both P_d and P_{fa} are functions of the predetection SNR_D. Furthermore, L impacts the SNR as discussed for equation (2.30). Under certain circumstances, however, L may be increased without appreciably altering P_d or P_{fa}. Namely, when there is a sufficient link margin, then L may be increased to reduce Z, the average number of cells searched, and n_{fa}, the average number of false alarms. Sometimes, though, the additional variance may exact too great a penalty on SNR_D and an increase in L could decrease performance. That is why proper sequence design is of the utmost importance, and use of a prebiased reference channel is desired.

2.3.1.2 Sequential Testing with the PMC

In order to reduce the time spent searching an invalid cell, Abraham Wald proposed a self-normalizing threshold to compare the dual hypotheses H_0 and H_1. For a given P_{fa} and P_d, the sequential detection algorithm is optimal in that it guarantees the minimum average number of samples of the random variable to be observed before a decision is reached. Inherently, this reduces the time spent in searching the uncertainty region.

Suppose that μ_i are independent samples of the random variable. Then, the sequential detection algorithm may be expressed by:

$$\Lambda_{\gamma}(\mu_i) = \frac{\prod_{i=1}^{\gamma} p(\mu_i/S+N)}{\prod_{i=1}^{\gamma} p(\mu_i/N)}$$

(2.42)

where $p(\mu_i/S+N)$ is the conditional probability density function (pdf) of μ_i given signal plus noise or partial correlation, and $p(\mu_i/N)$ is the conditional pdf of μ_i given noise only or very low correlation. The acceptance of the hypotheses H_0 and H_1 corresponds to achieving some threshold, β_1' or β_u' for the test. Figure 2.3-16 shows graphically how the test progresses for i samples. $\Lambda(\mu_i)$ is known as the likelihood ratio.

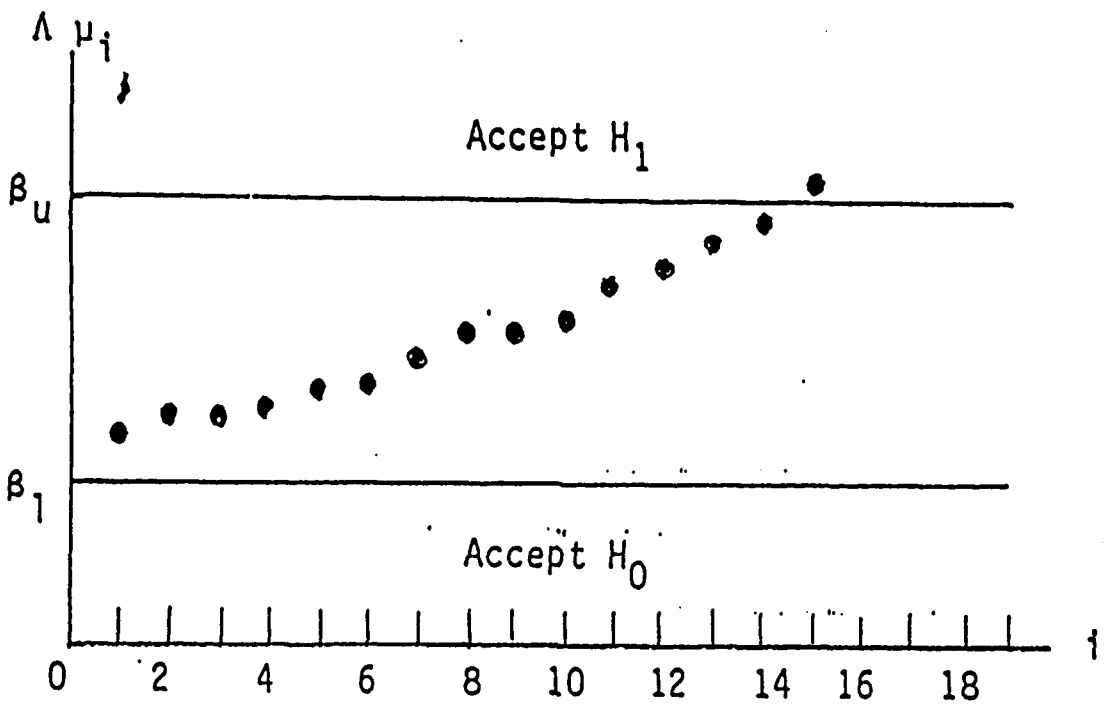

Figure 2.3-16 Likelihood ratio test boundaries.

Whenever:

$\Lambda(\mu_i) \geq \beta_u'$ the cell is correlated

$\Lambda(\mu_i) \leq \beta_l'$ the cell is uncorrelated

$\beta_l' < \Lambda(\mu_i) < \beta_u'$ continue sampling

Furthermore, the probability of detection is given by:

$$P_d = \int_{\Gamma_1} p(\mu_i/S+N)\ d\mu_i \qquad (2.43)$$

When H_o is accepted, the coarse acquisition loop flags the controller to search a new cell. When H_1 is accepted, the coarse acquisition loop flags the controller to pass synchronization responsibilities from the coarse acquisition loop to the code tracking loop for fine synchronization. The probability of false alarm is given by:

$$P_{fa} = \int_{\Gamma_1} p(\mu_i/N)\ d\mu_i \qquad (2.44)$$

where Γ_1 denotes the set of μ_i samples corresponding to the acceptance of H_1, and Γ_o denotes the set of samples corresponding to acceptance of H_0. Therefore, for the acceptance of H_1:

$$\int_{\Gamma_1} p(\mu_i/S+N)d\ \mu_i \geq \beta_u' \int_{\Gamma_1} p(\mu_i/N)\ d\mu_i \qquad (2.45)$$

Analogously, for the acceptance of H_o:

$$\int_{\Gamma_o} p(\mu_i/S+N)d\mu_i \leq \beta_1' \int_{\Gamma_o} p(\mu_i/N)d\mu_i \qquad (2.46)$$

Hence, equations (2.45) and (2.46) can be rewritten as (Holmes 1982):

$$P_d \geq \beta_u'\ P_{fa} \qquad (2.47)$$

$$1 - P_d \leq \beta_1\ (1 - P_{fa}) \qquad (2.48)$$

If the final sample of μ_i ends near the threshold boundary, then the threshold may be found from:

$$\beta_u' \approx \frac{P_d}{P_{fa}} \tag{2.49}$$

$$\beta_l' \approx \frac{1 - P_d}{1 - P_{fa}} \tag{2.50}$$

A bandpass filter and envelope detector or square law detector usually precede the sequential test hardware. Thus, the random variable of the detector output for the noise only case is Rayleigh distributed. For partial or full correlation, the output of the detector will be governed by Rician statistics (Schwartz 1980). Therefore, the pdfs of interest are:

$$p(\mu_i/S+N) = \left[\frac{\mu_i}{\sigma^2} e^{\frac{-(\mu_i + A_o)^2}{2\sigma^2}}\right] I_o\left(\frac{\mu_i A_o}{\sigma^2}\right) \tag{2.51}$$

$$p(\mu_i/N) = \frac{\mu_i}{\sigma^2} e^{\frac{-\mu_i^2}{2\sigma^2}} \tag{2.52}$$

where:

σ^2 = noise power

A_o = sine wave amplitude

$$I_o(p) = \frac{1}{2\pi}\int_o e^{p\cos\theta}\, d\theta \quad \text{(modified Bessel function of the first kind degree zero)}$$

$$I_o(p) = \left(1 + \frac{(p/2)^2}{(1!)^2} \quad \frac{(p/2)^4}{(2!)^2} \quad \frac{(p/2)^6}{(3!)^2} + \ldots\right.$$

Substitution of equations (2.51) and (2.52) into equation (2.42) yields:

$$\Lambda_\gamma = \frac{\prod_{i=1}^{\gamma} \left(\frac{\mu_i}{\sigma^2} \exp-\left(\frac{\mu_i^2 + A_o^2}{2\sigma^2}\right)\right) I_o\left(\frac{\mu_i A_o}{\sigma^2}\right)}{\prod_{i=1}^{\gamma} \frac{\mu_i}{\sigma^2} \exp-\left(\frac{\mu_i^2}{2\sigma^2}\right)} \qquad (2.53)$$

$$\Lambda_\gamma = \prod_{i=1}^{\gamma} \exp -\left(\frac{A_o^2}{2\sigma^2}\right) \; I_o \left(\frac{\mu_i A_o}{\sigma^2}\right) \qquad (2.54)$$

A convenient alternate form of equation (2.54) can be obtained by taking the natural logarithm of both sides. Thus, the log-likelihood ratio is given by:

$$\ln \Lambda_\gamma = \prod_{i=1}^{\gamma} \ln I_o \left(\frac{\mu_i A_o}{\sigma^2}\right) - \left(\frac{A_o^2}{2\sigma^2}\right) \qquad (2.55)$$

The test then becomes modified to the form:

$$\sum_{i=1}^{\gamma} \ln I_o \left(\frac{\mu_i A_o}{\sigma_2}\right) - \frac{A_o^2}{2\sigma^2} \geq \ln \beta_u', \qquad \text{correlation achieved}$$

$$\sum_{i=1}^{\gamma} \ln I_o \left(\frac{\mu_i A_o}{\sigma^2}\right) - \frac{A_o^2}{2\sigma^2} \leq \ln \beta_1', \qquad \text{uncorrelated}$$

$$\ln \beta_1' < \ln I_o \left(\frac{\mu_i A_o}{\sigma^2}\right) - \frac{A_o^2}{2\sigma^2} < \ln \beta_u', \qquad \text{take another sample}$$

This is the general result for the non-coherent sequential detector with the signal modeled as a sine wave in noise. This model is valid for the case of M-ARY PSK spreading, because each symbol is essentially a sine wave in the presence of bandlimited AWG noise. Figure 2.3-17 shows a basic block diagram of the sequential detector. Other simpler implementations are possible if the pre-detection SNR is low (Simon 1985).

In equation (2.55), $A_o^2/2\sigma^2$ is simply the SNR going into the envelope detector and can be used as a design parameter. Rubin has shown that the average number of samples to dismiss the uncorrelated case is given by (Bouvier 1980):

$$\overline{n_d} = \frac{(1 - P_{fa}) \ln\left(\frac{1 - P_d}{1 - P_{fa}}\right) + P_{fa} \ln\left(\frac{P_d}{P_{fa}}\right)}{E\left(\ln I_o \left(\frac{\mu_i A_o}{\sigma^2}\right) - \left(\frac{A_o^2}{2\sigma^2}\right)\right.} \qquad (2.56)$$

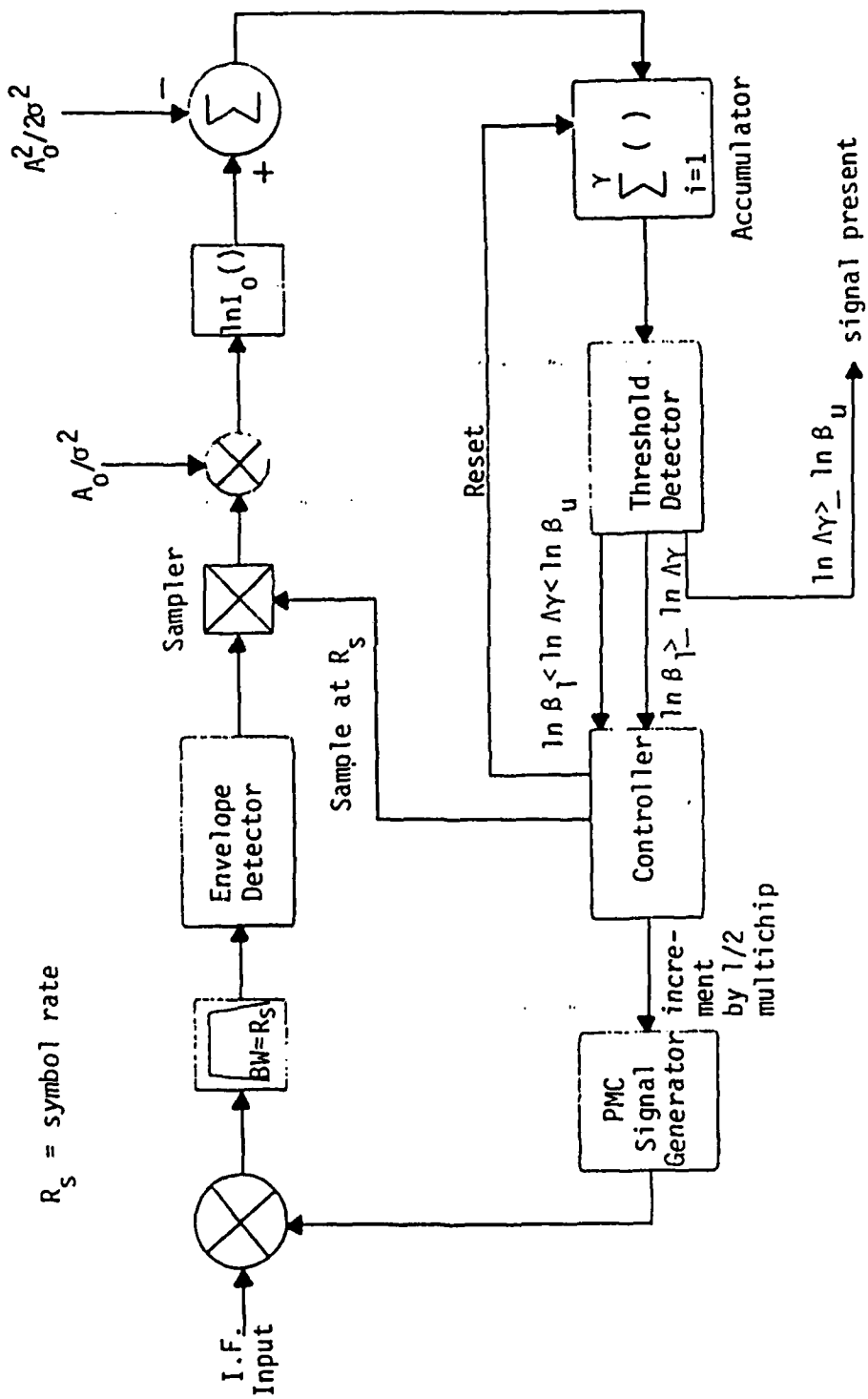

Figure 2.3-17 Sequential detector block diagram.

Therefore, the average search time for a $\overline{ST}$ cell is given by:

$$\overline{ST} = R_s^{-1} \overline{n_d} \qquad (2.57)$$

where R_s^{-1} is the time between samples. If we make the assumption that every false alarm incurs a penalty of K_p time units, then using equations (2.39), (2.41) and (2.57), a mean acquisition time may be calculated from:

$$\overline{T_{aq}} = \lambda(2/P_d - 1)(1+K_p P_{fa}) R_s^{-1} \overline{n_d} \qquad (2.58)$$

K_p accounts for the ime required by the receiver to recognize a false alarm and resume the sequential detection test. The difficulty with calculating equations (2.56, (2.57) and (2.58) is in finding the expectation of the log-likelihood ratio in the denominator of equation (2.56) (Simon 1985). There are many approximations based on assumptions about predetection SNR but computer simulation yields the most reliable results because of the inability of most analytical models to find the moments of ln (I_o) (Holmes 1982). A range of predetection SNRs must exist that will allow a decrease in (Rawlins 1987):

$$\lambda = N+1/L$$

by increasing the number of PMC phases L and thus decrease T_{aq}.

Most of the available literature points to system simulation as the viable analysis method for sequential detection (Simon 1985). While working for the Harris Corporation, Bouvier, Walls and Boyd compiled data based on such a simulation. The data is presented in a general manner that succumbs to the proposed application. The important parameters desired are predetection SNR or SNR_D, β_u and β_1. β_u and β_1 are defined by:

$$\beta_u = \ln \beta_u' = \ln \frac{P_d}{P_{fa}} \qquad (2.59)$$

$$\beta_1 = \ln \beta_1' = \ln \left(\frac{1 - P_d}{1 - P_{fa}}\right) \qquad (2.60)$$

SNR_D is the design value on which the design process hinges. The value, A_o, is calculated based on SNR_D. Figure (2.3-18) illustrates the probability of miss, P_m, versus SNR_D. P_m is defined as the probability of accepting hypothesis H_0 when in fact H_1 is true. P_m is given by:

$$P_m = \frac{\beta_u{}^h - 1}{\beta_u{}^h - \beta_1}$$

$$h \approx 1 - 2 \frac{(SNR_{IF})}{(SNR_D)}$$

SNR_{IF} is the actual signal to noise ratio in the I.F. bandwidth. Figure (2.3-19) defines the lower threshold sensitivity as a function, n_d, the mean number of samples to dismiss given SNR_D.

The sequential detector design process proceeds like the following:

1. Choose SNR_D as the lowest desired pre-detection SNR for synchronization.

2. Choose β_1 based on a compromise between figures 18 and 19.

3. Using SNR_o' from equation (28) as a design parameter, and SNR_D, calculate L from equation (31).

4. Estimate T_{aq} given by equation (58).

5. If the degradation in SNR_D is acceptable, then go to step 6. If not, iterate steps 3, 4 and 5 until the degradation of SNR_D from step 1 is acceptable. T_{aq} may have to be sacrificed in order that a particular BER or SNR_o' be accommodated.

6. Repeat step 2 with the new value for SNR_D, then go to step 7.

7. Choose β_u so that P_{fa} is low.

8. Design the phase multiplexed pseido-noise sequence and determine the partial autocorrelation/cross-correlation properties by computer simulation.

9. Simulate the sequential detector with a computer model and evaluate the performance.

10. Terminate the design process.

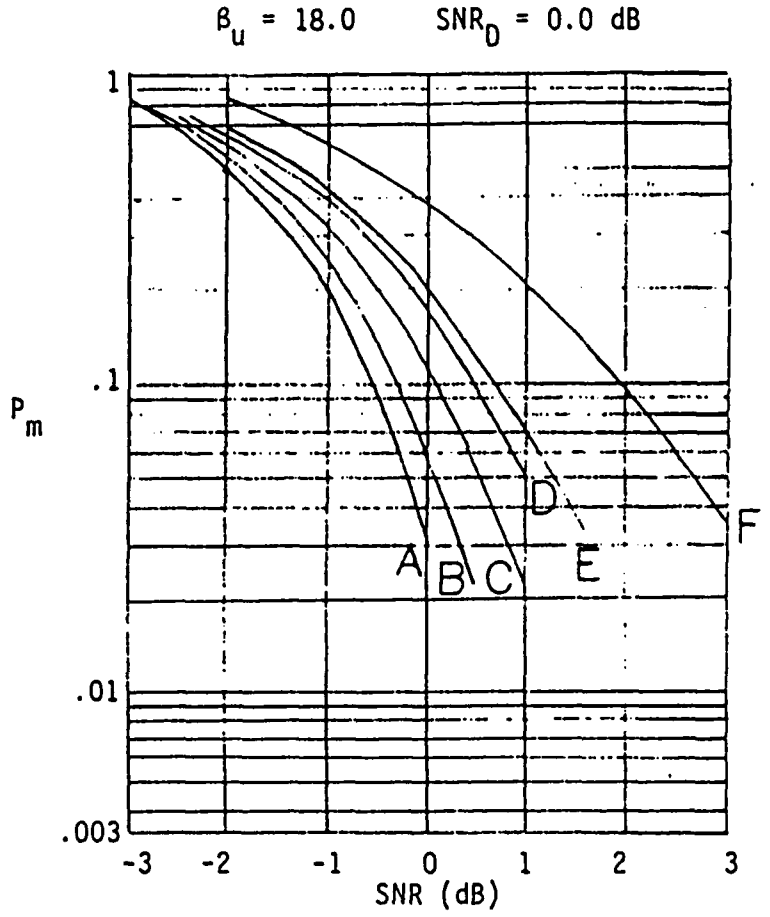

Curve Legend

A: β_1 = - 5.0

B: β_1 = - 4.0

C: β_1 = - 3.0

D: β_1 = - 2.5

E: β_1 = - 2.0

F: β_1 = - 1.0

Figure 2.3-18 Probability of Miss Versus SNR with SNR$_D$, β_1, and β_u as Parameters

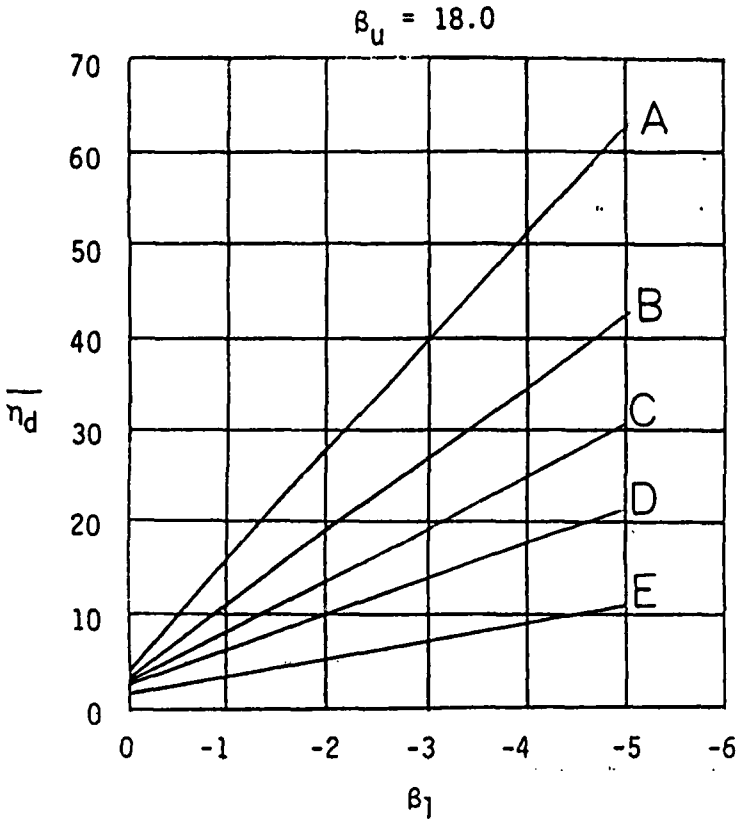

Curve Legend

A: SNR_D = - 3 dB

B: SNR_D = - 2 dB

C: SNR_D = - 1 dB

D: SNR_D = 0 dB

E: SNR_D = + 2 dB

Figure 2.3-19 Lower Threshold Sensitivity Versus the Mean Number of Samples to Dismiss Given SNR_D

This process may require several iterations before acceptable results are achieved. Of course, computer simulation will greatly enhance the design effort. Tradeoffs between SNR_D, SNR_o, and T_{aq} will inevitably have to be made.

Furthermore β_u and β_l will have a significant impact on acquisition performance. Figures 2.3-18, 2.3-19 present two of many possible sets of data. For instance $\beta_u = 18$ corresponds to a P_{fa} of 1.53×10^{-8} which is certainly overkill for most applications. Decreasing P_{fa} enhances acquisition speed drastically. Because, many scenarios are possible, the resulting simulation data for acquisition performance can be overwhelming. Therefore, any further study should define the mission accurately for precise simulation. Performance data from hardware under field tests can better be interpreted in light of theory if this approach is considered. Specific test case analysis is considered to be beyond the scope of the present Phase I program. The foregoing analyses simply justify the approach and bound the predicted behavior theoretically.

It is important to note that the analyses included in this section consider the worst case of non-coherent code acquisition. It is also possible to obtain increased performance if carrier tracking can be accomplished. This would result in a different test statistic for acquisition and a modification to the sequential test proposed. In many applications carrier tracking may be an option, particularly where the phase noise of the carrier at the transmitter can be controlled and ample transmitter power is available so that moderate to high SNR at the receiver is anticipated.

2.3.2 Fine Acquisition

Fine acquisition refers to code synchronization between the received waveform and local sequence at the sub-chip time interval. Coarse acquisition hands off the responsibility of synchronization at the sub-chip interval and fine acquisition maximizes the correlation peak out of the matched filter.

There are several types of control loops employed to obtain fine synchronization. These are: Delay locked loops (early late gate), Tau-dither loops, time gated loops, and hybrids of the above. All of these loops are compatible with coherent and non-coherent implementations. All of these loops depend on the cross-correlation properties of received waveforms and the local reference sequences. We have already shown exhaustive theoretical proofs substantiating the cross-correlation features of the waveform designs proposed here. This required feature of our codes is also shown in the section 4.3 of experimental results. Since it is not the intent of this report to redefine or redesign fine acquisition performance, we simply state that our waveform synthesis is compatible with the above mentioned approaches. A most probable implementation for a Phase II approach will be an early-late-on time delay locked loop. Holmes and Simon provide excellent tutorials on the various code tracking options available.

2.4 SYSTEM CONSIDERATIONS

2.4.1 Range and Range Rate: Range Resolution

Code length and chip rate determine the range accuracy/resolution of the system. For the Phase I base line experiment a binary sequence is emitted in the transmitter while a PMC is implemented in the receiver. The number L = 8 of linearly summed codes in the PMC waveform produces 8 significant correlation peaks out of 1023 transmitted code positions. Therefore, the number L also effects the range measurement unless each of the 8 possible correlation peaks are tested according to the procedure outlines by figure 2.2-12. If this procedure is utilized, it can be shown that the unambiguous maximum target range is given by:

$$d = \frac{N\ tc\ C}{2} \qquad (2.61)$$

where: d = maximum unambiguous range

$N = 2^n - 1$ = code length

tc = chip pulse length

For the Phase I experiment, N = 1023 and tc = 1 μsec, so that the maximum unambiguous range would be

$$d = \frac{(1023)\ (10^{-6})\ (3 \times 10^8)}{2} = 153 \text{ km}$$

Of course, this result is divided by L if the test given by 2.2-12 is not performed. Conversely, 2.61 may be used to determine the required code length for a particular mission by solving for;

$$N = \frac{2(d/c)}{tc} \qquad (2.62)$$

2.4.2 Doppler Ambiguity

Range rate can be measured if carrier tracking is possible. Signal Technologies typically implements a cascade of carrier acquisition technologies consisting of an FFT coarse acquisition phase and a fine carrier tracking phase accomplished via a Costas or modified Costas loop. It may be possible to utilize PMC structures as the arm filters for a modified Costas loop that is robust at low SNR because of the inherent processing gain of a local correlator. Since the output SNR of the PMC can be 20 dB or more greater than the input SNR carrier, tracking via a loop technique is an option. However, since the Costas loop technique is a baseband tracking loop, the Doppler sign is lost in the down conversion. Nevertheless, the frequency of a highly stable up convert/transmit oscillator can be compared to the Costas carrier tracking loop VCO to gain some insight into Doppler. This technique works in the case where the transmitted sequence is used to modulate a pure subcarrier and that result is used to modulate the optical carrier. Of course, the concomitant instabilities of the laser optical phase introduce other difficulties. If the chip rate of the PN sequence is much greater than the incoherent phase bandwidth of the laser source, then Costas subcarrier tracking with Doppler capability may be viable. For the case of Homodyne operation, the detected Doppler corrupted/phase noise corrupted signal could be translated to an IF/subcarrier that is suitable for tracking via the Costas loop. The average frequency value of the VCO within the Costas loop feed back could be monitored to strip off sign and magnitude of the Doppler component. Figure 2.4-1 shows a block diagram of the approach.

This might be considered a high risk approach compared to other traditional techniques using synchronous but non coherent detection. For instance figure 2.4-2 shows another approach for Doppler tracking that resolves range rate by using in phase and quadrature components of the down converted carrier after the PN sequence is stripped off.

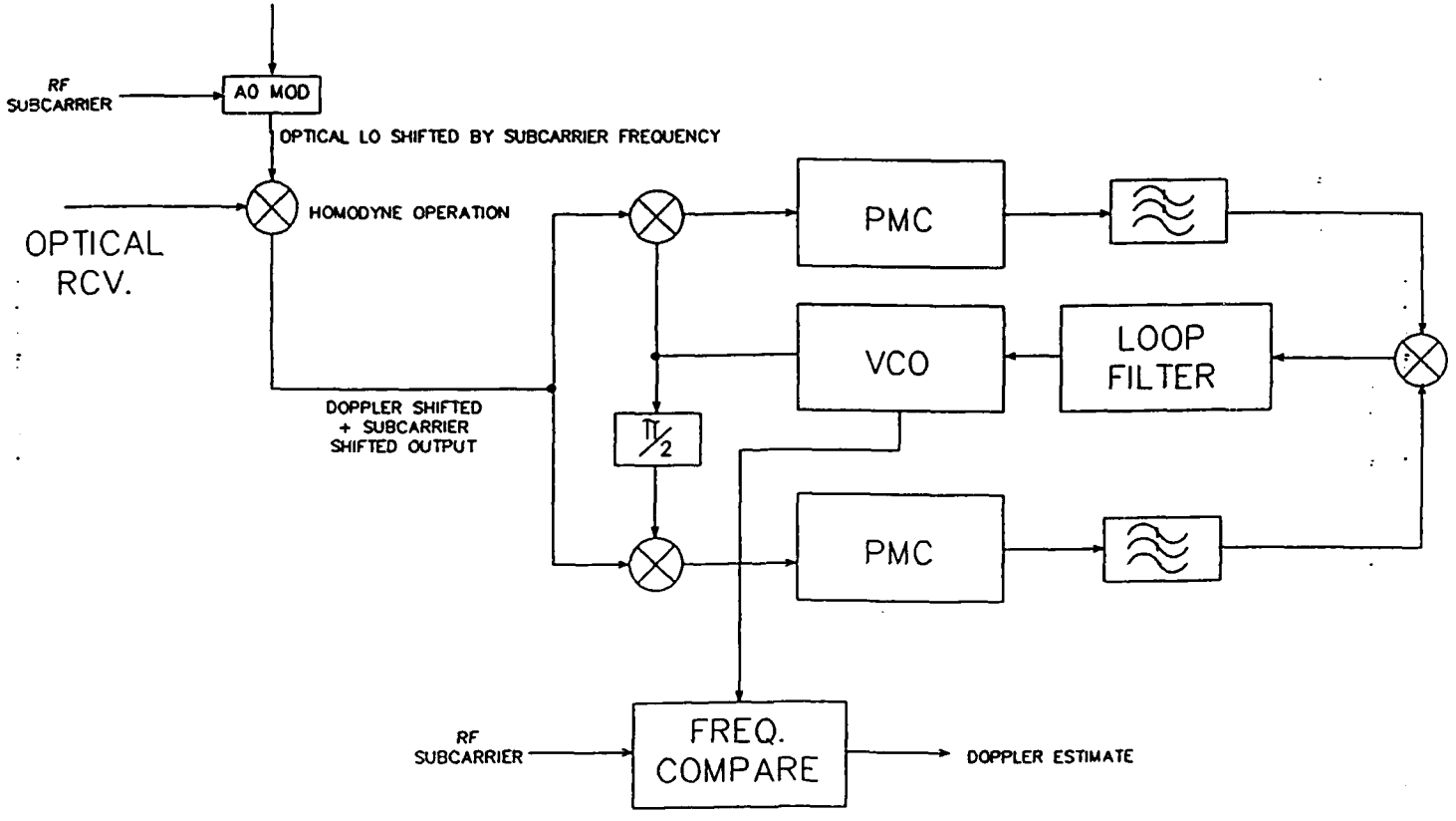
RF
SUBCARRIER
AO MOD
OPTICAL LO SHIFTED BY SUBCARRIER FREQUENCY
OPTICAL
RCV.
HOMODYNE OPERATION
PMC
VCO
LOOP
FILTER
DOPPLER SHIFTED
+ SUBCARRIER
SHIFTED OUTPUT
π/2
PMC
RF
SUBCARRIER
FREQ.
COMPARE
DOPPLER ESTIMATE

Figure 2.4-1

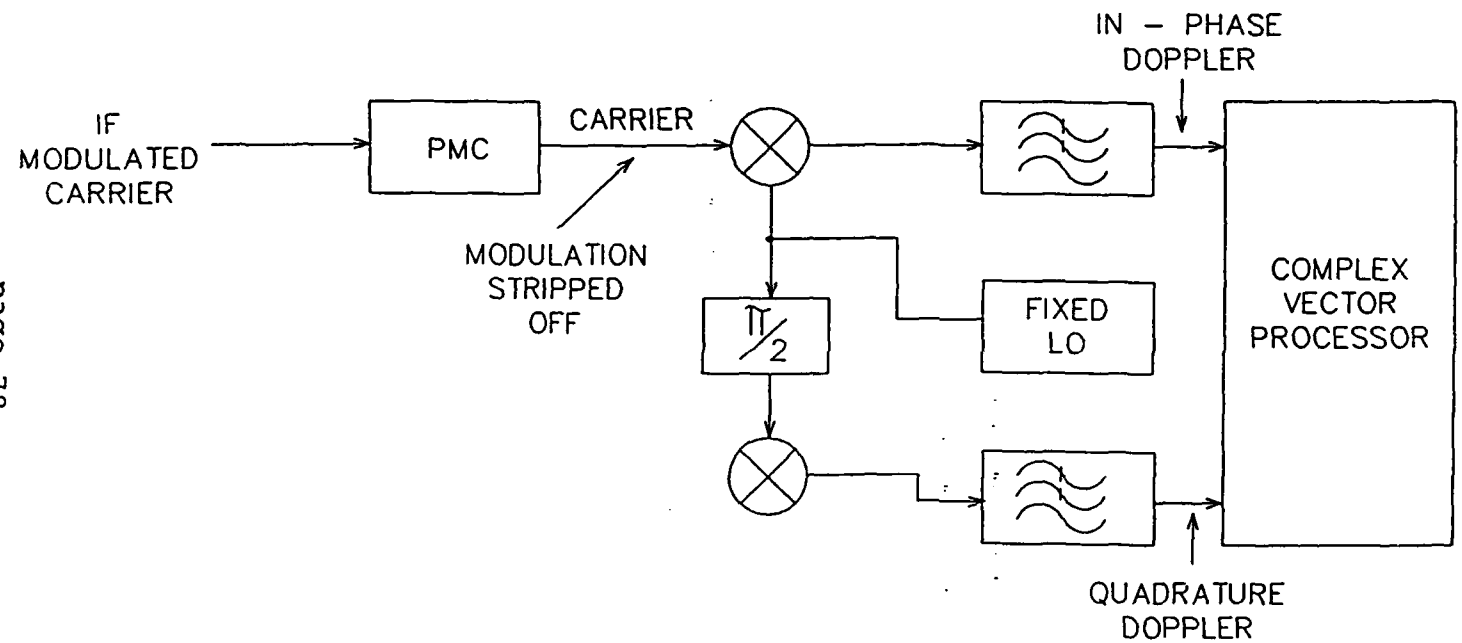
IN – PHASE
DOPPLER
IF
MODULATED
CARRIER
PMC
CARRIER
MODULATION
STRIPPED
OFF
π/2
FIXED
LO
COMPLEX
VECTOR
PROCESSOR
QUADRATURE
DOPPLER

Figure 2.4-2

By using I & Q components, the direction of the rate of change of phase (i.e. the direction of the frequency change) can be obtained. This is because a vector in the complex plane may be created via the in phase and quadrature Doppler terms. The phase of this vector retards for the low side Doppler shift and advances for the high side Doppler shift. Figure 2.4-3 illustrates the phasor notation.

Very often, frequency bin processing is used to resolve Doppler in a non coherent system. For this approach, spectral sidelobes on the received spread signal provide ambiguities because sidelobes will spill over into bins that represent false Doppler shifts. These spectral sidelobes are apparent for PN sequence waveforms by observation of equation 2.15. A contiguous band of matched filters may be used to accomplish Doppler processing, although that approach is usually hardware intensive. Doppler ambiguity may be reduced by pulse shaping the basic chip component of the waveform to reduce spectral content outside of the main lobe. Signal Technologies has used raised cosine pulse shaping and Gaussian pulse shaping previously and is presently investigating the Prolate Spheroidal wave function pulse family for reducing spectral side lobes.

The Doppler ambiguity function, as written by Eaves and Reedy (1987) is given by:

$$\phi = \left| \int_{-\infty}^{\infty} u(t)\ u^*(t+T_R)\ \exp(j2\pi f_d t)\ dt \right|^2 \qquad (2.63)$$

where:

$T_R \equiv$ response time coordinate of receiver matched filter output

$f_d \equiv$ Doppler frequency

$u(t) \equiv$ modulated waveform

Eq. 2.63 basically describes the energy density of a two dimensional Fourier transform, with one dimension time and the other frequency. For the PN modulated waveforms described in this report, range resolution and Doppler ambiguity are independent from one another. For the case of the FM chirp however, there is a cross-coupling of error in the range measurement due to Doppler shift according to eq. 2.63. Figure 2.4-4 shows how range and Doppler ambiguity are coupled for the FM chirp and decoupled for the 13 element Barker PN sequence. Each contour is a 3dB performance locus for the various radar schemes: pulse, Barker PN sequence, FM chirp. In general, PN sequences may be obtained to provide more accurate range resolution than other pulse compression waveforms.

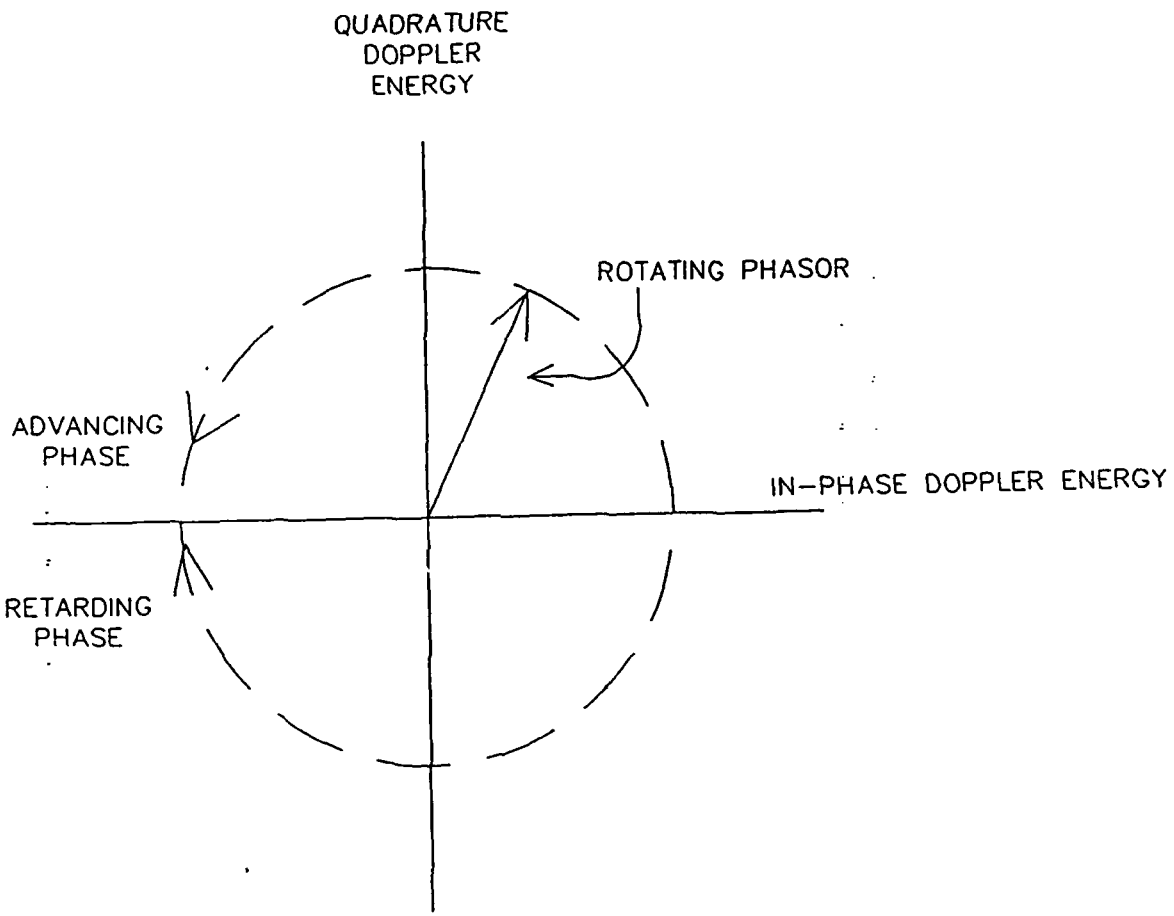
QUADRATURE
DOPPLER
ENERGY
ROTATING PHASOR
ADVANCING
PHASE
IN-PHASE DOPPLER ENERGY
RETARDING
PHASE

Figure 2.4-3

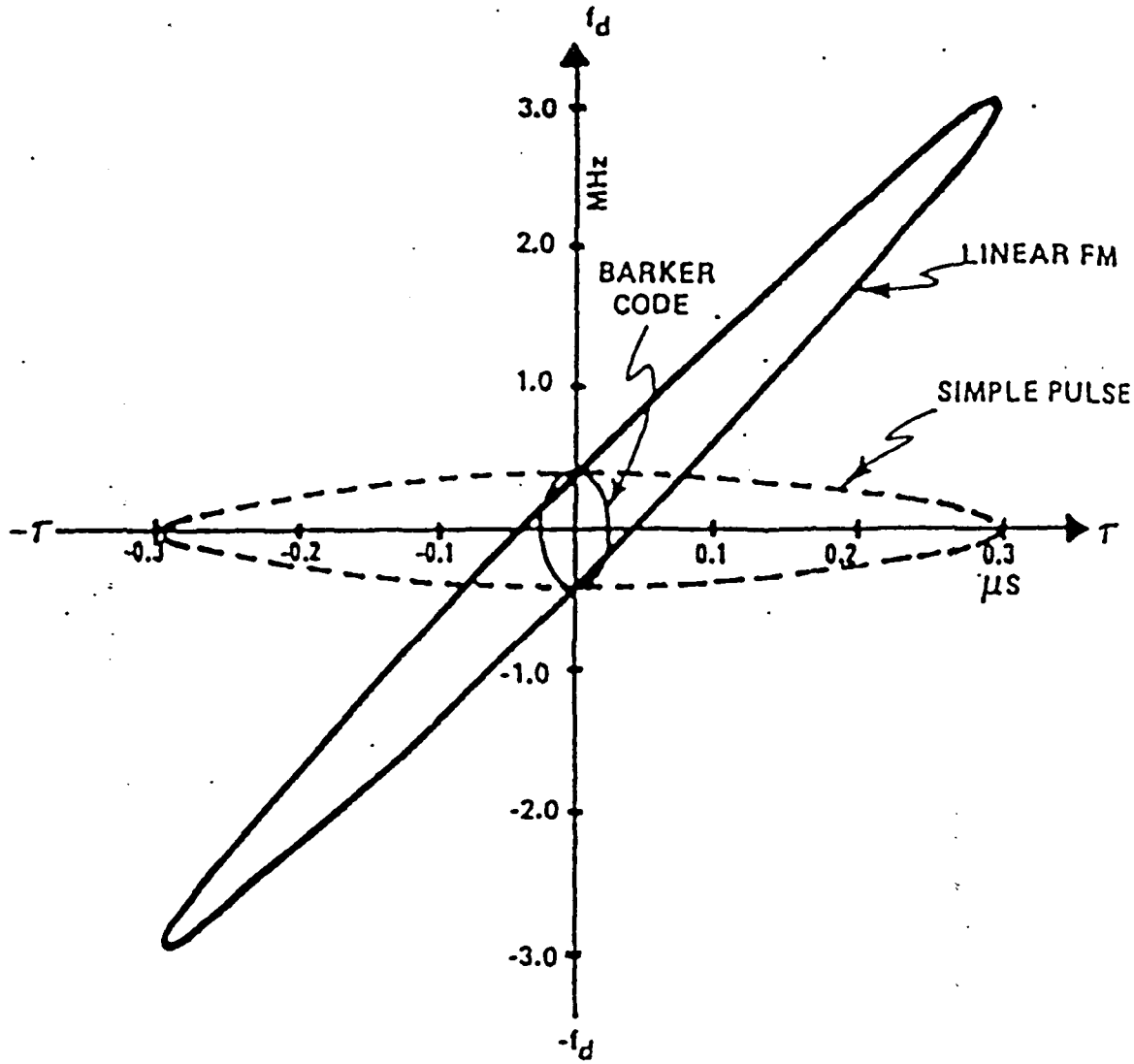

Ambiguity function 3-dB contours for simple pulse, linear FM pulse and 13-bit Barker code. (By permission, from Brookner, ref. 10; © 1982 Artech House, Inc.)

Figure 2.4-4

As already indicated, Doppler ambiguity and range resolution are decoupled for the class of PN sequence based waveforms presented in this report. Nevertheless, Doppler ambiguity can deteriorate the performance of the local correlator if the local correlator cannot be exactly coherent. For these cases a non coherent detector such as in Figure 2.4-2 may be used or multiple skewed bandpass matched filters can be used for bin processing. The basic model for a non coherent matched filter implementation is illustrated in Figure 2.4-5. T is the matched filter time constant. The central issue is the interaction of the integration period T with respect to harmonic content of X_c and X_s due to a Doppler component that has not been tracked by S(t). Furthermore, the configuration shown is also phase sensitive as well as frequency sensitive in terms of desired performance. It can be shown (Bouvier 1980) that the output Z without Doppler components is given by:

$$Z = S^2 R_c^2(\tau) \tag{2.64}$$

where:

$R_c(\tau)$ = autocorrelation function of the PN sequence

Moreover, when Doppler is present, eq. 5.4 modifies to:

$$Z = S^2 T^2 \mathrm{sinc}^2(f_d T) \tag{2.65}$$

From eq. 2.65 it is apparent that Doppler can degrade the detector performance. Figure 2.4-6 shows the degradation of the correlator peak for a corresponding Doppler shift. For a 1μsec pulse shape or chip duration a 3 dB degradation occurs at a Doppler shift of approximately 600 kHz. Figures 2.4-7 through 2.4-9 show normalized correlation functions as a function of time shift with Doppler shift, f_d, as a parameter.

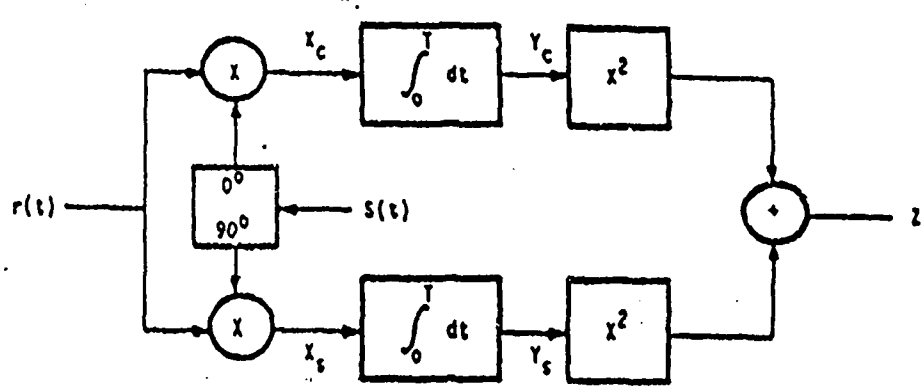

Figure 2.4-5 Noncoherent detector

$$r(t) = \sqrt{2S}\ C(t) \cos([\omega+\omega_d]t)$$

S = signal power

C(t) = PN code [±1]

ω_d = doppler

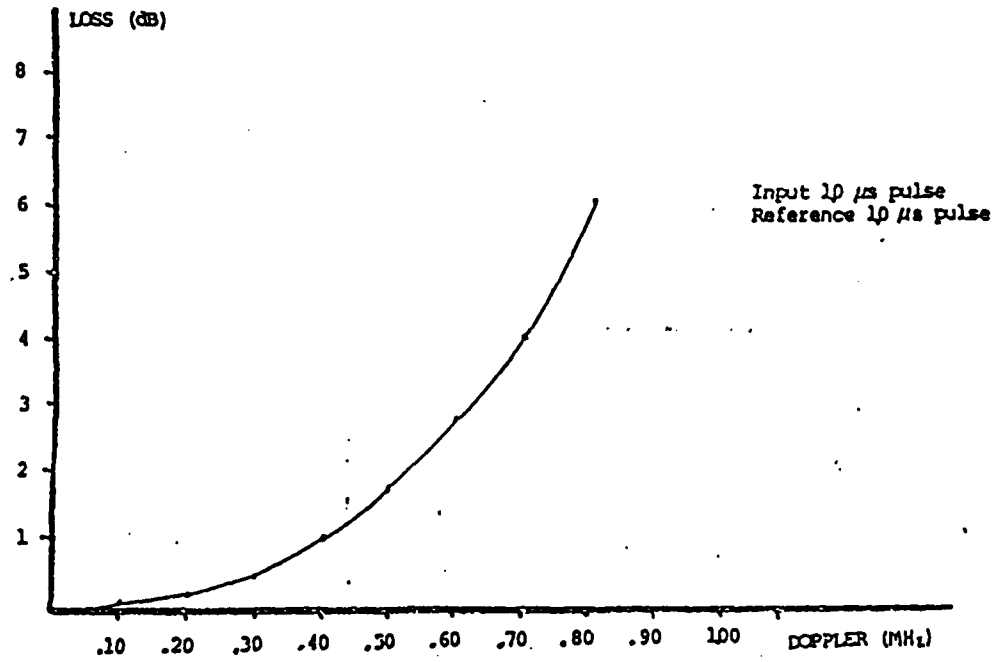

Figure 2.4-6 Loss in Convolver Peak Output Due to Doppler for the Input and Reference Waveforms being 10μs Pulses

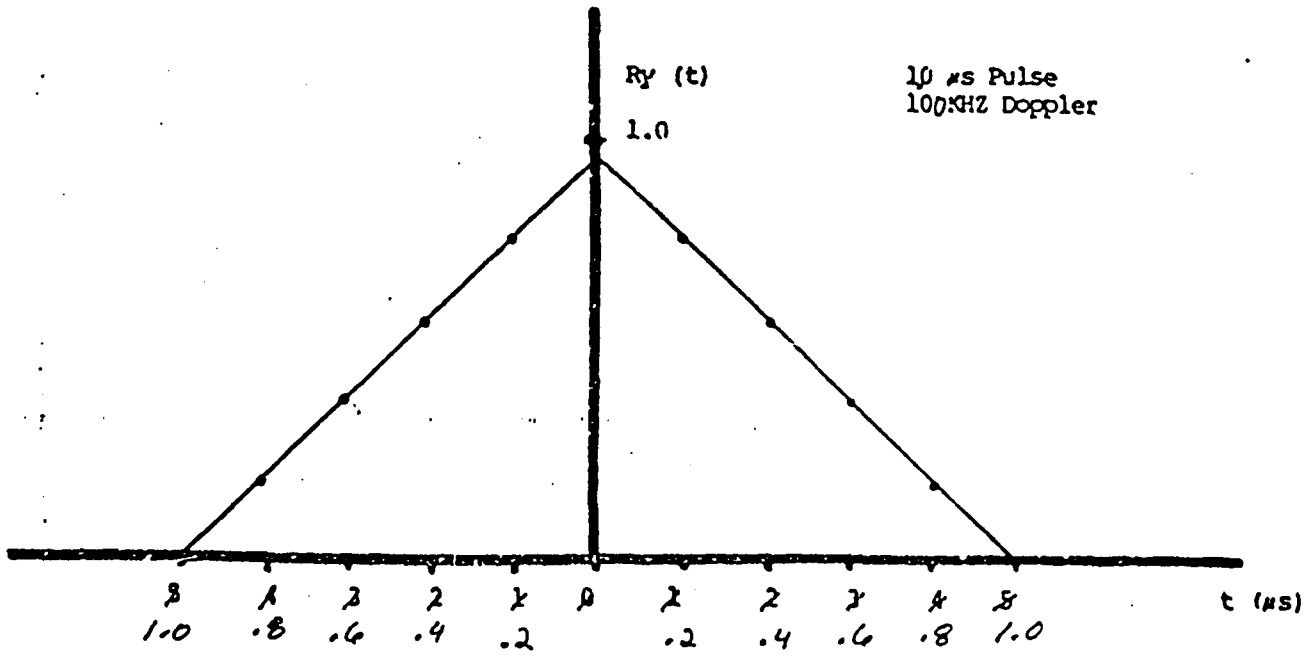

Figure 2.4-7

Normalized Correlation Function for Output of Convolver with the Input and Reference Waveforms Being 10μs Pulses with 10 kHz of Doppler

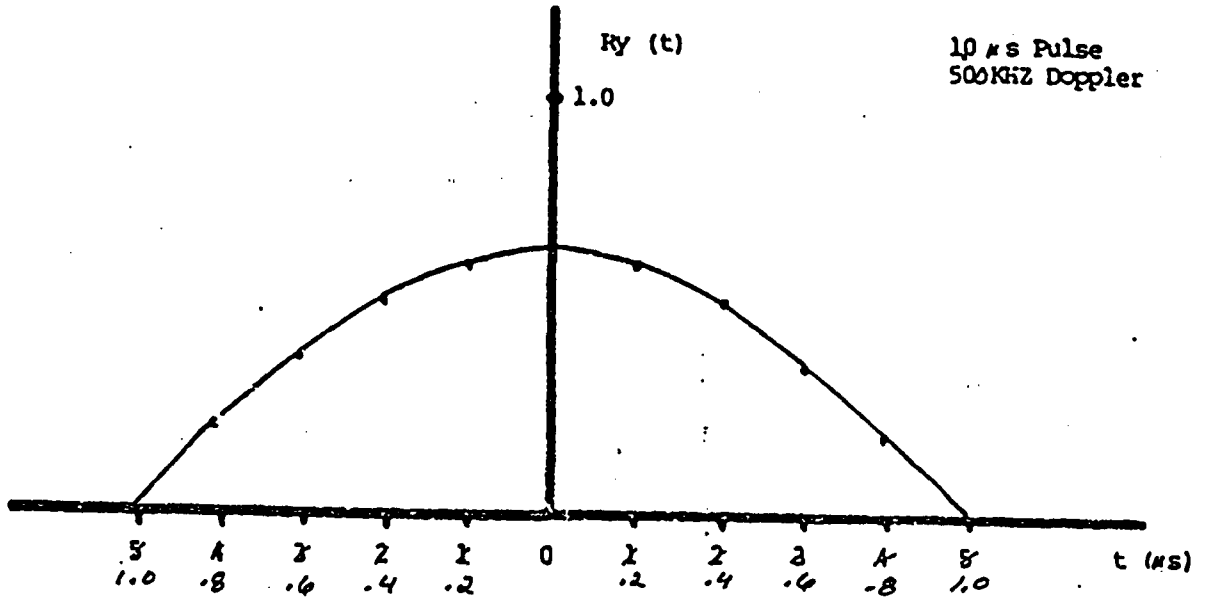

Figure 2.4-8
Normalized Correlation Function for Output of Convolver with the Input and Reference Waveforms Being 10μs Pulses with 500 kHz of Doppler

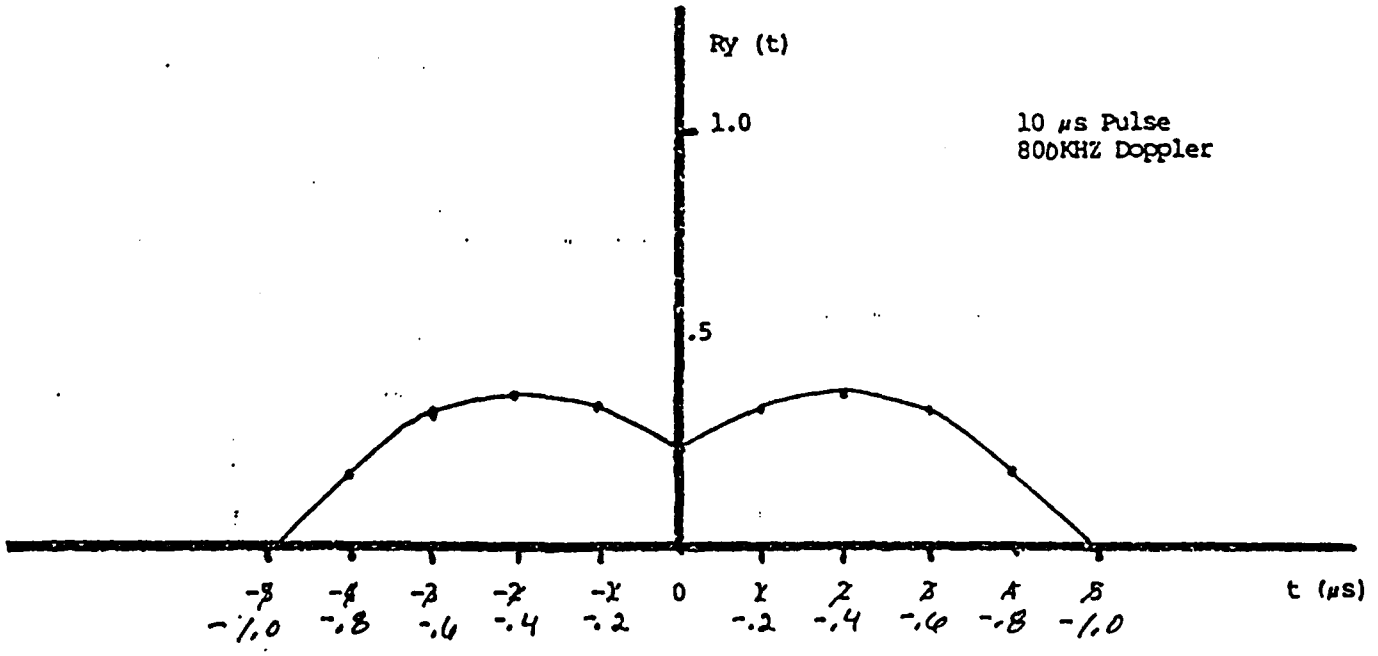

Figure 2.4-9
Normalized Correlation Function for Output of Convolver with the Input and Reference Waveforms Being 10μs Pulses with 800 kHz of Doppler

If the effects of a uniformly distributed random phase are considered along with Doppler, then further distortion of the correlation peak results. Since the phase is distributed from 0 to 2π, we consider the mean square output for the matched filter as a function of time misalignment with Doppler as a parameter in Figures 2.4-10 through 2.4-14. It is important to note that the previously examined 3 dB loss in correlator peak energy occurs at 430 kHz rather than 600 kHz. Of course, each matched filter type and technology whether transversal filters, or SAW convolvers may have certain peculiar responses. Figures 2.4-7 through 2.4-14 establish the expected trend for correlator operation in the presence of Doppler shift and random phase when adequate carrier tracking is not an option.

2.4-.3 Doppler Invariant Design

It is possible to build a Doppler invariant correlator by differentially encoding the transmit sequence before modulation. Signal Technologies had employed such a scheme on previous programs/studies for non coherent demodulation of phase shift keyed waveforms. The technique requires that the chip sequence in the transmitter be encoded by the rule:

$$d_k = d_{k-1} + d_{k-1}b_k,\ b_k \equiv \text{input sequence} \qquad (2.66)$$

The receiver strips off the encoding process by a delay multiply operation. Figure 2.4-15 illustrates the technique. Table 2-7 shows how the PN sequence stream is recovered via the delay multiply operation in the receiver. It is necessary to obtain an IF in the receiver and to obtain an accurate delay line for τ over the expected Doppler bandwidth. Therefore, laser radars which modify their chipping rates must also modify τ. Of course, there is a performance penalty to be paid for this approach. Even though the IF frequency is identically stripped off by the delay multiply operation, the pseudo-carrier stripping is affected by signal noise processes. However, for a 0 dB chip energy to noise density ratio only a 1.5 dB degradation in performance is anticipated. Therefore, this approach may be an attractive alternative for a Doppler hardened design.

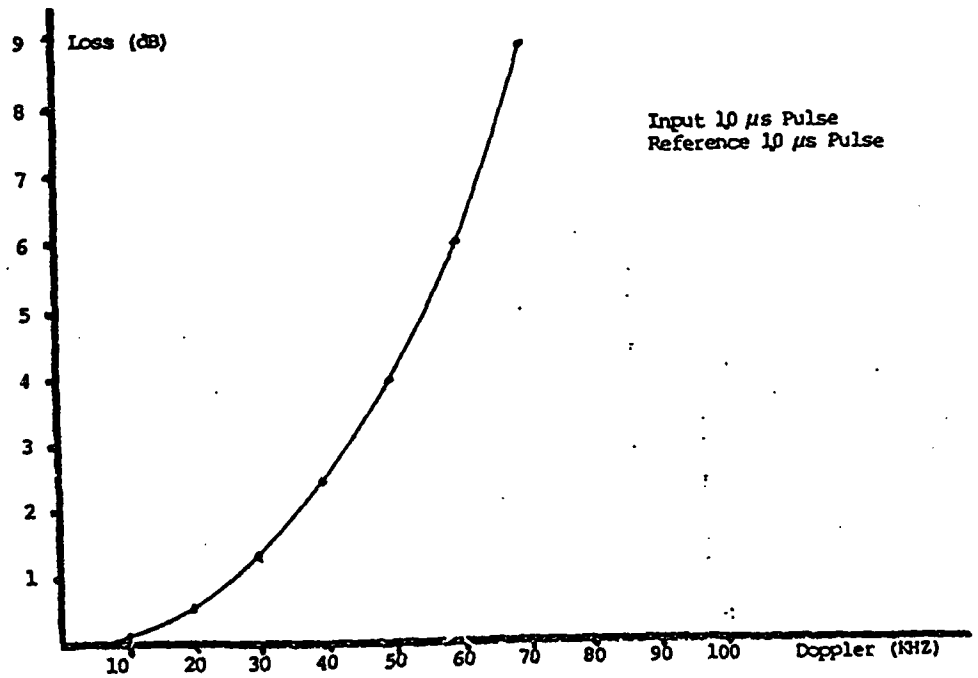

Figure 2.4-10 Loss in convolver mean square output due to doppler and random phase variations

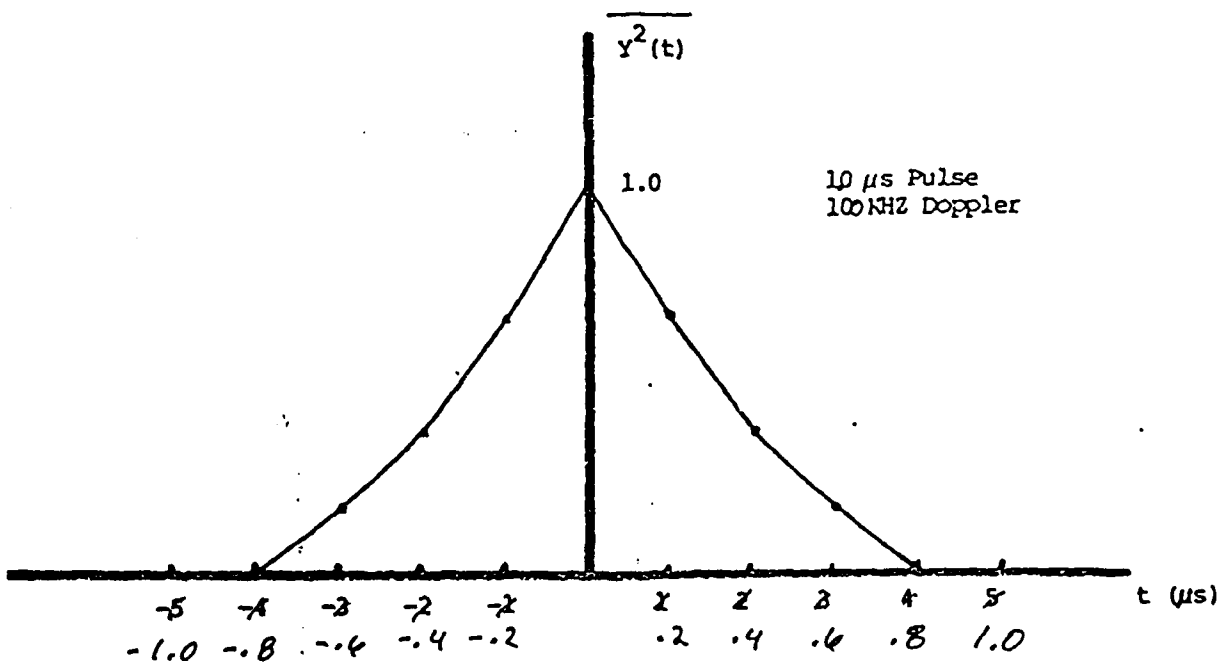

Figure 2.4-11 Normalized mean square value of convolver output with random phase input

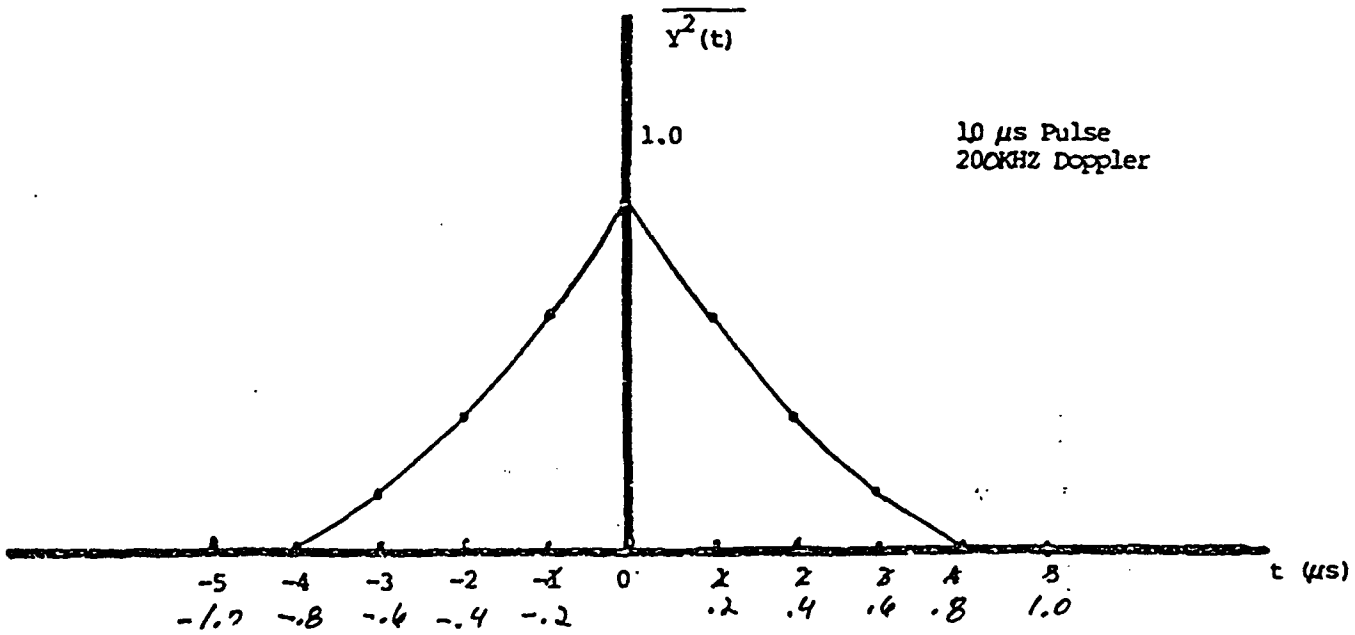

Figure 2.4-12 Normalized mean square value of convolver output with random phase input

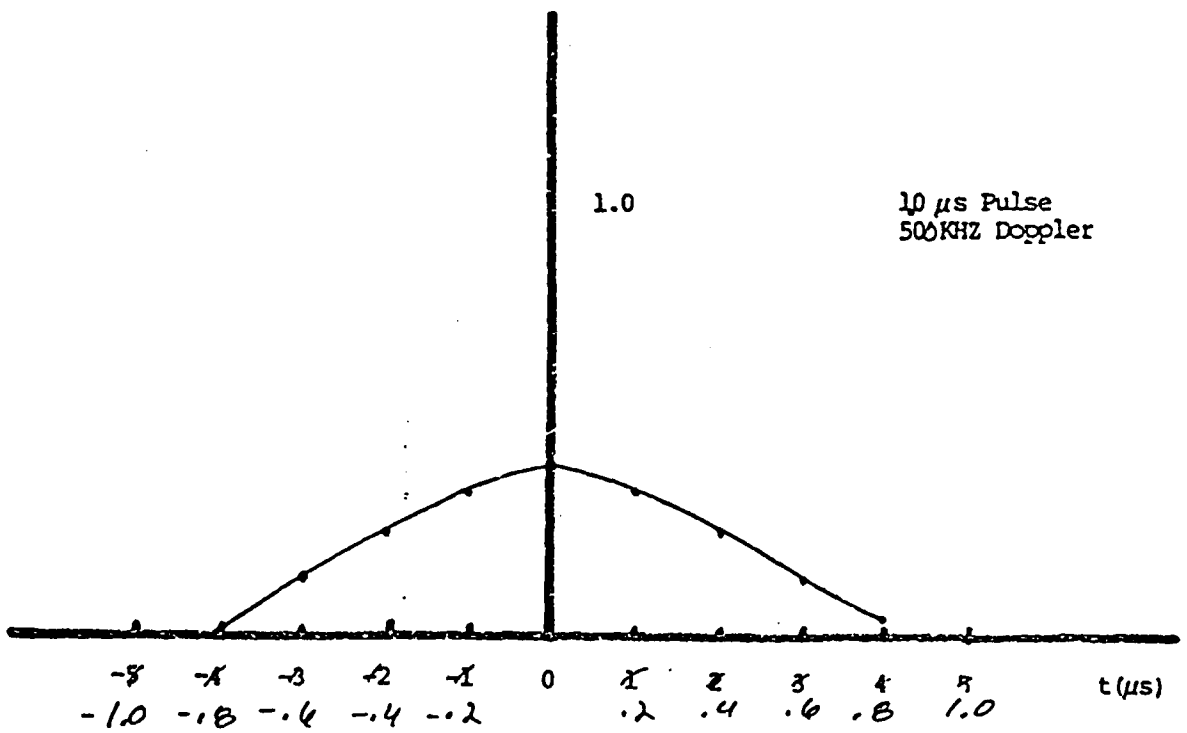

Figure 2.4-13 Normalized mean square value of convolver output with random phase input

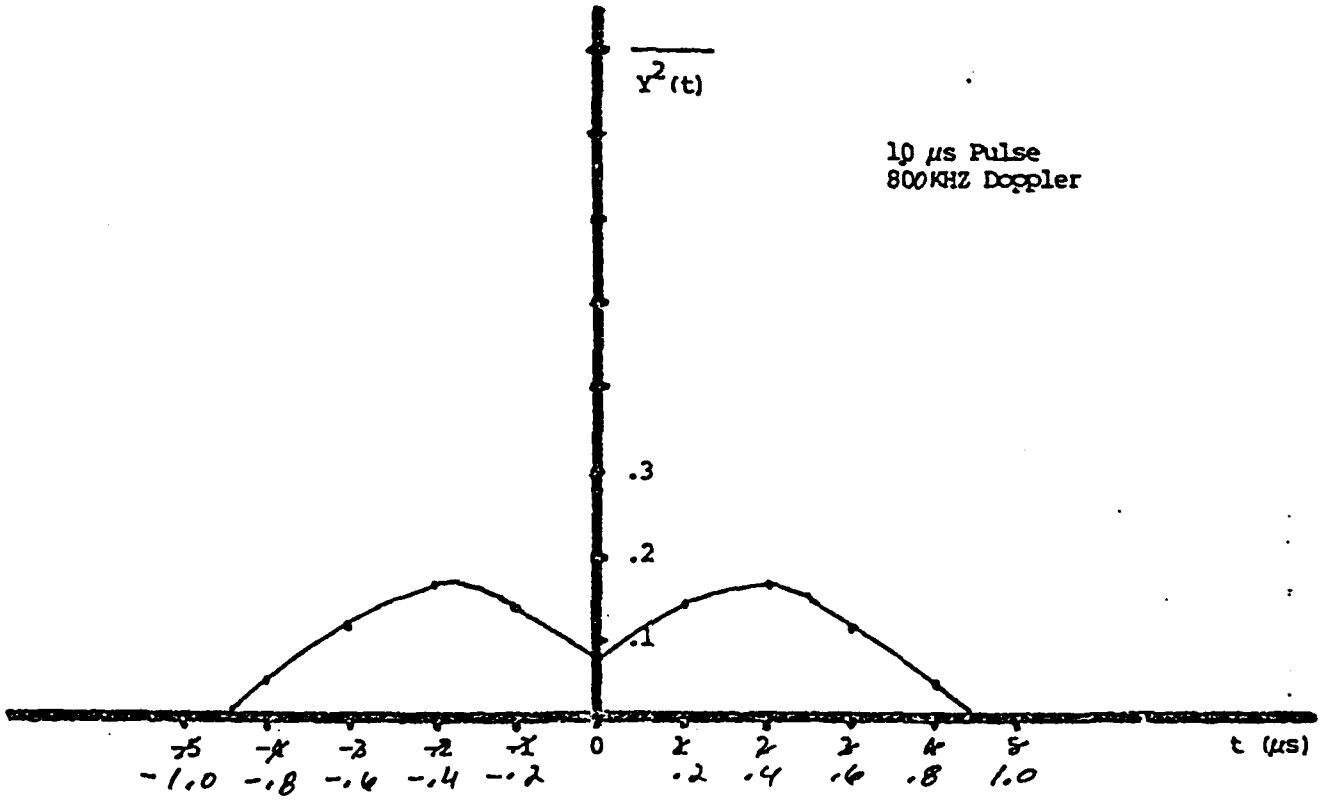

Figure 2.4-14 Normalized mean square value of convolver output with random phase input

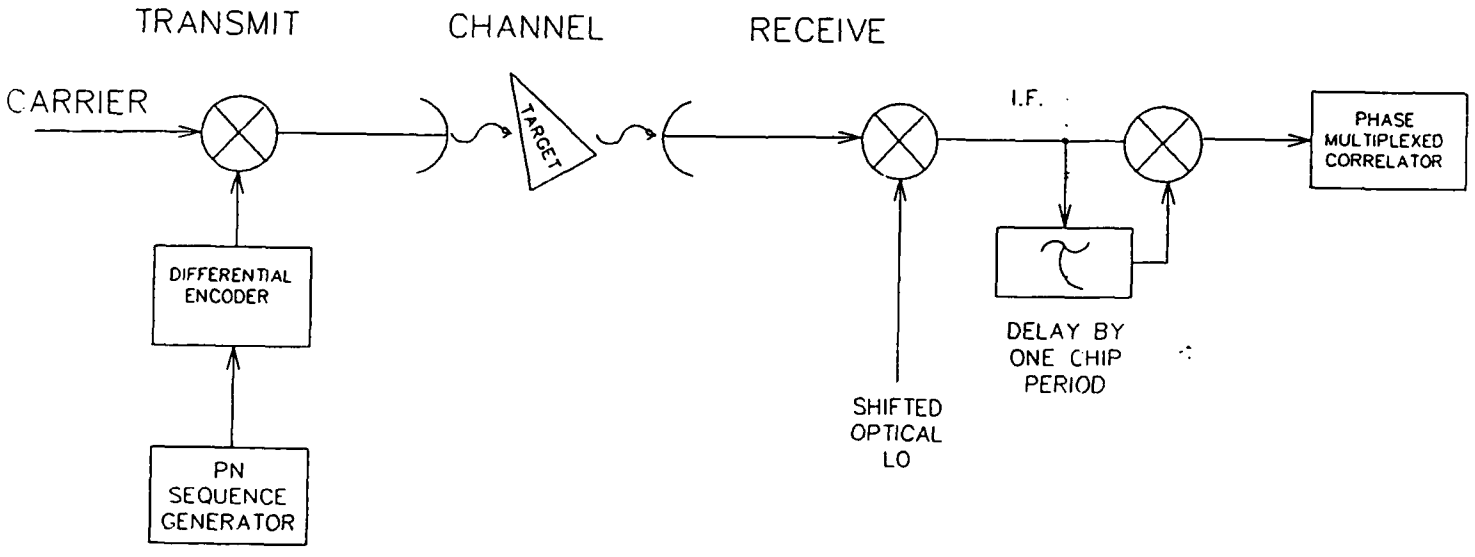
TRANSMIT
CHANNEL
RECEIVE
CARRIER
TARGET
I.F.
PHASE MULTIPLEXED CORRELATOR
DIFFERENTIAL ENCODER
PN SEQUENCE GENERATOR
SHIFTED OPTICAL LO
DELAY BY ONE CHIP PERIOD

Figure 2.4-15

TABLE 2-7 DIFFERENTIAL ENCODING AND DECODING

Input sequence (b_k)			1	1	0	1	0	0	0	1	1
Encoded sequence (d_k)	1[a]	1	1	0	0	1	0	1	1	1
Transmitted phase	0	0	0	π	π	0	π	0	0	0
Phase comparison output		+	+	-	+	-	-	-	+	+
Output sequence		1	1	0	1	0	0	0	1	1

[a]Arbitrary starting reference chip.

3.0 PHASE I PN LADAR OPTICAL IMPLEMENTATION

The Phase I PN LADAR opto-mechanical configuration is based upon the ATC developed Compact Interferometer (CI).

The CI has been designed and fabricated for maximum flexibility and optical component reconfigurability. Photographs of the laser, the CI with mounts and optics, and of the complete LADAR transceiver are shown on the following page in Figures 3-1, 3-2, and 3-3, respectively.

3.1 Opto-Mechanical Hardware

3.1.1 Laser

The laser is a Hughes CO_2 rf excited waveguide with a PZT tuned intracavity grating and the following specifications:

Output Power	2.0 Watts Measured
Polarization	Linear
Mode	EH_{11} Waveguide Mode TEMoo Free Space Mode
Wavelength	10.59 um(P20 line)
Beam Diameter ($1/e^2$)	1.4mm
Divergence Full Angle	10 mr

The RF power supply operates off of 28 volts DC, 3.5 amps, and the rf output power is 66 watts, at a frequency of 74.5 MHz. At this drive power, the laser power is 2 watts.

3.1.2 Compact Interferometer

The Phase I transceiver approach is bistatic, ie: separate transmit and receive apertures. The Phase I PN LADAR transceiver optical schematic is shown in figure (3-4). The 1.4 mm $1/e^2$ is first expanded with a 3.57x afocal telescope up to the nominal working aperture of 5mm. All CI optical component diameters are 12.7mm (1/2" nominal), so that even with 45° mirrors and beamsplitters, the beam will propagate untruncated. Referring to the figure, the laser polarization is into the page, ie. "s" polarization.

The beam is split by beamsplitter BS1 (10% reflecting). The reflected portion becomes the optical local oscillator (LO). The LO is then reflected from BS2 (10% R) and mirror M7 to the detector. The 1-2 milliwatt LO incident on the detector provides the correct optical bias for shot noise limited heterodyne operation.

After BS1, the beam is directed by mirrors M3 and M4 to an acousto-optic modulator (Bragg Cell), Intra-Action model AGM-402. The modulator operates at a center frequency of 40 MHz, effectively frequency upshifting the optical carrier by 40 MHz. Additionally, the PN code sequence modulates the 40 MHz acoustic carrier. Details of the Phase I vs. Phase II modulation approach will be discussed in the next section.

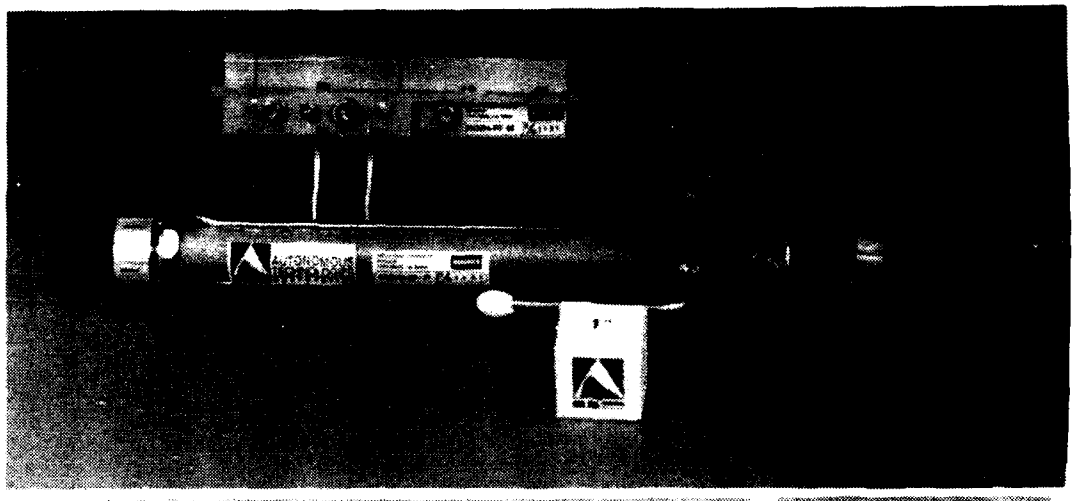

Figure 3-1

PHOTO Laser

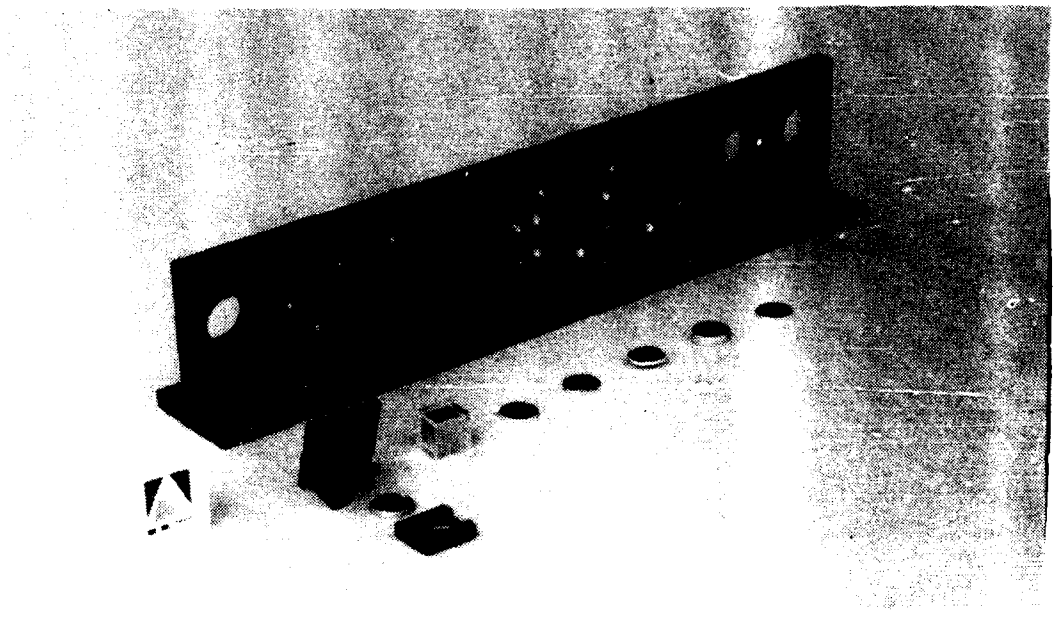

Figure 3-2

PHOTO CI and Mounts

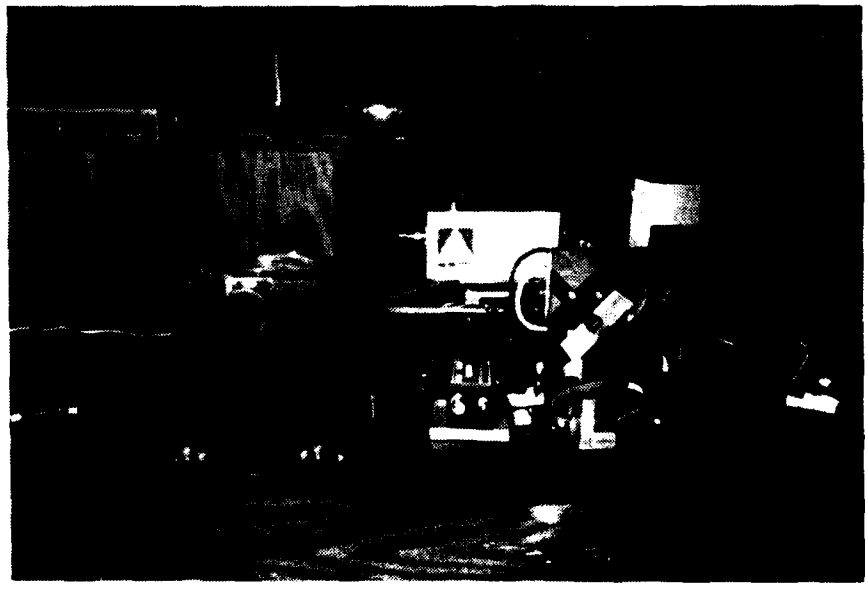

Figure 3-3

PHOTO Complete Transceiver

PN LADAR
OPTICAL SCHEMATIC

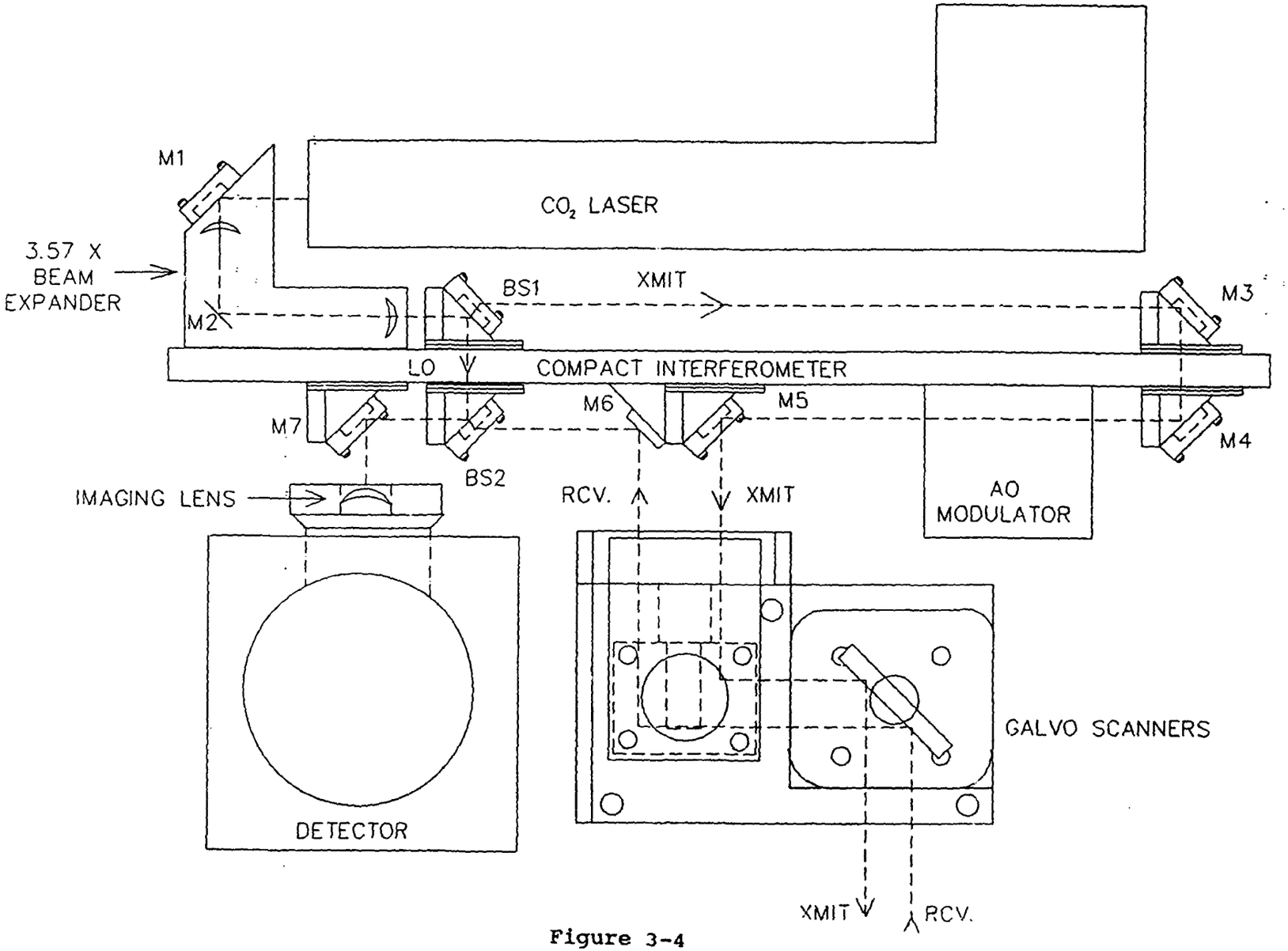

Figure 3-4

AD-A207 454 DEEP SPACE LADAR SBIR PHASE 1(U) AUTONOMOUS TECHNOLOGIES CORP ORLANDO FL R W FREY ET AL. 27 MAR 89 DASG60-88-C-0076 2/2

UNCLASSIFIED F/G 17/5.1 NL

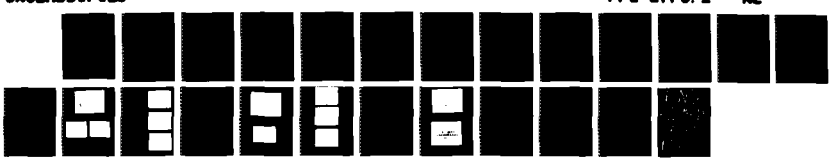

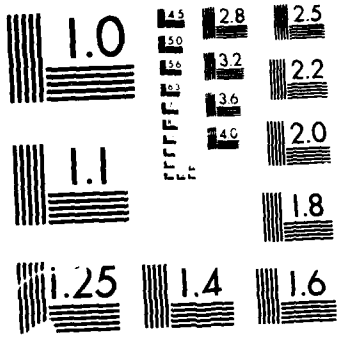

UTION TEST CHART

After being modulated by the Bragg Cell, the beam reflects off mirror M5, then to a pair of Galvo scanners, used for directing the beam in azimuth and elevation to targets in the lab. Upon reflection from a target, the received energy reflects off the galvo pair and M6 to beamsplitter BS2 (10% R, approximately 90% T), where it combines with the LO. This is the so called heterodyne mixing surface. The receive and LO beams are then imaged onto the detector. Thus we have an offset homodyne laser radar (LADAR).

3.1.3 Compact Interferometer Mechanical Design Considerations

During the past year, the compact interferometer was designed and built by ATC and successfully incorporated into several ATC programs. The design approach used in the development of the hardware incorporated modular optical mounts on an optical bed. Using the modular optical mounts facilitated flexibility of location on the optical bed. This hardware versatility allows the testing of many different approaches without building new hardware.

An important opto-mechanical design consideration for the optical mo nts was the minimization of the size and mass of the mounts while properly holding the optics. Most of the elements are mounted in retainers using a non-outgassing silicon RTV. The RTV is used to hold the optic in place and apply pressure against an optical registration surface. This preload from the RTV will enable the optics to endure a 10g environment. The mounts incorporate a precision pilot mounting diameter that allows the units to be accurately located on the optical bed. To aid in the alignment of the system, clearance holes are used to allow rotation of the mounts in the pilot diameters on the optical bed.

Other features incorporated into the compact interferometer include: 1) liquid cooling of the laser, the laser power supply and the AO modulator; 2) the ability to remove and replace both the laser and detector while maintaining system alignment; and 3) use of a modular scanner mount to allow multiple positions in the CI.

3.1.4 PN LADAR Transmitter Optical Carrier Modulation

The Phase I approach to optical carrier modulation utilized an acousto-optic (Bragg Cell) modulator. The modulator is single crystal germanium, manufactured by Intra-Action Corp., model #AGM 402. The acoustic driver, IntraAction Model GE4030, used an RF carrier at 40 MHz. For acousto optic modulators, maximum diffraction efficiency occurs when the optical field is at an angle of incidence with respect ot the acoustic field at the Bragg angle α_b:

$$\sin \alpha_b = \frac{\lambda_L}{2\ \lambda_s}$$

where :

α_b = the Bragg angle,

λ_L = wavelength of light (in air)

λ_s = sound wavelength (in the material)

For Germanium, the velocity of acousitc waves is V_s = 5500 meters/sec, and the center frequency fs = 40 MHz, therefore $\lambda_s = V_s/f_s = 5500/40x10^6 = 138$ mm. For $\lambda_L = 10.59\ \mu$m, $\alpha_b = \sin^{-1}(10.59)/(2)(138) = 38.5$ milliradians.

The angular deviation between the undesired zero order (undiffracted) and desired first order diffracted beams is $2\alpha_b = 77$ mrad. The alignment in the compact interferometer was compensated for, such that the zero order beam was blocked and the diffracted, beam was used. This first order diffracted beam, ie. the optical carrier, is also frequency shifted by the frequency of the acoustic carrier, ie. 40 MHz.

The frequency shifted optical carrier is such that the heterodyne return signal from a stationary target is centered at 40 MHz. For an unmodulated, frequency shifted carrier, this eliminates baseband fold over and allows differentiation of approaching and receding Doppler.

For optical modulation, this allowed either double sideband full carrier (DSC) or double sideband suppressed carrier (DSSC) modulation of the optical carrier. The DSSC modulation, which is spectrally equivalent to the desired 0°/180° PSK modulation was implemented as the Phase I modulation approach. The spectrum of the Phase I PN codes used (see eq. 2.14-2.16) has a sinx/x distribution. This was experimentally verified (see section 5).

The Phase I modulation rate was limited to 1 MHz for the following reason. The spectral width of the acoustic signal into the A-O modulator was limited to avoid excessive first order diffracted beam spread. For a 2 mm diameter acoustic aperture, the optical beam has 6.75 mrad divergence at 10.6 μm. It is therefore desireable to limit the spectral input such that the acoustic spectral width induced optical divergence increase is 1/5 to 1/10 of the optical divergence or .67 to 1.34 mrad. Given the Germanium Bragg cell with acoustic velocity 5500 m/s and center frequency 40 MHz, the

modulation bandwidth limit is .7 MHz to 1.4 MHz. For Phase I, a 1 μsec minimum chip width, corresponding to a first null in the sinx/x distribution at 1 MHz, were employed.

Cadmium Telluride (CdTe) electro-optic (EO) modulators, which have the ability to directly phase modulate as well as intensity modulate, are more suitable for the pseudo noise LADAR. However, their use in a Phase I program was not considered due to their high cost and higher voltage (>1kv) drive requirements. The Phase II program will consider their use due to the high payoff technical characteristics of E-O over AO modulators: direct phase modulation, and higher frequency operation, providing payoffs for SDI missions of interest. Additional payoffs will include implementation of the ATC-STI developed proprietary Pseudo Noise Imaging concept, to be further discussed in the Phase II proposal.

4.0 PHASE I RECEIVER HARDWARE

4.1 Receiver Noise Considerations

All receiver designs must start with a derivation for the noise power expected in the final IF bandwidth. The Phase I IF bandwidth was 10 MHz, so chosen to preserve harmonics of the PN code sequence, and to allow for growth. In a 50 ohm system, one starts with the noise power generated by a 50 Ω resistor in a 1 Hz bandwidth:

$$kTB = -174 \text{ dBm/Hz}$$

Where k = Boltzmans constant, and T = front end noise temperature, 293°k, and B = Bandwidth = 1 Hz. Then one adds the increase in noise power due to system bandwidth:

$$10 \log \pm BW = 10 \log (2x10\ x10^{6}) = +73 \text{ dB}$$

For shot noise limited heterodyne detection, there is approximately 5 dB optical local oscillator induced shot noise. Finally, a worst case value for the first preamp noise figure is added in, ie: approximately 3 dB

To summarize:

kTB	-174 dBm/Hz
Bandwidth 10 MHz	+ 73 dB
LO shot noise	+ 5 dB
Pre-Amp NF	+ 3 dB
	- 93 dBm

The receiver noise floor is then -93 dBm in a 10MHz IF bandwidth.

4.2 Receiver Intermediate Frequency (IF) Electronics

The PN LADAR Phase I receiver electronics consisted of the following sub components.

1) HgCdTe wideband, high quantum efficiency detector
2) Current limiting bias network
3) Low noise pre-amp and filter
4) RF amplifiers and filters---Additional IF electronics
5) IF to baseband video down convert
6) Video amp and filter
7) Pseudo random bit sequence (PRBS) test set

The block diagram of the receiver is shown in Figure (4-1). The diagram also shows the PN code modulation section for clarity. The function of each of these will now be described.

PN LADAR
RF-IF PROCESSING BLOCK DIAGRAM

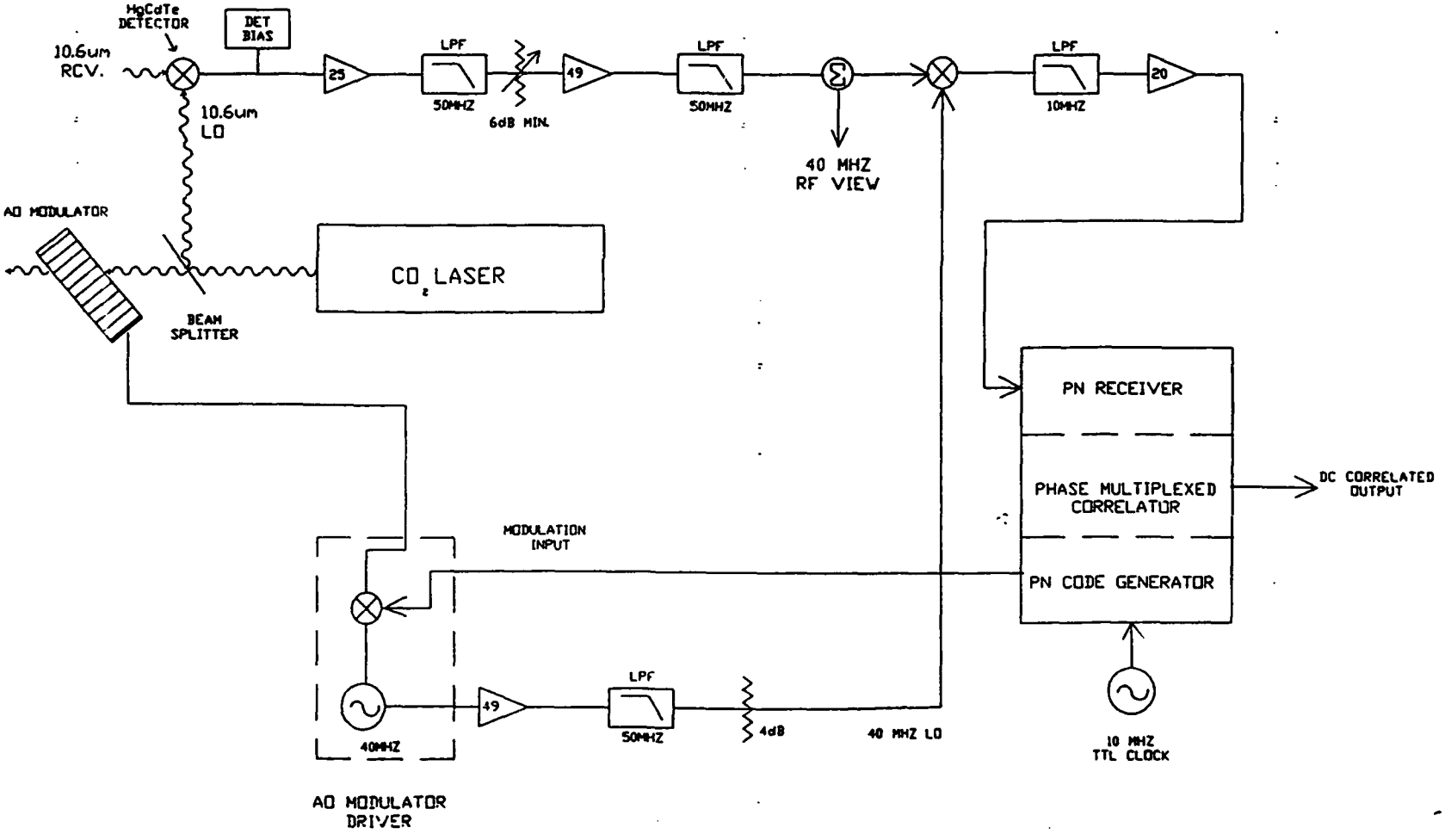

Figure 4-1,

4.2.1. Optical Detector

The optical detector is a high quality mercury cadmium telluride (HgCdTe) diode operating at 77°K. It is mounted in a liquid nitrogen dewar with a Germanium AR coated window, and has a LN_2 hold time of approximately 8 hours. The sensitive area is 100um in diameter. At $\lambda = 10.6\mu m$, the D^* is 3.4×10^{10} cm root Hz per watt, the DC quantum efficiency is 47%, and the bandwidth is >200 MHz. The detector was manufactured by SAT.

Heterodyne efficiency measurements for the detector were not made in Phase I. Detailed heterodyne efficiency measurements will be made so that detector operations will be optimized for the Phase II program.

4.2.2 Bias Network

The detector bias network for the MCT diode was designed and fabricated at ATC to provide the correct voltage and current bias for efficient heterodyne detection. It is fully regulated and current limiting but provides sufficient current swing to optimize the detector's heterodyne efficiency with approximately 1 mw of local oscillator power.

The schematic of the bias network is shown on the following page in Figure (4-2).

The photovoltaic detector diode is used in reverse biased operation. The dewar housing is electronically isolated from the compact interferometer bed, so that the first ground point is actually located at the first preamp. This arrangement was found to be very useful in eliminating ground loops. This bias network approach proved excellent for Phase I, and a similar, but RFI hardened approach will be implemented in Phase II.

4.2.3 Pre-amp and Filter

The Vanguard Labs model MX500 preamp used in the PN LADAR is a wideband, low noise device. It has a gain of 25 dB, a 1 dB compression point of 0 dBm, a noise figure of 1.5 dB and a 3 dB bandwidth of 200 MHz. The low end cutoff is approximately 1MHz. A 50 MHz low pass filter was used to attenuate narrowband interference caused by the laser transmitter's RF power supply at 75 MHz, and also broadband noise due to the wideband preamp.

4.2.4 Additional RF Components

Following the pre-amp and filter, additional RF components were used. A precision variable attenuator following the pre-amp was used for manual gain control, so strong return signals would not saturate amplifiers further down the RF chain. Next, a side band, low noise amp was used to boost the signal. This amp, Miteq Corp. model AU-3A-0110, has a gain of 49 dB, a noise figure of 1-5 dB and a 1 dB compression point of 13 dBm. An additional 50 MHz low pass filter, followed this amp. A wide band 3 dB splitter was used to view the 40 MHz IF carrier with a spectrum analyzer.

SAT BIAS NETWORK

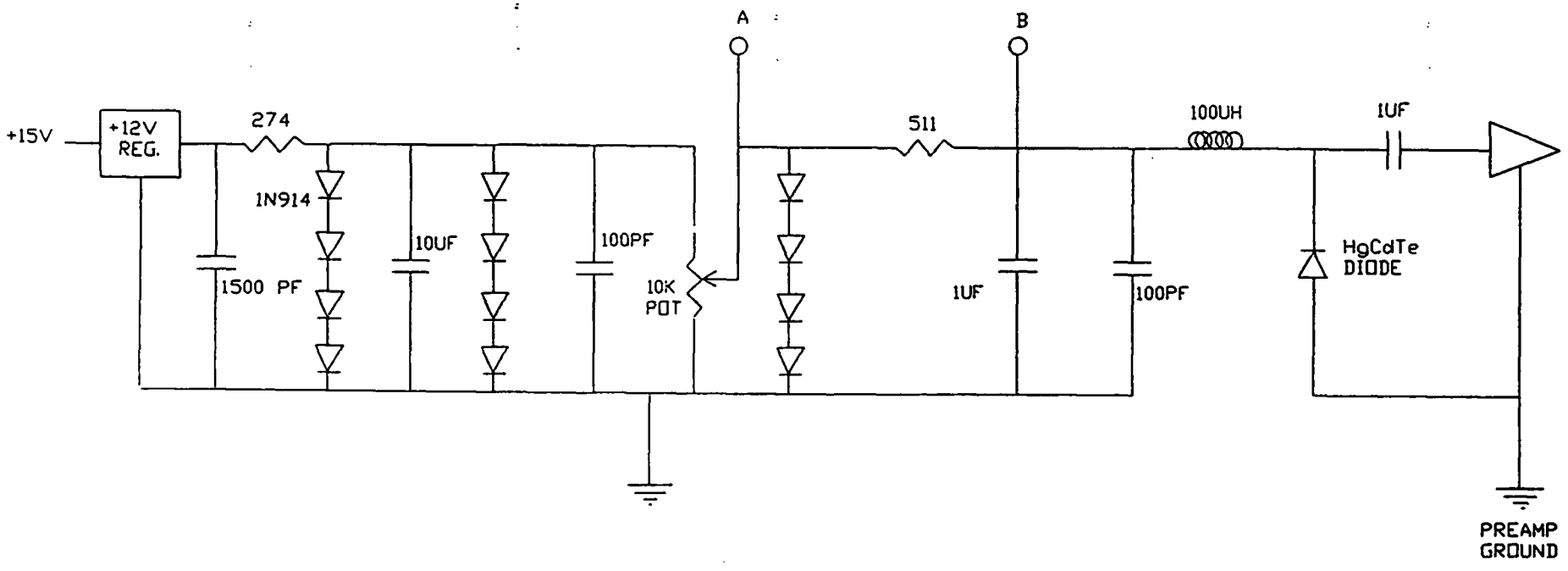

Figure 4-2

4.2.5 RF Conversion to Baseband

The 40 MHz IF signals are then mixed in a double balanced mixer and converted to baseband. The 40 MHz local oscillator (LO) was derived from the same crystal reference used to drive the acousto-optic modulator, to preserve system coherence. The low amplitude signal was inductively coupled out of the Intra-Action Modulator Driver; then amplified, filtered and padded before mixing with the 40 MHz IF signal in the double balanced mixer. The output of the mixer has components at $f_{LO} + f_{RF} = 80$ MHz and $f_{LO} - f_{RF} = 0$ Hz. The upper mixing product at 80 MHz was filtered out, and the baseband signal from DC to 10 MHz was amplified by 20 dB and sent to the PN receiver.

4.3 Pseudo Random Bit Sequence (PRBS) Test Set

Hardware developed on Phase I by Signal Technologies consists of transmit and receive sections. Both transmit and receive functions were designed to operate at baseband with a minimum bandwidth of 10MHz. The test set is responsible for generating the spread spectrum Gold Code and correlating the channel corrupted received Gold Code with a phased multiplexed correlator (PMC) signal. The following sections describe the various functions of the hardware and aspects of the design. A block diagram of the PN transmit section is shown in figure 4-3.

4.3.1 Transmit Sequence:

The transmitter sequence is based on the modulo two sum of two maximal length pseudo random sequences. The two primitive generator polynomials are given by:

$$g_1 = X^{10} + X^9 + X^8 + X^6 + X^3 + X^2 + 1$$

$$g_2 = X^{10} + X^3 + 1$$

A resulting Gold Code family is generated from relative phase shifted versions of g1 and g2.

4.3.1.1 Phase Multiplexed Correlator Signal:

This signal is built from a linear phase shifted sum of up to 8 Gold Codes corresponding to the transmit sequence. This signals cross correlation coefficient with respect to the transmitted sequence was key to the success of the Phase I effort. The composition of this signal permits rapid acquisition of the received waveform. A block diagram of the PMC receiver is shown in figure 4-4.

4.3.2 Inputs:

± 15 volts and +5v DC are supplied via a terminal block on the back of the test set. An external clock of up to 16MHz can be supplied via a BNC located on the back panel. This signal is specified as a standard TTL input. A 10MHz clock was used for the Phase I effort. A 50Ω receive input with 10MHz bandwidth is located on the front panel of the unit and comes from the optical receiver (see Fig. 4-1).

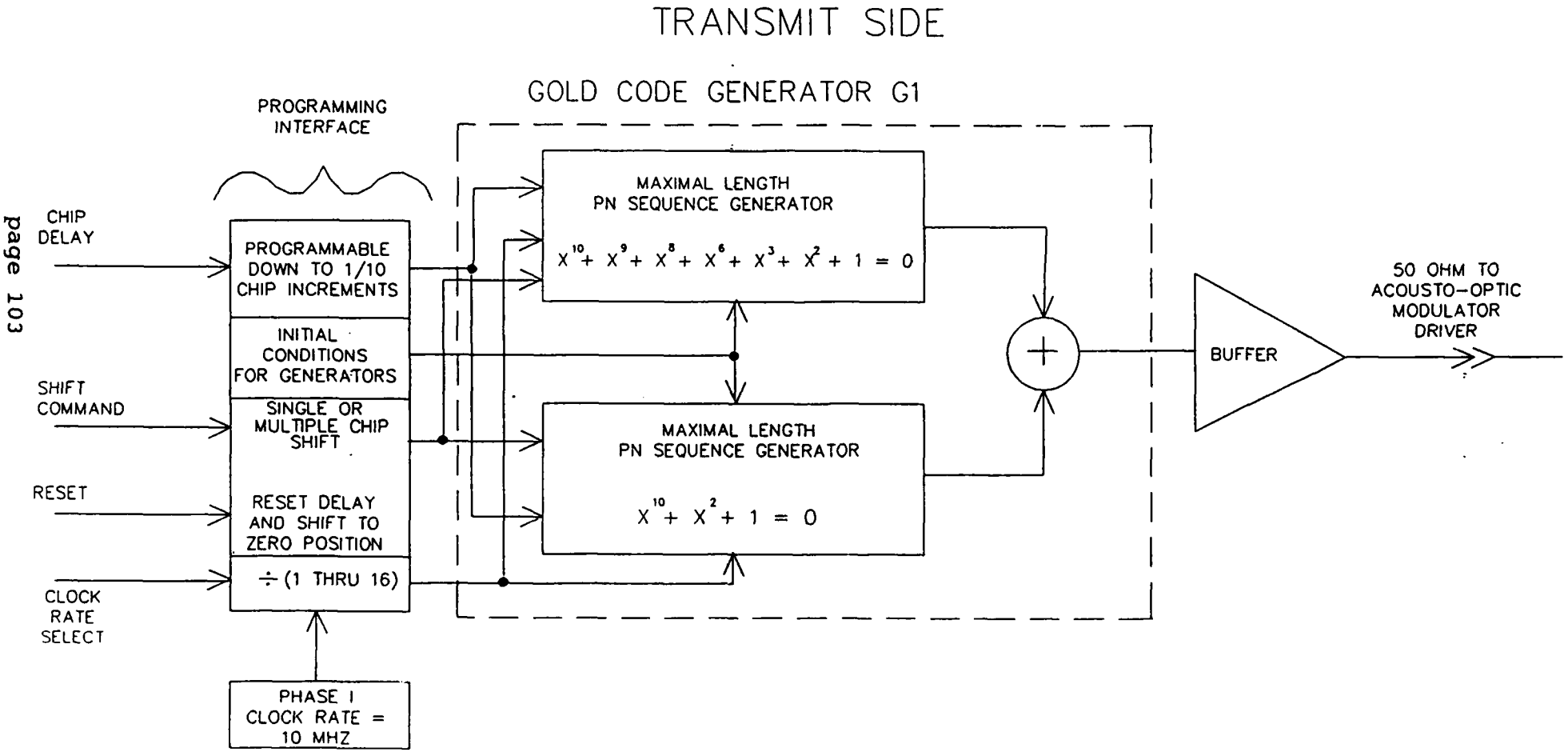
TRANSMIT SIDE
GOLD CODE GENERATOR G1
PROGRAMMING INTERFACE
CHIP DELAY
SHIFT COMMAND
RESET
CLOCK RATE SELECT
PROGRAMMABLE DOWN TO 1/10 CHIP INCREMENTS
INITIAL CONDITIONS FOR GENERATORS
SINGLE OR MULTIPLE CHIP SHIFT
RESET DELAY AND SHIFT TO ZERO POSITION
÷ (1 THRU 16)
PHASE I CLOCK RATE = 10 MHZ
MAXIMAL LENGTH PN SEQUENCE GENERATOR
$X^{10} + X^9 + X^8 + X^6 + X^3 + X^2 + 1 = 0$
MAXIMAL LENGTH PN SEQUENCE GENERATOR
$X^{10} + X^2 + 1 = 0$
BUFFER
50 OHM TO ACOUSTO-OPTIC MODULATOR DRIVER

Figure 4-3

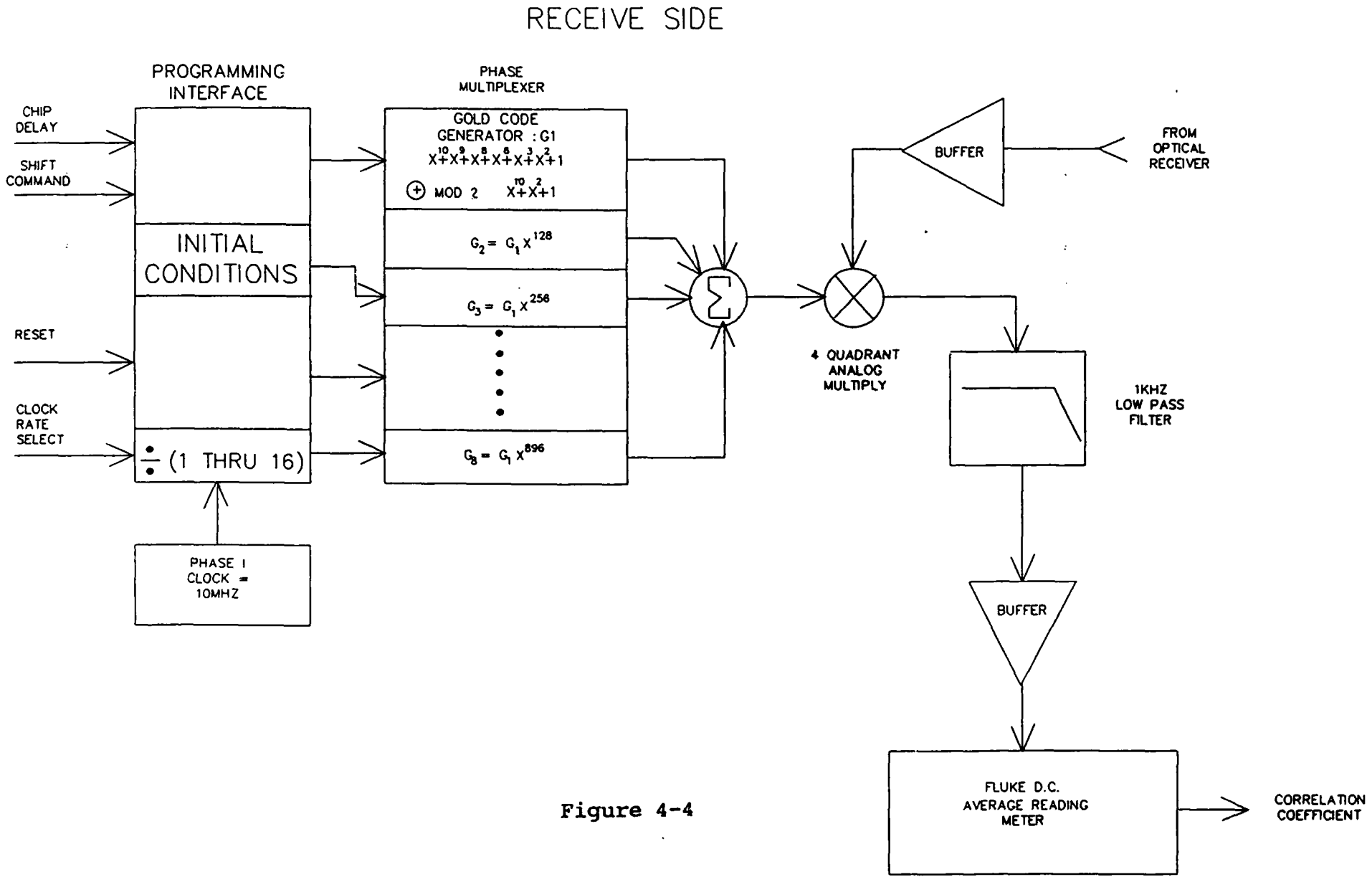
RECEIVE SIDE
PROGRAMMING INTERFACE
PHASE MULTIPLEXER
CHIP DELAY
SHIFT COMMAND
INITIAL CONDITIONS
RESET
CLOCK RATE SELECT
÷ (1 THRU 16)
PHASE I CLOCK = 10MHZ
GOLD CODE GENERATOR : G1
$X^{10}+X^{9}+X^{8}+X^{6}+X^{3}+X^{2}+1$
⊕ MOD 2 $X^{10}+X^{2}+1$
$G_2 = G_1 X^{128}$
$G_3 = G_1 X^{256}$
$G_8 = G_1 X^{896}$
BUFFER
FROM OPTICAL RECEIVER
4 QUADRANT ANALOG MULTIPLY
1KHZ LOW PASS FILTER
BUFFER
FLUKE D.C. AVERAGE READING METER
CORRELATION COEFFICIENT

Figure 4-4

The external clock drives all of the functions of the box and determines the chip rate as well as the phase resolution of the delay function. An auxiliary data input with TTL interface is located on the back panel. This data input accepts data rates of up to 300 BPS NRZ or RZ format. The purpose of this input is to allow covert jam resistant data transfer over a link.

4.3.3 Outputs:

The transmit out signal is a 50Ω 10 MHz wideband port used to deliver the conditioned Gold Code to the acousto-optic modulator driver (see figs. 4-3 and 4-4). A correlation coefficient output is provided on the rear panel. The expected value of the signal from this port is a direct measure of the correlation between the PMC signal of the receiver and the received waveform. This output is designed to drive a digital voltmeter or similar device. The correlation coefficient is read directly from the display of the DVM while operating in the DC measurement mode. In addition, despread data received and correlated from the transmitter is available as an output.

4.3.4. Programming Interface:

The Programming Interface is identical for the transmit and receive sections. The external clock input can be divided down by 1 through 16 to select various chip rates. Likewise, delay increments and shift increments are programmable from 1 to 16 clock cycles and 1 to 16 chips respectively. Furthermore, initial conditions on g1 and g2 can be programmed in order to select the appropriate Gold Code. These programming options are fixed by dip switches located on the boards.

4.3.5 Shift:

The Shift control is implemented by a positive feedback front panel push button. Each detent of the button creates a delay of some multiple number of chips, programmed via a dip switch. For the purposes of this experiment, a delay of one chip per detent was used. Both transmit and receive waveforms can be shifted independently by the transmit shift and receive shift controls.

4.3.6 Delay:

The Delay push buttons are also located on the front panel for both transmit and receive sections. The Delay function operates similarly to the shift command except that the fundamental delay unit is a sub-multiple of one chip. For this experiment 1/10 chip increments were programmed via a dip switch.

4.3.7 Reset:

The Reset function resets transmit and receive sections simultaneously so that the transmit sequence is optimally aligned to the PMC signal in the receiver within a fraction of one chip. This control is a front panel mounted push button.

4.4 Theory of Operation:

The PRBS test set generates the ranging, spread spectrum, Gold Code at baseband and routes this signal to the acousto-optic modulator through an SMA interface. This output can be phase shifted by delay and shift controls to obtain multiple chip and sub-multiple chip delays of the output sequence with respect to the PMC signal in the receive section. The output signal modulates the acoustic carrier, which modulates the laser, transverses the channel, illuminates the target, is processed by the receiver, and is routed back to the receive input of the box. The receive input is routed to a correlation assembly consisting of a 4 quadrant analog multiplier and image filter. The PMC signal supplies the other input of the analog multiply. It can be shifted in phase with respect to the transmit output by using the receive section delay and shift controls. The shift and delay controls on both the receive and transmit sections are used to adjust for channel delays. Hence, optimal correlation can always be obtained with some manipulation. Of course, due to the nature of the PMC design, this optimal correlation is achieved every 128 chip increments even though the transmitted sequence repeats only every $2^{10}-1 = 1023$ chips. The expected value of the correlator output becomes the measure of the correlation coefficient.

5.0 PHASE I EXPERIMENTAL CONFIGURATION AND RESULTS

5.1 Configuration

The Phase I experiment system configuration is shown in the block diagram in Figure (4-1). Measurements were individually performed on both the optical, RF and PMC subsystems of the system. These subsystems were then integrated, and end to end experiments were performed. Results were obtained from laboratory targets. The principle targets used were a stationary glint target at a range of 70 feet, and a diffuse, low reflectivity target at a range of 30 feet. The glint target was a 1" reflector located across the hallway in the opposite corner of the building occupied by ATC. The diffuse target was a cone with a height of 18" and a base 9" in diameter. This conical target was affixed to a turntable mount, rotating at 78 rpm, yielding a maximum rotational Doppler component of ≈ 1 meter per second.

5.2 Results

When integrating a coherent heterodyne LADAR, achieving shot noise limited operation of the heterodyne receiver is the principle indication of a working system. The spectrum analyzer photo in Figure (5-1a) shows shot noise limited operation out to 50 Mhz.

The lower trace is the optical local oscillator blocked.

The upper trace shows the approximate 3 dB increase in noise power due to LO induced shot noise out to 50 MHz.

The narrow band CW interference at 40 MHz is RF bleed through from the acousto-optic RF driver.

The Phase II program approach will utilize higher carrier frequencies and wider bandwidths, and therefore shot noise limited operation out to frequencies > 1 GHz will be required. However, on a previous SDI program, ATC has demonstrated the capability of obtaining shot noise limited heterodyne detection out to 1.5 GHz on the LASE program at the RADC/AMOS facility. Figure 5-1b shows the shot noise limited response for the LASE program.

The next sign of successful operation of the Phase I LADAR was detection of a Doppler target. For the unmodulated frequency shifted optical carrier, measurements were made on the laboratory spinning conical target. The spectrum analyzer photos in Figures (5-2, 5-3, and 5-4) show returns from the spinning conical target. Figure (5-2) is the return from the center of the target. The finite spectral width (20-30 KHz) is due to the finite beam size on the target, indicating returns having positive, zero and negative radial Doppler components. The next photo Figure (5-3), is a return from the approaching side of the cone. The radial Doppler component

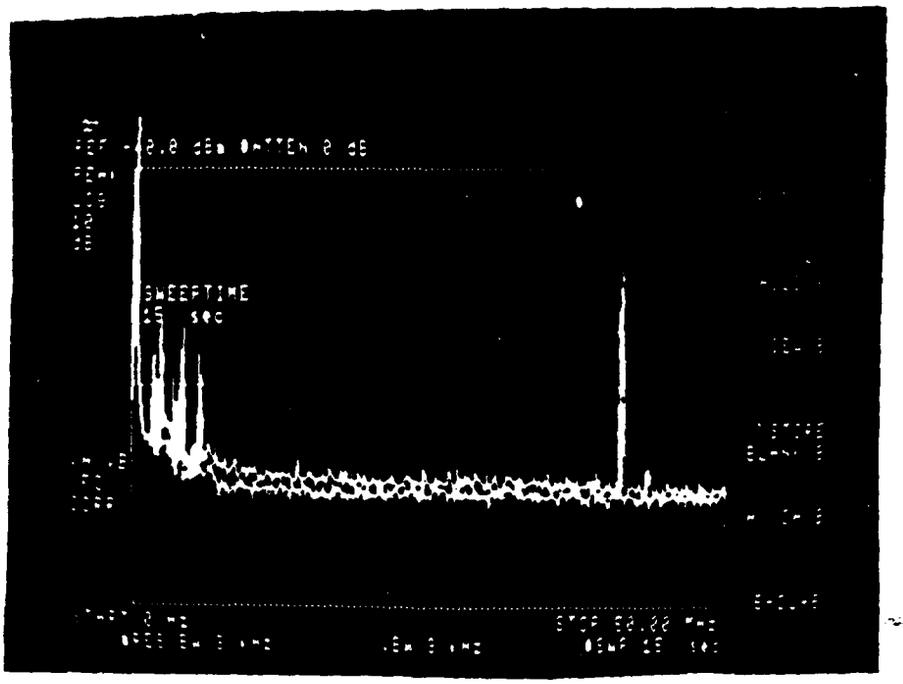

PHASE I PN LADAR

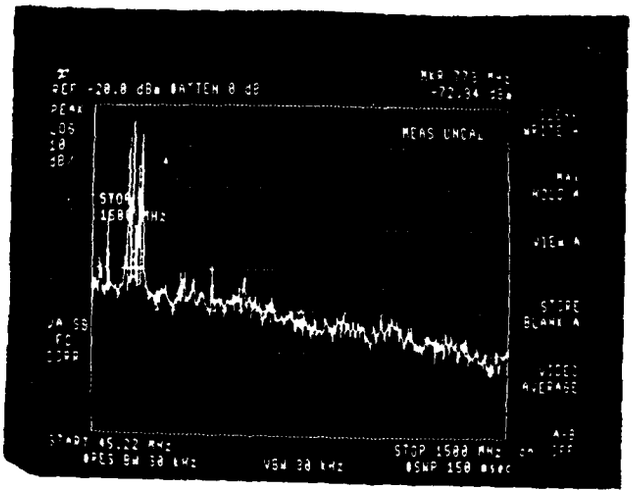

A. LO OFF

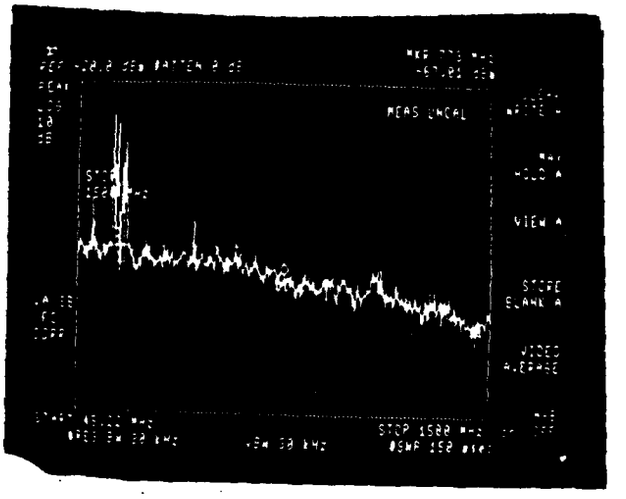

B. LO ON

LASE

Figure 5-1 Shot Noise Limited Heterodyne Detection

Figure 5-2 Center of Target

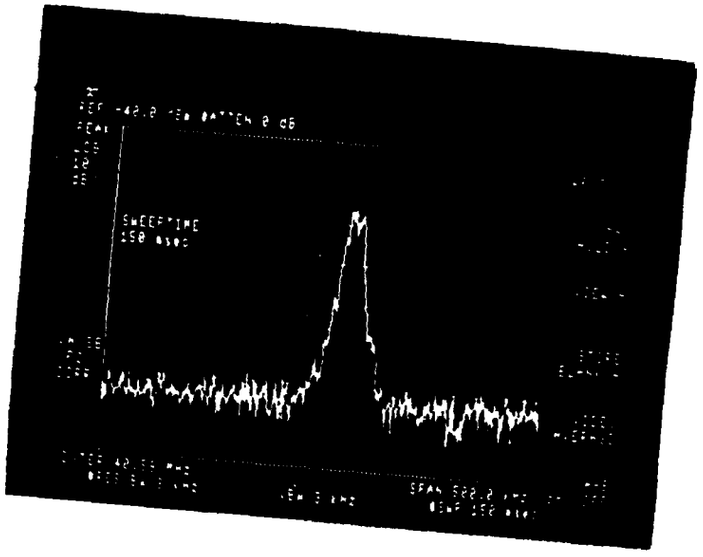

Figure 5-3 Approaching Side of Target

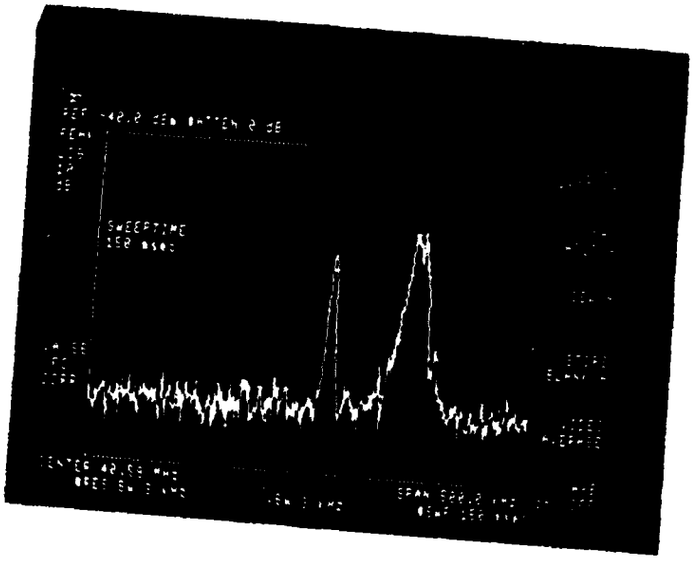

Figure 5-4 Receding Side of Target

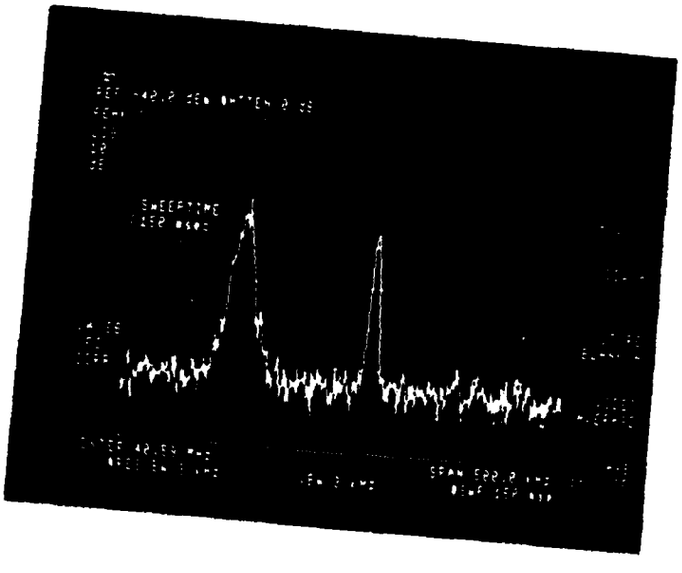

is ≈ 100 KHz, corresponding to a radial velocity component of ≈ .53 meters/second.

The narrow band cw interference in the photo is the RF bleed through from the AO modulator driver. Although quite large for the non-suppressed carrier Doppler experiment, this interference is still 6 dB below the carrier, and we still obtained performance at the target center . A novel approach for coherent cancellation of this narrow band cw interference will be discussed in the Phase II proposal and implemented in the Phase II program.

The third photo, Figure (5-4), is the return from the receding side of the cone, with a radial Doppler component of 165 kHz (≈ .87 m/sec.).

The returns from this low reflectivity diffuse target have a carrier to noise ratio (CNR) of 45 dB in the 3 kHz noise bandwidth of the spectrum analyzer. This is equivalent to a 10 dB CNR in the Phase I system noise bandwidth of 10 MHz.

The Phase I PN transmit and PMC receive electronics were tested, and the pseudo noise and phase multiplex local correlator waveforms were recorded. The top trace in Figure (5-5), shows a portion of the transmitted PN waveform. For a 1 μsec chip width and a code length of 1023, the total code length is 1023 μsec. The bottom trace shows the phase multiplexed local correlator waveform. Note the horizontal scale of 10 μsec/div = 100 μsec full scale. This lower trace clearly shows the successful implementation of the phase multiplex correlator concept discussed in detail in section 2. For a code length = 1023, and the Phase I 8 level multiplexing implementation, the PMC local waveform repeats every 128 μsec. The 8 level multiplexed structure of the coded waveform is clearly visible in this photo. Transmit and receive shift and delay functions were also verified, respectively.

The PN transmit, PMC correlator and RF electronics were then all integrated into the optical transceiver to form the complete PN LADAR. End to end system experiments were performed against targets in the lab environment. The results of these experiments will now be described.

The PN transmit sequence modulated the 40 MHz acoustic carrier, which in turn modulated the optical carrier. Heterodyne returns from the lab targets were observed and recorded. The spectrum analyzer photos in Figures (5-6 through 5-9) are of signals out of the RF viewport (see Figure 4-1). Figure (5-6) shows the spectrum of the noise generated by the RF carrier bleed through. Figure (5-7) is the spectrum of the return from the diffuse rotating conical target. The transmit beam was aimed at the center of the target, where the magnitude of the rotational Doppler component was at its minimum. This target was the same target as in Figure (5-2). Comparing Figures (5-6 and 5-7), the signal and noise/interference and noise ratio is ≈ 10 dB. Figure (5-8) shows the return from the receding side of the cone, corresponding to the target in Figure (5-4). The frequency shift is just apparent, due to the expanded frequency scale as compared to Figure (5-4).

Figure 5-5 PN Transmit Sequence Waveform (top trace) and PMC Local Correlator Reference Waveform

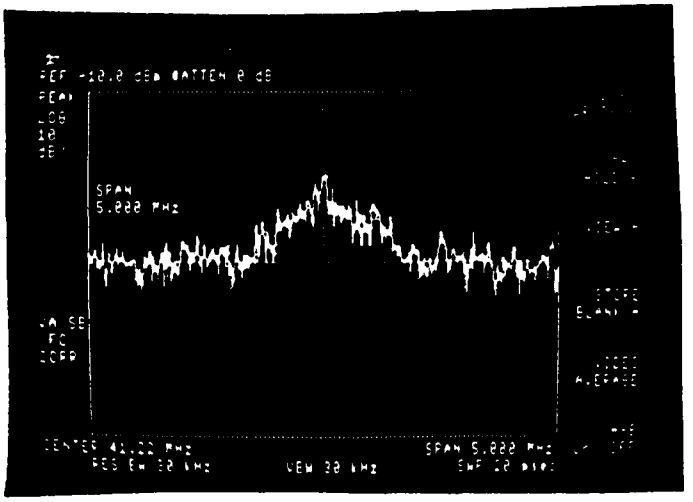

Figure 5-6 Spectrum of RF Bleedthrough with PN Modulation on the Optical Carrier

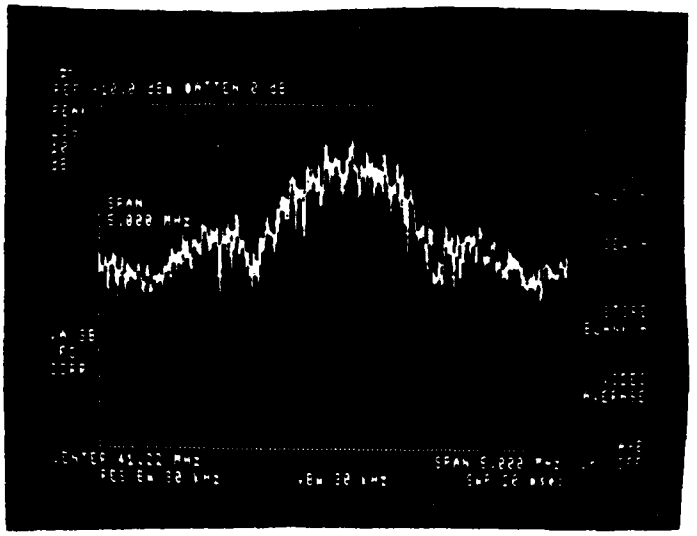

Figure 5-7 Spectrum of the Pseudo Noise Return from the Center of the Diffuse Rotating Conical Target

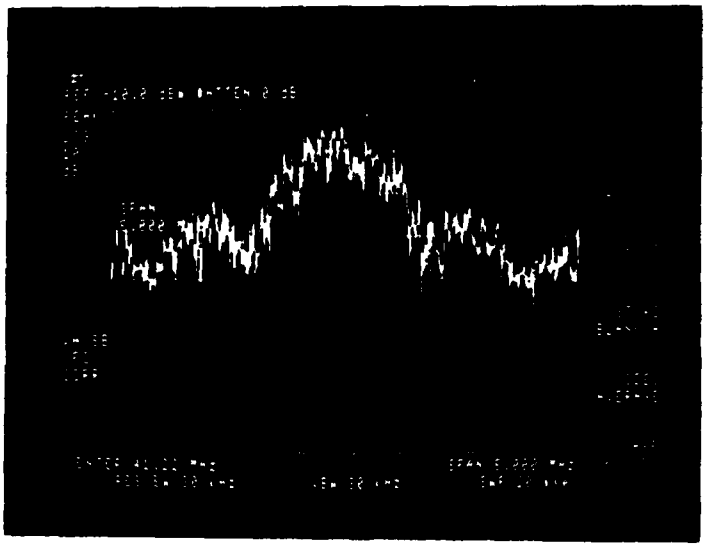

Figure 5-8 Spectrum of the Pseudo Noise Return from Diffuse Rotating Conical Target with Receding Rotational Doppler

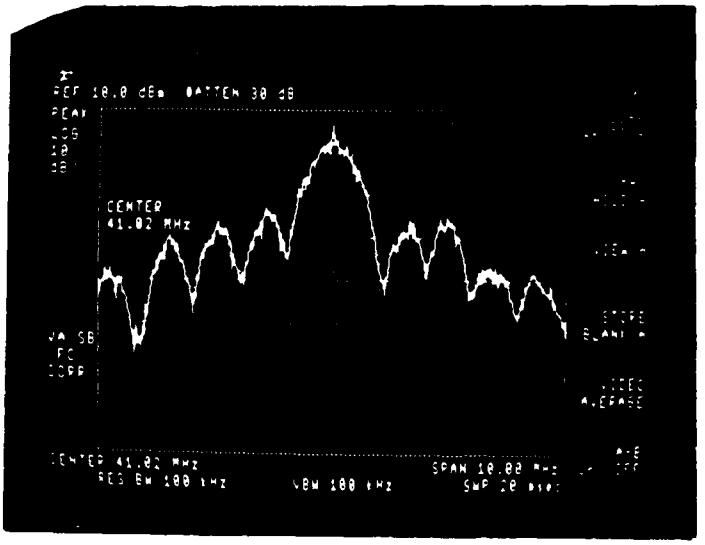

Figure 5-9 Spectrum of the Return from a Stationary Glint Target

Figure (5-9) shows the spectrum of the return from the stationary glint target. The sinx/x distribution of the PN modulation, with the first null at 1 MHz, corresponding to the minimum chip width of 1 μsec, is clearly visible in this spectrum analyzer photo.

Figures (5-10 and 5-11) are scope photos of the carrier stripped baseband received time waveform before going to the PMC correlator. The return was from a stationary diffuse target of low reflectivity (ie. a wall in ATC's laboratory) at a range of ≈ 40 feet. Figure (5-11) shows the phase instabilities due to the lack of a carrier tracking loop. Waveforms typical of this were also observed from returns of Doppler targets. The Phase II approach will include carrier tracking loops to eliminate effects of random phase returns. The PMC receiver correlator was then exercised against the various lab targets. Figure (5-12) shows the correlations measured from the best case and worst case scenario targets. The solid line is the correlation obtained by going directly from the PN transmit to the PMC receive ports of the test set described in section 4.3. This is the best case no noise situation. The dashed curve represents the correlation measured from the complete **END to END Phase I PN LADAR** system against a diffuse rotating conical target. As one can observe, substantial correlation peaks were still measured.

5.3 Conclusion

Given this, we feel strongly that the Phase I concepts were successfully demonstrated, and we are eager to extend the innovative theoretical concepts and hardware implementations in a successful **PHASE II PROGRAM.**

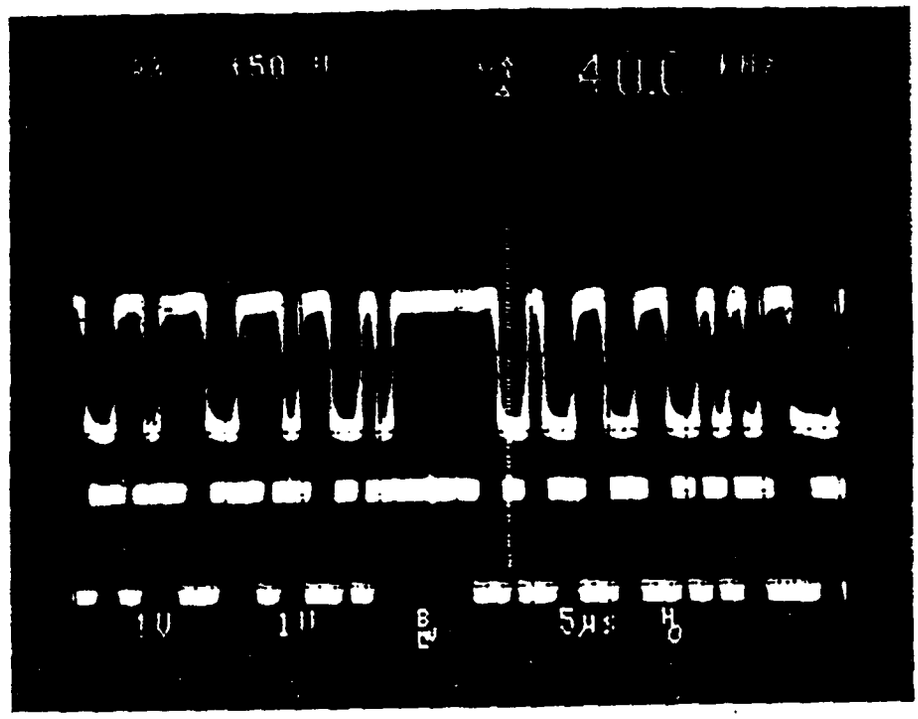

Figure 5-10 Baseband Received PN Waveform from a Stationary Diffuse Target

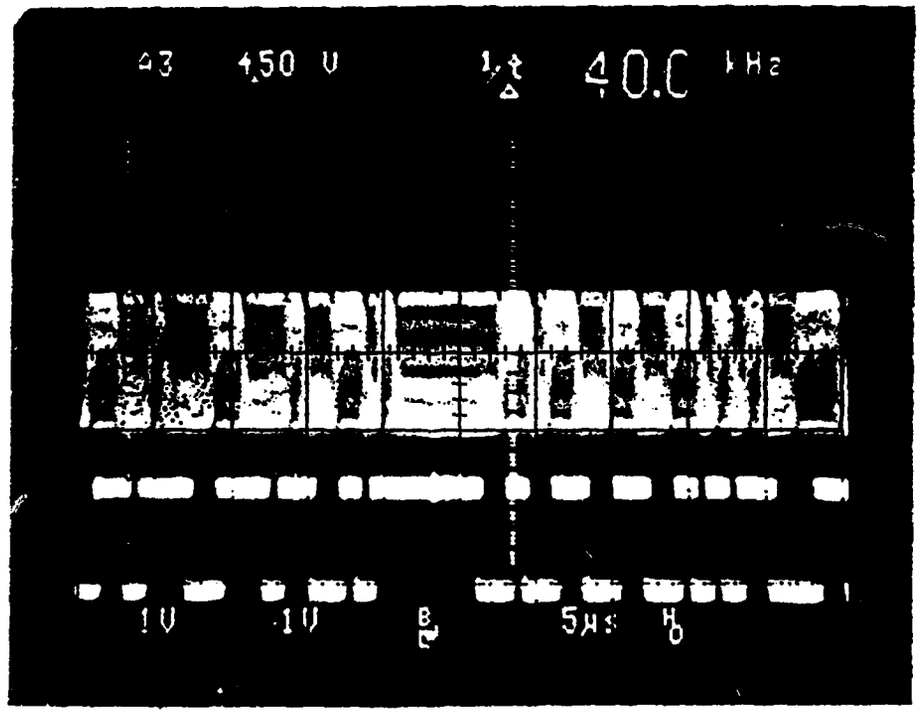

Figure 5-11 Baseband Received PN Waveform from a Stationary Diffuse Target showing Phase Instability [In the Absence ofa Carrier Tracking Loop]

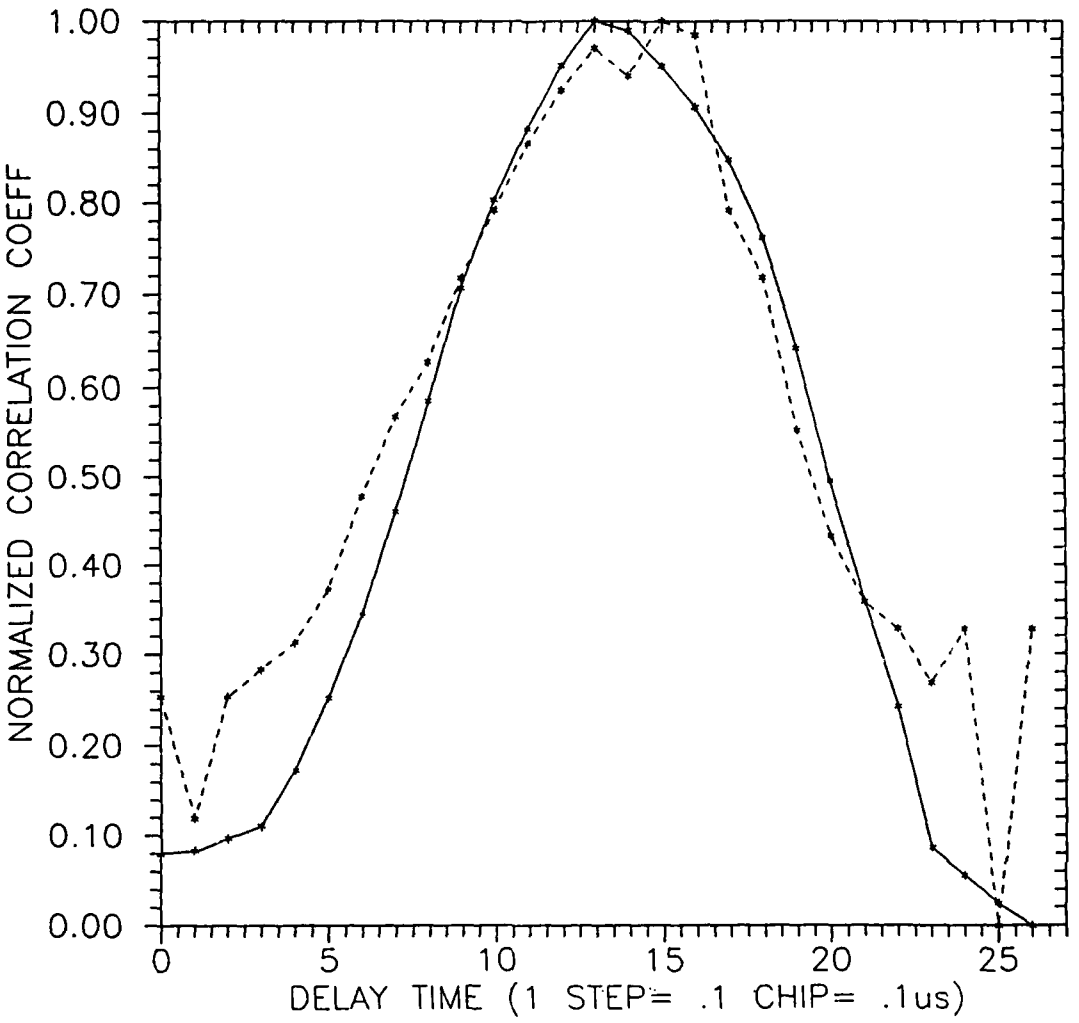

Figure 5-12 Normalized Correlation Coefficient
——— No Noise Electronics Only Correlation
-------End to End Optical Correlation

REFERENCES

Bouvier, M. J.; Walls, H. J.; and Boyd, R. V. Rapid Acquisition of Spread Spectrum Systems. Final Report to Army Research Office, Contract #DAAG29-80-C-0005 (1980).

Cooper, George R., and McGillem, Clare D. Probabalistic Methods of Signal and System Analysis. New York: Holt, Rinehart and Winston, Inc., 1971.

Cooper, George R., and McGillem, Clare D. Modern Communications and Spread Spectrum. New York: McGraw-Hill Book Company, 1986.

Holmes, Jack K. Coherent Spread Spectrum Systems. New York: John Wiley and Sons, Inc., 1982.

Lane, Barry. "Digital Communications System Evaluation: Design Developments in Pseudorandom Sequence Usage, Signal Conditioning and Timing Regeneration." Master's Thesis, University of Central Florida, Orlando, FL., 1983.

Papoulis, Athanasios. Probability, Random Variables and Stochastic Processes. New York: McGraw-Hill Book Company, 1984.

Pickholtz, Raymond L.; Schilling, Donald L.; and Milstein, Laurence B. "Theory of Spread Spectrum Communications." IEEE Transactions on Communications COM-30 (May 1982): 855-884

Polydoros, Andreas, and Weber, Charles L. "Worst-Case Considerations for Coherent Serial Acquisition of PN Sequences." IEEE 1980 Symposium on Communications 24 (1980): 24.6.1-24.6.5

Proakis, John G. Digital Communications. New York: McGraw-Hill Book Company, 1983.

Sage, Gerald F. "Serial Synchronization of Pseudonoise Systems." IEEE Transactions on Communication Technology (December 1964): 123-127

Schwartz, Mischa. Information Transmission Modulation and Noise. New York: McGraw-Hill Book Company, 1980.

Simon, Marvin K.; Omura, Jim K.; Scholtz, Robert A.; and Levitt, Barry K. Spread Spectrum Communications, Volumes I, II, III. Rockville, MD: Computer Science Press, 1985.

Torrieri, Don J. Principles of Military Communication Systems. Dedham: Artech House, Inc., 1981.

Young, Mark W. "Design of a Gold Code Generator for use in a Code Division Multiple Access Communications Systems." Master's Thesis, University of Central Florida, Orlando, FL., 1985.

Eaves, Jerry L.; Reedy, Edward K. Principles of Modern Radar. New York: Van Nostrand Reinhold Co., 1987.

Skolnik, Merrill I. Radar Handbook. New York: McGraw Hill Book Co., 1970.

Rawlins, Gregory S. "A Rapid Acquisition Technique for Direct Sequence Spread Spectrum Systems." Master's Thesis, University of Central Florida, Orlando, Fl., 1987.

END

FILMED

6-89

DTIC